



Coherent states of photonic dimers

Qihang Liu , Yao Zhou, and Jung-Tsung Shen **Department of Electrical and Systems Engineering, Washington University in St. Louis, St. Louis, Missouri 63130, USA*

(Received 29 May 2023; accepted 11 October 2023; published 7 November 2023)

The concept of coherent states of single photons is generalized to the scenario wherein the fundamental building blocks are entangled two-photon states rather than single-photon states. To provide a concrete discussion, the case of photonic dimers (two-photon bound states) is explored. The coherent states of photonic dimers are defined. The correlation functions are calculated and expressed in terms of series expansion which is suitable for computational investigations. The quadrature properties and the squeezing effects are computed and compared with the experimental results at suitable regimes. Finally, the statistical properties of the coherent states of photonic dimers in the BEC and BCS limits are investigated. The correlation functions are shown to exhibit a BEC-BCS crossover behavior when the two-photon pairing correlations (i.e., the size of photonic dimers) are comparable to the average spacing between the dimer pairs.

DOI: [10.1103/PhysRevA.108.053705](https://doi.org/10.1103/PhysRevA.108.053705)

I. INTRODUCTION

Photon-photon correlations have long been recognized to play a fundamental role in the concept of optical coherence [1]. Techniques for both generation and manipulation of various types of interphoton correlations at few-photon levels have advanced rapidly in the past decades and photonic quantum technologies, in particular, are expected to provide extraordinary applications in quantum information science [2,3]. At a separate forefront, the developments of masers and lasers have led to the generation of coherent electromagnetic radiation in a wide range of frequencies, wherein an ensemble of single photons are made to work coherently. To date, the laser remains the dominant coherent many-photon quantum light source. Nonetheless, it is of its intrinsic interest to discuss the possibilities of new many-photon quantum photonic states because laser light represents only one of the simplest forms of possible many-photon quantum photonic states. Such new states, if they exist, in addition to enabling unprecedented applications in quantum information science, will also shed light on our understanding of the collective behavior of the quantum nature of many-photon systems [4].

In recent years, the bound states of light quanta were theoretically proposed in engineered nonlinear optical media [5–10], and have since been experimentally confirmed in ultracold atom systems [11,12]. The simplest realization of the photonic bound states is a two-photon dimer. Inspired by the remarkable optical properties of lasers and the penetrating insights into the role played by photons in the description of light beams offered by the coherent states [13], the present paper is devoted to investigating the scenarios of a different type of coherent many-photon quantum light source which, instead of single photons, outputs a coherent state of photonic dimers, and to the optical coherence properties of the photonic

dimers. We do so by first describing the generation of the coherent states of dimers from an idealized quantum optical system, which consists of a pumped spontaneous parametric down-conversion (SPDC) crystal in a resonant cavity, and the consequences of certain assumptions about their properties. We then provide a comprehensive discussion of the quantum statistical properties of such coherent states. Finally, we discuss, from a theoretical point of view, the generalizations of the coherent states of dimers when the overlaps between the dimers are varied via the controlled parameters of the system. In particular, we discuss the two limits which are of great scientific interests, namely, Bose-Einstein condensation (BEC) and the Bardeen-Cooper-Schrieffer (BCS) limit, respectively. In our approach, the field of light quanta is treated fully quantum mechanically while the pumping field is treated classically. We construct the evolution operator of the system and calculate the state of the system at the large-time limit for the case when initially the system contains no photons. We show that the final output state is a coherent state of dimers when certain conditions are met. As a partial assurance, we also apply the same approach to a collection of classical oscillating dipoles in a cavity and show that our approach yields the desired final output state as a coherent state of single photons.

This paper is constructed as follows: Section II introduces the properties of a photonic dimer and defines a set of operators to describe the photonic dimer as an entity. In this section, it is also shown that photonic dimers exhibit bosonic nature under the so-called condensation limit. Section III introduces the basic Hamiltonians and discusses the generation of single-photon coherent states from oscillating dipoles. We detail our approach in diagonalization of the Hamiltonian and describe the steps in constructing the evolution operator and calculating its large-time limit. We then apply the approach to the case of single-photon lasers. Section IV describes the generation of the coherent states of photonic dimers. Section V provides a detailed calculations of the correlation functions. In Sec. VI

*jushen@wustl.edu

we discuss the quadrature properties of the coherent states of photonic dimers. In Sec. VII we estimate the experimental conditions for creating the coherent states of dimers. Section VIII discusses the statistical properties of the coherent states of dimers in the BEC and BCS limits. Finally, Section IX summarizes the work of the coherent states of photonic dimers. Several aspects of the approach presented in this work are considered; in particular, the time-ordering effect, the undepletion assumption, and the comparison with the input-output formalism and the quantum Langevin approach are discussed.

II. BASIC PROPERTIES OF PHOTONIC DIMERS

Photons, despite being electrically neutral, have been shown to form bound states wherein the relative wave function between any two photons decays exponentially when the interphoton distance increases [8–10]. The simplest realization of the photonic bound states is a photonic dimer consisting of two entangled photons and is mathematically described by the following two-photon wave function [8,9]:

$$|B_\mu\rangle = \sqrt{\frac{\Gamma}{4\pi v_g^2}} \iint dx_1 dx_2 e^{i\frac{\mu}{2v_g}(x_1+x_2) - \frac{\Gamma}{v_g}|x_1-x_2|} \hat{c}^\dagger(x_1)\hat{c}^\dagger(x_2)|\emptyset\rangle. \quad (1)$$

The relative wave function is described by the exponentially decaying term $\exp(-\frac{\Gamma}{v_g}|x_1-x_2|)$ in Eq. (1), with a spatial width of v_g/Γ , which gives rise to photonic bunching behavior. It follows from the form of the relative wave function that the two photons are energy anticorrelated. When the photonic dimer is formed via interacting with an intermediary two-level atom, Γ is the reciprocal of the spontaneous emission lifetime of the atom. The center of mass degree of freedom is described by the term $\exp[i\frac{\mu}{2v_g}(x_1+x_2)]$, where $\mu\hbar$ denotes the total energy of the two-photon state. v_g is the group velocity of the photons. $\hat{c}^\dagger(x)$ is the creation operator of a single photon at location x and $\hat{c}(x)$ is the adjoint single-photon annihilation operator, following the bosonic commutation relation $[\hat{c}(x), \hat{c}^\dagger(x')] = \delta(x-x')$. $|\emptyset\rangle$ is the zero-photon vacuum state.

Figure 1(a) plots the modulus of the dimer state, $|\langle x_1, x_2 | B_\mu \rangle|$, which distributes uniformly along the diagonal axis $x_1 = x_2$ and decays exponentially away from the diagonal axis. A time scale metric, namely, the correlation time of a photonic dimer, is defined as $1/2\Gamma$ to characterize such time difference of detecting two photons of a photonic dimer, which provides the information of the width for $|\langle x_1, x_2 | B_\mu \rangle|^2$. Thus a larger Γ yields a shorter correlation time and correspondingly a shorter temporal spread of the dimer relative wave function.

The formation of individual photonic dimers has recently been demonstrated in ultracold atoms [11] and has the potential to open up new possibilities for nonlinear quantum optical physics. For example, the unusual temporal and frequency entanglement properties between the constituent photons in photonic dimers endow multiphoton excitation processes with the enhanced efficiency necessary for many scientific and industrial applications, including three-dimensional optical memory [14], sensitivity enhancement in the molecular Stark

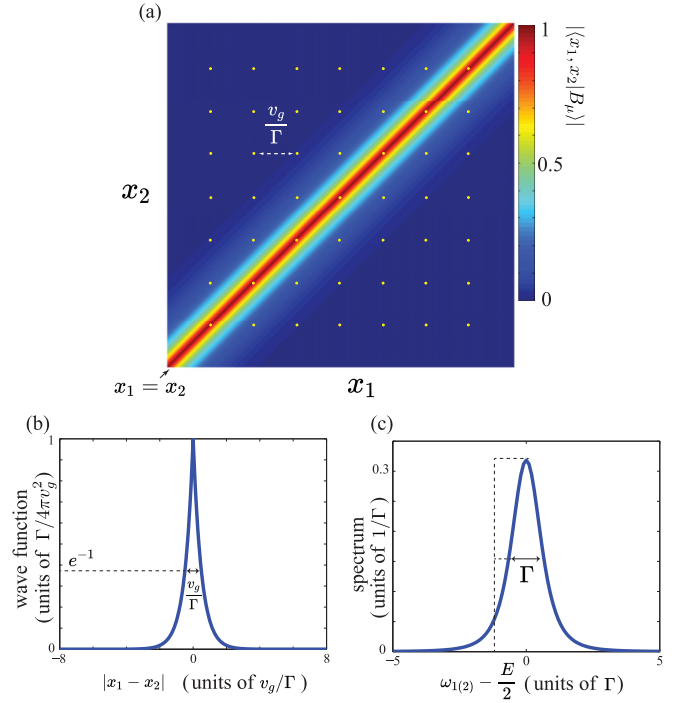


FIG. 1. (a) The modulus of the dimer state, $|\langle x_1, x_2 | B_\mu \rangle|$. The distance between grid points equals v_g/Γ . The maximum of the plot is normalized to a value of 1. (b) The relative wave function of the dimer. The full width at $1/e$ equals v_g/Γ . (c) Single-photon frequency spectrum in a dimer. The full width at half maximum equals Γ .

effect [15], coherent quantum control of multiphoton transitions [16], and quantum biophotonics. By exploiting the energy anticorrelation and the temporal proximity between the constituent photons in the photonic dimers, it has been shown that the two-photon excitation efficiency of a fluorophore by photonic dimers can be improved by orders of magnitude [17]. It is of great interest to go beyond the individual-dimers regime to investigate the scenario when the optical excitation is a coherent states of photonic dimers.

Before we embark on the development of the theory of an ensemble of photonic dimers, in the following section we digress momentarily to discuss the theory of an ensemble of single photons so as to introduce the machinery and the notations that are used later.

III. GENERATION OF SINGLE-PHOTON COHERENT STATES

In the semiclassical treatment of the light-matter interactions, light is described as a classical Maxwell field while the medium is described as a collection of atoms whose dynamic evolution is governed by the Schrödinger equation. The semiclassical theory is sufficient to describe a rich variety of phenomena. However, questions regarding the quantum nature of the optical field, e.g., the photon statistics and linewidth of the output optical field, require a fully quantized theory of the radiation. For example, the density-matrix formalism and the Heisenberg-Langevin approach are developed as the full quantum theories of a laser [18]. Nonetheless, the

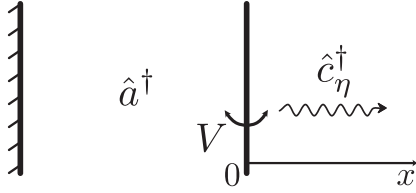


FIG. 2. Schematic of single-mode cavity system. The cavity mode \hat{a}^\dagger is coupled to the free-space modes \hat{c}_η^\dagger with the coupling strength V .

complexities of these full quantum theories make it challenging to investigate the various single- and two-photon processes in the atomic medium. In the following, we develop a phenomenological theory to describe the generation of the photon field in a real-space formalism. One feature of the effective theory is that the medium is treated classically as a collection of oscillating dipoles while the optical field is fully quantized. We start with the full quantum theory for the single-photon processes and derive the effective Hamiltonian to justify the approach. Similar approaches have been employed in describing the parametric amplification and squeezing via nonlinear optical processes [18,19].

A. Single-mode cavity without the gain medium

Our starting point is the Gardiner-Collett Hamiltonian [20,21], which describes the case when there is no nonlinear medium but only discrete cavity modes coupled to the continuum of modes of the output (hereafter we restrict ourselves to the single-cavity-mode case with a mode frequency ω_0):

$$\hat{H}_0 = \hbar\omega_0\hat{a}^\dagger\hat{a} + \hbar \int d\eta \eta \hat{c}_\eta^\dagger \hat{c}_\eta + \hbar \int d\eta (V\hat{a}^\dagger \hat{c}_\eta + V^*\hat{a} \hat{c}_\eta^\dagger), \quad (2)$$

as shown in Fig. 2. In this Hamiltonian, \hat{a} (\hat{a}^\dagger) is the annihilation (creation) operator of the cavity-mode photons with the frequency ω_0 . The output channel here is treated simply as free space, with the mode annihilation (creation) operator of frequency η defined as \hat{c}_η (\hat{c}_η^\dagger). The coupling strength between the cavity mode and the free-space modes is denoted V .

The coupling creates a linear superposition between the cavity photons and the free-space photons. Taking into account of the superposition, H_0 can be diagonalized in terms of the dressed operators which incorporate the superposition states of photons [22]. To proceed, the diagonalized H_0 is assumed to follow the form:

$$\hat{H}_0 = \int d\omega \hbar\omega \hat{A}^\dagger(\omega) \hat{A}(\omega), \quad (3a)$$

$$\hat{A}(\omega) = \alpha(\omega)\hat{a} + \int d\eta \beta(\omega, \eta)\hat{c}_\eta, \quad (3b)$$

where the dressed operator \hat{A} describes the linear superposition, and $\alpha(\omega)$ and $\beta(\omega, \eta)$ are the coefficients of the cavity and the free-space modes, respectively. After imposing the

following commutation relations:

$$[\hat{A}(\omega), \hat{H}_0] = \hbar\omega\hat{A}(\omega), \quad (4a)$$

$$[\hat{A}(\omega), \hat{A}^\dagger(\omega')] = \delta(\omega - \omega'), \quad (4b)$$

the coefficients $\alpha(\omega)$ and $\beta(\omega, \eta)$ can be determined as

$$\alpha(\omega) = \frac{V^*}{\omega - \omega_0 + i\pi|V|^2}, \quad (5a)$$

$$\beta(\omega, \eta) = \left[|V|^2 \mathcal{P} \frac{1}{\omega - \eta} + (\omega - \omega_0)\delta(\omega - \eta) \right] \times \frac{1}{\omega - \omega_0 + i\pi|V|^2}, \quad (5b)$$

where \mathcal{P} denotes the Cauchy principal integral. Moreover, using the fact that the mode operators \hat{a} and \hat{c}_η commute, the cavity mode operator can be expressed in terms of the diagonalized operator:

$$\hat{a} = \int d\omega \alpha^*(\omega) \hat{A}(\omega). \quad (6)$$

As shown below, Eq. (6) plays an important role in deriving the quantum optical states of the interacting system.

The effective cavity mode strength is proportional to

$$|\alpha(\omega)|^2 = \frac{|V|^2}{(\omega - \omega_0)^2 + \pi^2|V|^4}.$$

Compared with the classical result where in the mode strength

$$\propto \frac{1}{(1-r)^2 + 4r \sin^2(kL)}$$

(r is the reflection coefficient of the semitransparent mirror), the coupling strength V can be expressed as $\Delta B = 2\pi|V|^2 = 2[(1-r)^2 c^2]/4rL^2$, so that $V = \frac{(1-r)c}{2\sqrt{\pi r}L} e^{i\phi}$, in the good cavity limit (i.e., high Q factor). This also yields directly that the transmission coefficient $|T|^2 = (2L/c)2\pi|V|^2$, which is also given in Ref. [23].

It is often advantageous to describe the output photons in a real-space representation:

$$\hat{c}_\eta^\dagger = \frac{1}{\sqrt{2\pi v_g}} \int_{-\infty}^{\infty} dx e^{ik_\eta x} \hat{c}^\dagger(x), \quad (7)$$

where $\eta = v_g k_\eta$. The real-space Hamiltonian for single-mode cavity case is

$$\begin{aligned} \hat{H}_0 = & \hbar\omega_0\hat{a}^\dagger\hat{a} + \hbar \int_{-\infty}^{\infty} dx (-iv_g) \hat{c}^\dagger(x) \frac{\partial}{\partial x} \hat{c}(x) \\ & + \hbar \int_{-\infty}^{\infty} dx V \delta(x) [\hat{c}^\dagger(x)\hat{a} + \hat{a}^\dagger\hat{c}(x)], \end{aligned} \quad (8)$$

where $\hat{c}^\dagger(x)$ is the creation operator for a right-going photon at position x . Here $\delta(x)$ indicates the photon generation position

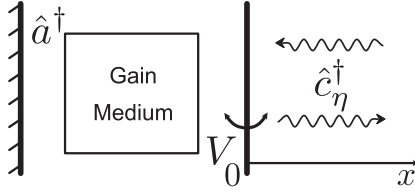


FIG. 3. Schematic of single-mode cavity with the gain medium system. The cavity mode \hat{a}^\dagger is coupled to the gain medium which is treated as a collection of dipoles oscillating at frequency Ω . The dipoles are resonant with the cavity ($\Omega = \omega_0$). The cavity-gain medium interaction is described by Eq. (11).

(position the semitransparent mirror of the cavity) is $x_0 = 0$. The configuration is effectively a chiral system where only one-way propagating photons are allowed [24].

H_0 can also be diagonalized by $\hat{A}(\omega)$, which now takes the following form:

$$\hat{A}(\omega) = \alpha(\omega)\hat{a} + \int dx \bar{\beta}(\omega, x)\hat{c}(x), \quad (9)$$

Writing \hat{H}_{mc} in the interaction picture and using Eq. (6):

$$\begin{aligned} \hat{H}_I(t) &= e^{\frac{i}{\hbar}\hat{H}_0 t} \hat{H}_{mc} e^{-\frac{i}{\hbar}\hat{H}_0 t} \\ &= \hbar\chi \int_{-\infty}^{\infty} d\omega e^{i\Omega t - i\omega t} \alpha^*(\omega) \hat{A}(\omega) + \text{H.c.} \\ &= \hbar\chi \int_{-\infty}^{\infty} d\omega e^{i\Omega t - i\omega t} \left(|\alpha(\omega)|^2 \hat{a} + \int_{-\infty}^{\infty} d\eta \alpha^*(\omega) \beta(\omega, \eta) \hat{c}_\eta \right) + \text{H.c.} \\ &= \hbar\chi \int_{-\infty}^{\infty} d\omega e^{i\Omega t - i\omega t} \left(\frac{|V|^2}{(\omega - \omega_0)^2 + \pi^2|V|^4} \hat{a} + \frac{(\omega - \omega_0)V}{(\omega - \omega_0)^2 + \pi^2|V|^4} \hat{c}_\omega + \int_{-\infty}^{\infty} d\eta \frac{|V|^2}{(\omega - \omega_0)^2 + \pi^2|V|^4} P \frac{V}{\omega - \eta} \hat{c}_\eta \right) + \text{H.c.}, \end{aligned} \quad (12)$$

which governs the system dynamics of a laser cavity containing pumped gain medium. At the large- t limit ($t \rightarrow \infty$), the system reaches a steady state; thus we shall be interested in the same limit of the evolution operator $\hat{U}(t) = e^{-\frac{i}{\hbar} \int_0^t dt' \hat{H}_I(t')}$, especially the exponential term:

$$\begin{aligned} \lim_{t \rightarrow \infty} -\frac{i}{\hbar} \int_0^t dt' \hat{H}_I(t') &= \lim_{t \rightarrow \infty} -i\chi \int_{-\infty}^{\infty} d\omega \frac{e^{-i(\omega - \Omega)t} - 1}{-i(\omega - \Omega)} \left(\frac{|V|^2}{(\omega - \omega_0)^2 + \pi^2|V|^4} \hat{a} + \frac{(\omega - \omega_0)V}{(\omega - \omega_0)^2 + \pi^2|V|^4} \hat{c}_\omega \right. \\ &\quad \left. + \int_{-\infty}^{\infty} d\eta \frac{|V|^2}{(\omega - \omega_0)^2 + \pi^2|V|^4} P \frac{V}{\omega - \eta} \hat{c}_\eta \right) - \text{H.c.} \\ &= -i \frac{\chi}{\pi|V|^2} \hat{a} - \frac{\chi}{V^*} \hat{c}_{\omega_0} + \frac{i\chi}{\pi V^*} \int_{-\infty}^{\infty} d\eta P \frac{1}{\omega_0 - \eta} \hat{c}_\eta - \text{H.c.} \end{aligned} \quad (13)$$

The first three terms in Eq. (13) correspond to the cavity mode, the output free-space mode at the cavity resonance, and the cross-talk to other weaker free-space nonresonant modes due to interactions. Together with the complex-conjugate terms, the evolution operator at the large- t limit thus has the form of the product of the Glauber displacement operators of the cavity mode and the free-space modes, which can be symbolically represented as

$$\lim_{t \rightarrow \infty} \hat{U}(t) = \hat{D}(\hat{a}) \Pi_\eta \hat{D}(\hat{c}_\eta), \quad (14)$$

where

$$\begin{aligned} \alpha(\omega) &= \frac{V^*}{\omega - \omega_0 + i\pi|V|^2}, \\ \bar{\beta}(\omega, x) &= \frac{1}{\sqrt{2\pi}} e^{-i\omega x/v_g} \left[\Theta(x) + \frac{\omega - \omega_0 - i\pi V^2}{\omega - \omega_0 + i\pi V^2} \Theta(-x) \right]. \end{aligned} \quad (10)$$

B. Single-mode cavity with the gain medium

When the gain medium is embedded and is pumped far above threshold, the atoms behave as dipoles oscillating at the pumping field frequency Ω , as depicted in Fig. 3. Such an approach has been employed in the literature; we also provide a heuristic derivation in Appendix A. In this regime, the interaction Hamiltonian describing the gain medium-cavity photon field is given by the following effective form:

$$\hat{H}_{mc} = \hbar[\chi e^{i\Omega t} \hat{a} + \chi^* e^{-i\Omega t} \hat{a}^\dagger], \quad (11)$$

where χ is the Rabi frequency and the dipoles are resonant with the cavity ($\Omega = \omega_0$).

where η includes both resonant and nonresonant frequencies. It follows immediately that when the initial state is a vacuum state, the steady state which the system evolves into is a product of the coherent states over the cavity mode and the free-space modes. By using a suitable filter, the output field contains only the resonant mode

$$e^{\frac{\chi}{V} \hat{c}_{\omega_0}^\dagger - \frac{\chi}{V^*} \hat{c}_{\omega_0}} |\emptyset\rangle, \quad (15)$$

which is a coherent state with an average photon number of $|\chi/V|^2$.

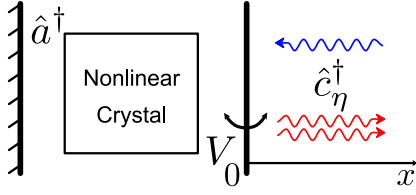


FIG. 4. Schematic of single-mode cavity with the SPDC nonlinear crystal system. The cavity mode \hat{a}^\dagger is coupled to the gain medium which is treated as a collection of dipoles oscillating at frequency ω_p . The cavity-SPDC interaction is described by Eq. (16).

As has been shown above, the approach of treating the gain medium as oscillating dipoles and the optical field quantum-mechanical reproduces the well-known results for an ideal laser operating above the threshold. We also note that a semi-classical approach of the same spirit has been employed to show that the radiation emitted by a classical current distribution is a coherent state of single photons [25].

In the following, we apply the same strategy to the generation of the coherent states of photonic dimers.

IV. GENERATION OF COHERENT STATES OF PHOTONIC DIMERS

The prerequisite of the generation of coherent states of photonic dimers is a gain medium that produces dimers. To date, although efficient generation of individual dimers has been suggested [17], a medium that generates an ensemble of dimers has yet to be engineered. Nonetheless, many electronic transitions lead to the generation of correlated photon pairs. In this section, we show that, under certain conditions, an optical cavity can shape the optical spectrum of the correlated photon pairs and creates coherent states of photonic dimers.

Specifically, here we describe a mechanism to generate coherent states of photonic dimers using a degenerate type-0 spontaneous parametric down-conversion (SPDC) nonlinear crystal in a single-mode resonant cavity, as depicted in Fig. 4. In the configuration, both the pumping light and the SPDC

photons are blocked by the left wall of the cavity and can only pass through via the right wall. The configuration and operating scheme is equivalent to the optical parametric oscillator (OPO) scheme where the parametric down conversion process takes place inside a cavity and the optical gain is from parametric amplification rather than from stimulated emission of radiation. The oscillation wavelength is determined by the phase-matching details, which offers the potential for wavelength tuning with extremely wide tuning ranges.

The degenerate collinear SPDC Hamiltonian in a single-mode cavity is given by [26,27]

$$\begin{aligned} \hat{H}_{\text{SPDC}} &= \sum_{k,k'} \Gamma_{k,k'} L h(L\Delta_{k,k'}) e^{-i\omega_p t} \hat{a}_k^\dagger \hat{a}_{k'}^\dagger + \text{H.c.} \\ &= \Gamma_{0,0} L e^{-i\omega_p t} \hat{a}^\dagger \hat{a}^\dagger + \text{H.c.}, \end{aligned} \quad (16)$$

where the summation of k represents the photons with different momentum generated in the nonlinear medium. Here the parameter $\Gamma_{k,k'} = E_k E_{k'} 2\pi \epsilon_0 \chi^{(2)} E_0 A$, where

$$E_k = i \sqrt{\frac{\hbar \omega_k}{2\epsilon_0 n^2 V_c}}$$

is the electric field of generated photon state, V_c is the volume of the cavity, n is the effective refractive index of the nonlinear crystal for SPDC photon pairs, $h(x) = (1 - e^{-ix})/ix$, and $\Delta_{k,k'} = k_p - k - k'$ is the momentum difference between pump photon and the sum of two degenerate SPDC photons. In the single-mode cavity scheme, $h(L\Delta_{k,p-k}) \approx 1$. $\Gamma_{0,0}$ is the parameter when both signal and idler photons have the same frequency ω_0 . The pumping light is treated as a classical optical field with an electric-field amplitude E_0 and a frequency $\omega_p = 2\omega_0$.

Below, we solve for the output states using both the interaction picture and the Schrödinger picture.

A. The interaction picture of the photonic states

In the interaction picture, the SPDC Hamiltonian becomes (the SPDC subscript is omitted)

$$\begin{aligned} \hat{H}_I(t) &= \Gamma_{0,0} L e^{-i\omega_p t} e^{i\frac{\hbar_0}{\hbar} t} \hat{a}^\dagger \hat{a}^\dagger e^{-i\frac{\hbar_0}{\hbar} t} + \text{H.c.} \\ &= \Gamma_{0,0} L \int d\omega_1 d\omega_2 e^{-i\omega_p t + i\omega_1 t + i\omega_2 t} \alpha(\omega_1) \alpha(\omega_2) \hat{A}^\dagger(\omega_1) \hat{A}^\dagger(\omega_2) + \text{H.c.} \\ &= \Gamma_{0,0} L \int d\omega_1 d\omega_2 e^{-i\omega_p t + i\omega_1 t + i\omega_2 t} \alpha(\omega_1) \alpha(\omega_2) \left[\alpha^*(\omega_1) \hat{a}^\dagger + \int d\eta_1 \beta^*(\omega_1, \eta_1) \hat{c}_{\eta_1}^\dagger \right] \\ &\quad \times \left[\alpha^*(\omega_2) \hat{a}^\dagger + \int d\eta_2 \beta^*(\omega_2, \eta_2) \hat{c}_{\eta_2}^\dagger \right] + \text{H.c.}, \end{aligned} \quad (17)$$

where $\alpha(\omega) = V^*/(\omega - \omega_0 + i\pi|V|^2)$, $\beta(\omega, \eta) = [|V|^2 P \frac{1}{\omega - \eta} + (\omega - \omega_0) \delta(\omega - \eta)] (\omega - \omega_0 + i\pi|V|^2)^{-1}$. The optical state of the system in the interaction picture is

$$|\psi\rangle = \hat{T} e^{-\frac{i}{\hbar} \int_0^t \hat{H}_I(t') dt'} |\emptyset\rangle_I, \quad (18)$$

where $|\emptyset\rangle_I$ is the vacuum state with zero cavity-mode photon and zero free photon in the interaction picture. The time-ordering operator \hat{T} takes any product of operators and changes the order so that operators with a later time variable are placed to the left. As the Hamiltonians at different times in general do not commute, the time-ordering operator cannot be neglected. Nonetheless, retaining the time-ordering operator greatly increases the computational complexities. In the following, we omit the time-ordering operator and discuss the limitations and validity of the results thus obtained in Sec. IX.

Following Eq. (17), there are three terms in the exponent $-\frac{i}{\hbar} \int_0^\infty \hat{H}_I(t') dt'$.

(1) The first term contains only the cavity-mode operators,

$$-\frac{i}{\hbar} \int_0^\infty dt' \left[\Gamma_{0,0} L \int d\omega_1 d\omega_2 e^{-i\omega_p t' + i\omega_1 t' + i\omega_2 t'} |\alpha(\omega_1)|^2 |\alpha(\omega_2)|^2 \hat{a}^\dagger \hat{a}^\dagger + \text{H.c.} \right] = -i \frac{\Gamma_{0,0} L}{2\pi \hbar V^2} \hat{a}^\dagger \hat{a}^\dagger - i \frac{\Gamma_{0,0} L}{2\pi \hbar V^2} \hat{a} \hat{a} = \xi \hat{a}^\dagger \hat{a}^\dagger - \xi^* \hat{a} \hat{a}, \quad (19)$$

where $\xi = -i(\Gamma_{0,0} L)/2\pi \hbar V^2$. This term represents a two-photon coherent state.

(2) The second term contains both the cavity-mode operator and free-space operator,

$$-\frac{i}{\hbar} \int_0^\infty dt' \Gamma_{0,0} L \int d\omega_1 d\omega_2 e^{-i\omega_p t' + i\omega_1 t' + i\omega_2 t'} \left[|\alpha(\omega_1)|^2 \alpha(\omega_2) \int d\eta_2 \beta^*(\omega_2, \eta_2) \hat{a}^\dagger \hat{c}_{\eta_2}^\dagger + |\alpha(\omega_2)|^2 \alpha(\omega_1) \int d\eta_1 \beta^*(\omega_1, \eta_1) \hat{a}^\dagger \hat{c}_{\eta_1}^\dagger \right] - \text{H.c.} \\ = i \frac{\Gamma_{0,0} L}{\pi \hbar V} \int d\eta \frac{1}{\eta - \omega_0 + i\pi V^2} \hat{a}^\dagger \hat{c}_\eta^\dagger - \text{H.c.} = \int d\eta f_\eta \hat{a}^\dagger \hat{c}_\eta^\dagger - \text{H.c.}, \quad (20)$$

where

$$f_\eta = i \frac{\Gamma_{0,0} L}{\pi \hbar V} \frac{1}{\eta - \omega_0 + i\pi V^2}.$$

(3) The third term contains only the free-space operator,

$$-\frac{i}{\hbar} \int_0^\infty dt' \Gamma_{0,0} L \int d\omega_1 d\omega_2 e^{-i\omega_p t' + i\omega_1 t' + i\omega_2 t'} \alpha(\omega_1) \alpha(\omega_2) \int d\eta_1 d\eta_2 \beta^*(\omega_1, \eta_1) \beta^*(\omega_2, \eta_2) \hat{c}_{\eta_1}^\dagger \hat{c}_{\eta_2}^\dagger - \text{H.c.} \\ = -i \frac{\Gamma_{0,0} L}{\hbar} \int d\eta_1 d\eta_2 \frac{V^2}{(\eta_1 - \omega_0 - i\pi V^2)(\eta_2 - \omega_0 - i\pi V^2)} \\ \times \left[\pi \delta(\eta_1 + \eta_2 - \omega_p) + iP \frac{1}{\eta_1 + \eta_2 - \omega_p} - \frac{i}{\eta_1 - \omega_0 + i\pi V^2} - \frac{i}{\eta_2 - \omega_0 + i\pi V^2} + \frac{1}{2\pi V^2} \right] \hat{c}_{\eta_1}^\dagger \hat{c}_{\eta_2}^\dagger - \text{H.c.} \\ = \int d\eta_1 d\eta_2 \phi_{\eta_1, \eta_2} \hat{c}_{\eta_1}^\dagger \hat{c}_{\eta_2}^\dagger - \text{H.c.}, \quad (21)$$

where

$$\phi_{\eta_1, \eta_2} = -i \frac{\Gamma_{0,0} L}{\hbar} \frac{V^2}{(\eta_1 - \omega_0 - i\pi V^2)(\eta_2 - \omega_0 - i\pi V^2)} \left[\pi \delta(\eta_1 + \eta_2 - \omega_p) + iP \frac{1}{\eta_1 + \eta_2 - \omega_p} - \frac{i}{\eta_1 - \omega_0 + i\pi V^2} - \frac{i}{\eta_2 - \omega_0 + i\pi V^2} + \frac{1}{2\pi V^2} \right].$$

Combining the three terms together, the state of the system can be written as

$$|\psi\rangle_I = e^{\xi \hat{a}^\dagger \hat{a}^\dagger + f d\eta f_\eta \hat{a}^\dagger \hat{c}_\eta^\dagger + f d\eta_1 d\eta_2 \phi_{\eta_1, \eta_2} \hat{c}_{\eta_1}^\dagger \hat{c}_{\eta_2}^\dagger - \text{H.c.}} |\emptyset\rangle_I \\ = e^{\hat{F}^\dagger - \hat{F}} |\emptyset\rangle_I, \quad (22)$$

where $\hat{F}^\dagger = \xi \hat{a}^\dagger \hat{a}^\dagger + \int d\eta f_\eta \hat{a}^\dagger \hat{c}_\eta^\dagger + \int d\eta_1 d\eta_2 \phi_{\eta_1, \eta_2} \hat{c}_{\eta_1}^\dagger \hat{c}_{\eta_2}^\dagger$. Here $[\hat{a}, \hat{a}^\dagger] = 1$ and $[\hat{c}_\eta, \hat{c}_{\eta'}^\dagger] = \delta(\eta - \eta')$. Due to the second term, the system cannot be separated as a product of the cavity mode and free-space mode. In other words, the cavity-mode photons and free-space-mode photons are entangled and cannot be written as a product state.

Nonetheless, the frequency representation of the state, as shown above, masks some important information regarding the entangled term between the cavity-mode photons and free-space-mode photons. By Fourier transforming the state into the real-space representation, it is shown that the amplitude of this entangled term f_η decays exponentially, which indicates

that the photonic state described by this term is spatially localized in space.

The Fourier transformation $\hat{c}_\eta^\dagger = \frac{1}{\sqrt{2\pi v_g}} \int dx e^{ik_\eta x} \hat{c}^\dagger(x)$ gives rise to the following commutation relations:

$$[\hat{c}(x), \hat{c}^\dagger(x')] = \delta(x - x'), \\ [\hat{c}_\eta, \hat{c}_{\eta'}^\dagger] = \frac{1}{2\pi v_g} \int dx dx' e^{-ik_\eta x + ik_{\eta'} x'} [\hat{c}(x), \hat{c}^\dagger(x')] \\ = \frac{1}{2\pi v_g} \int dx e^{-i(k_\eta - k_{\eta'})x} \\ = \delta(\eta - \eta').$$

Thus, in the real-space representation, the state is given by

$$|\psi\rangle_I = e^{\xi \hat{a}^\dagger \hat{a}^\dagger + f d\eta f_\eta \hat{a}^\dagger \hat{c}_\eta^\dagger + f d\eta_1 d\eta_2 \phi_{\eta_1, \eta_2} \hat{c}_{\eta_1}^\dagger \hat{c}_{\eta_2}^\dagger - \text{H.c.}} |\emptyset\rangle_I \\ = e^{\xi \hat{a}^\dagger \hat{a}^\dagger + f dx \tilde{f}(x) \hat{a}^\dagger \hat{c}^\dagger(x) + f dx_1 dx_2 \tilde{\phi}(x_1, x_2) \hat{c}^\dagger(x_1) \hat{c}^\dagger(x_2) - \text{H.c.}} |\emptyset\rangle_I \quad (23)$$

where

$$\begin{aligned}\bar{f}(x) &= \frac{1}{\sqrt{2\pi v_g}} \int d\eta f_\eta e^{i\eta x} \\ &= \frac{1}{\sqrt{2\pi v_g}} 2\kappa V e^{i\frac{\omega_0}{v_g}x + \frac{\pi V^2}{v_g}x} \Theta(-x),\end{aligned}\quad (24)$$

$$\begin{aligned}\bar{\phi}(x_1, x_2) &= \frac{1}{2\pi v_g} \int d\eta_1 d\eta_2 \phi_{\eta_1, \eta_2} e^{i\eta_1 x_1 + i\eta_2 x_2} \\ &= \frac{i\kappa V^2}{v_g} e^{i\frac{\omega_0}{v_g}(x_1+x_2) - \frac{\pi V^2}{v_g}|x_1-x_2|} \Theta(-x_1)\Theta(-x_2).\end{aligned}\quad (25)$$

Detailed calculations will be discussed in Appendix C. Here $\kappa = \Gamma_{0,0}L/\hbar V^2$ is a real number characterizing the configuration and will be discussed in detail later when we estimate the values in experiment. Thus, the photonic state described by the $\hat{a}^\dagger \hat{c}^\dagger(x)$ term is an evanescent wave that is localized to the wall of the cavity. This term can be regarded as a localized

where

$$\begin{aligned}\hat{H}_0 &= \hbar \int d\omega \omega \hat{A}^\dagger(\omega) \hat{A}(\omega), \\ \hat{H}_I(t) &= \Gamma_{0,0}L \int d\omega_1 d\omega_2 e^{-i\omega_1 t + i\omega_1 t + i\omega_2 t} \alpha(\omega_1) \alpha(\omega_2) \hat{A}^\dagger(\omega_1) \hat{A}^\dagger(\omega_2) + \text{H.c.}\end{aligned}\quad (27)$$

The exponent of the time-evolution operator in the Schrödinger picture now becomes

$$\ln[\hat{U}_S(t)] = e^{-i\frac{\hat{H}_0}{\hbar}t} \left(-\frac{i}{\hbar} \int_0^t dt' \hat{H}_I(t') \right) e^{i\frac{\hat{H}_0}{\hbar}t} = \xi^S \hat{a}^\dagger \hat{a}^\dagger + \int d\eta f_\eta^S \hat{a}^\dagger \hat{c}_\eta^\dagger + \int d\eta_1 d\eta_2 \phi_{\eta_1, \eta_2}^S \hat{c}_{\eta_1}^\dagger \hat{c}_{\eta_2}^\dagger - \text{H.c.},\quad (28)$$

where

$$\begin{aligned}\xi^S &= \frac{i\kappa e^{-i2\omega_0 t}}{2\pi}, \quad f_\eta^S = \frac{-i\kappa e^{-i2\omega_0 t}}{\pi} \frac{V}{\eta - \omega_0 - i\pi V^2}, \\ \phi_{\eta_1, \eta_2}^S &= i\kappa V^2 e^{-2i\omega_0 t} \frac{V^2}{(\eta_1 - \omega_0 + i\pi V^2)(\eta_2 - \omega_0 + i\pi V^2)} \left[\pi \delta(2\omega_0 - \eta_1 - \eta_2) + iP \frac{1}{2\omega_0 - \eta_1 - \eta_2} + \frac{i}{\eta_1 - \omega_0 - i\pi V^2} \right. \\ &\quad \left. + \frac{i}{\eta_2 - \omega_0 - i\pi V^2} + \frac{1}{2\pi V^2} \right].\end{aligned}$$

Thus the state of the system in the Schrödinger picture in the frequency representation takes the following form:

$$|\psi(t)\rangle_S = \exp \left[\xi^S \hat{a}^\dagger \hat{a}^\dagger + \int d\eta f_\eta^S \hat{a}^\dagger \hat{c}_\eta^\dagger + \int d\eta_1 d\eta_2 \phi_{\eta_1, \eta_2}^S \hat{c}_{\eta_1}^\dagger \hat{c}_{\eta_2}^\dagger - \text{H.c.} \right] |\emptyset\rangle.\quad (29)$$

The details are provided in Appendix B.

2. Real-space representation

To better understand the state, we perform the Fourier transform [$\hat{c}_\eta^\dagger = \frac{1}{\sqrt{2\pi v_g}} \int_{-\infty}^{\infty} dx e^{i\eta x/v_g} \hat{c}^\dagger(x)$] to get the wave function in the real-space representation.

bound state of the cavity-mode photon and the free-space photon. The $\hat{c}^\dagger(x_1)\hat{c}^\dagger(x_2)$ term describes a two-photon bound state, or photonic dimers that travels afar, and the output state in the interaction picture is a coherent state of photonic dimers.

B. The Schrödinger picture of the photonic state

1. Frequency representation

To obtain a direct expression of the photonic state in the laboratory frame, here we calculate the state in the Schrödinger picture. It turns out that it is rather involving to transform the state in the interaction picture, Eq. (22), to the Schrödinger picture of the state. Here we employ the dressed operator \hat{A} [Eq. (3b)] that the diagonalized Hamiltonian \hat{H}_0 [Eq. (3b)] to get the final state in the Schrödinger picture. The relation of the state between the two pictures yields

$$|\psi(t)\rangle_S = e^{-i\frac{\hat{H}_0}{\hbar}t} e^{-\frac{i}{\hbar} \int_0^t dt' \hat{H}_I(t')} e^{i\frac{\hat{H}_0}{\hbar}t} |\emptyset\rangle_S,\quad (26)$$

For the second term $\int d\eta f_{\eta}^S \hat{a}^{\dagger} \hat{c}_{\eta}^{\dagger}$:

$$\begin{aligned} \int d\eta f_{\eta}^S \hat{a}^{\dagger} \hat{c}_{\eta}^{\dagger} - \text{H.c.} &= \frac{2i\Gamma_{0,0} L e^{-i\omega_0 t}}{\sqrt{2\pi v_g \hbar}} \hat{a}^{\dagger} \int dx \frac{-i}{V} e^{i\omega_0(x/v_g - t) - \pi V^2 x} [1 - e^{-\pi V^2(t-x/v_g) - \pi V^2 |t-x/v_g|}] \Theta(x) \hat{c}^{\dagger}(x) - \text{H.c.} \\ &\equiv a^{\dagger} \int dx \bar{f}^S(x, t) \hat{c}^{\dagger}(x) - \text{H.c.}, \end{aligned} \quad (30)$$

where

$$\begin{aligned} \bar{f}^S(x, t) &= \frac{2\Gamma_{0,0} L e^{-i\omega_0 t}}{\sqrt{2\pi v_g \hbar} V} e^{i\omega_0(x/v_g - t) - \pi V^2 x/v_g} [1 - e^{-\pi V^2(t-x/v_g) - \pi V^2 |t-x/v_g|}] \Theta(x) \\ &\approx \frac{2\kappa V e^{-i\omega_0 t}}{\sqrt{2\pi v_g}} e^{i\omega_0(x/v_g - t) - \pi V^2 x/v_g} \Theta(x) \quad (t \rightarrow \infty). \end{aligned} \quad (31)$$

The causality factor $\Theta(t - x/v_g)$ indicates that photons can only exist in the region behind the wave front. In the third line, as we are only interested in the steady case, the large- t limit ($t \rightarrow \infty$) is taken. At the large- t limit, the wave function of the output single-photon $\bar{f}^S(x, t)$ decays exponentially away from the cavity and becomes an evanescent wave with a width of $v_g/\pi V^2$. At time $t = 0$, the amplitudes are zero at all positions, due to the causality factor $\Theta(t - x/v_g)$. At later times, the amplitude at position $x = 0^+$ increases as $\bar{f}^S(0^+, t) = \frac{2\kappa V}{\sqrt{2\pi v_g}} e^{-2i\omega_0 t} (1 - e^{-2\pi V^2 t})$. For any x , $|\bar{f}^S(x, t)|^2$ becomes stationary at the large- t limit.

For the third term $\int d\eta_1 d\eta_2 \phi_{\eta_1, \eta_2}^S \hat{c}_{\eta_1}^{\dagger} \hat{c}_{\eta_2}^{\dagger}$ in Eq. (B4):

$$\begin{aligned} \int d\eta_1 d\eta_2 \phi_{\eta_1, \eta_2}^S \hat{c}_{\eta_1}^{\dagger} \hat{c}_{\eta_2}^{\dagger} - \text{H.c.} &= -\frac{i\kappa V^2}{v_g} \int dx_1 dx_2 e^{i2\omega_0(\frac{x_1+x_2}{2v_g} - t) - \pi V^2 |x_1-x_2|/v_g} \Theta(x_1) \Theta(x_2) \hat{c}^{\dagger}(x_1) \hat{c}^{\dagger}(x_2) - \text{H.c.} \\ &\equiv \int dx_1 dx_2 \bar{\phi}^S(x_1, x_2) \hat{c}^{\dagger}(x_1) \hat{c}^{\dagger}(x_2) - \text{H.c.}, \end{aligned} \quad (32)$$

where

$$\bar{\phi}^S(x_1, x_2, t) = -\frac{i\kappa V^2}{v_g} e^{i2\omega_0(\frac{x_1+x_2}{2v_g} - t) - \pi V^2 |x_1-x_2|/v_g} \Theta(x_1) \Theta(x_2). \quad (33)$$

In the above calculation, the large- t limit is also taken. $\Theta(x)$ factors are contributed by the last four terms of the wave function in the frequency domain. Figure 5 plots the probability distribution of the two-photon dimer state.

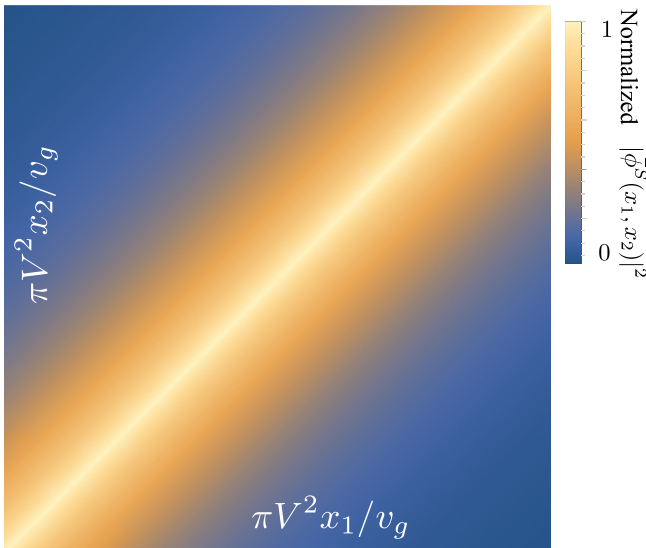


FIG. 5. Spatial distribution of two-photon state $|\bar{\phi}^S(x_1, x_2)|^2$.

In the real-space domain, the state of the system is

$$\begin{aligned} |\psi(t)\rangle_S &= \exp \left[\xi^S \hat{a}^{\dagger} \hat{a}^{\dagger} + \int dx \bar{f}^S(x, t) \hat{a}^{\dagger} \hat{c}^{\dagger}(x) \right. \\ &\quad \left. + \int dx_1 dx_2 \bar{\phi}^S(x_1, x_2, t) \hat{c}^{\dagger}(x_1) \hat{c}^{\dagger}(x_2) - \text{H.c.} \right] |\emptyset\rangle, \end{aligned} \quad (34)$$

where

$$\begin{aligned} \xi^S &= \frac{i\kappa e^{-i2\omega_0 t}}{2\pi}, \\ \bar{f}^S(x, t) &= \frac{2\kappa V e^{-i\omega_0 t}}{\sqrt{2\pi v_g}} e^{i\omega_0(x/v_g - t) - \pi V^2 x/v_g} \Theta(x), \\ \bar{\phi}^S(x_1, x_2, t) &= -\frac{i\kappa V^2}{v_g} e^{i2\omega_0(\frac{x_1+x_2}{2v_g} - t) - \pi V^2 |x_1-x_2|/v_g} \Theta(x_1) \Theta(x_2). \end{aligned}$$

Since we are only interested in the region far away from the cavity, the $\Theta(x)$ factors in the two-photon term can be neglected. After a sufficiently long time, the system tends to be steady and the emitted two-photon state amplitude is only a function of the distance between two photons. Writing $\bar{\phi}^S(x_1, x_2, t)$ as $\bar{\phi}^S(x_1, x_2) e^{-i2\omega_0 t}$, the spatial part of the wave function of the two-photon part is

$$\bar{\phi}^S(x_1, x_2) = -\frac{i\kappa V^2}{v_g} e^{i2\omega_0 \frac{x_1+x_2}{2v_g} - \pi V^2 \frac{|x_1-x_2|}{v_g}}, \quad (35)$$

which indicates that the output two-photon wave function is exactly that of the photonic dimer.

C. Coherent states of photonic dimers

From Eq. (B12), it thus follows immediately that at the large- t and large- x limits (away from the cavity but is nonetheless subject to the causality condition $t - x/v_g > 0$), the spatial part of the stationary output state becomes

$$|\psi\rangle = e^{\int dx_1 dx_2 \bar{\phi}^S(x_1, x_2) \hat{c}^\dagger(x_1) \hat{c}^\dagger(x_2) - \text{H.c.}} |\emptyset\rangle, \quad (36)$$

which is the coherent state of the photonic dimers. In the weak-pumping limit, $\kappa V^2/v_g$ is a small number, the state can be expanded in a Taylor series where we keep the lowest order:

$$|\psi\rangle \approx \left(1 + \int dx_1 dx_2 \bar{\phi}^S(x_1, x_2) \hat{c}^\dagger(x_1) \hat{c}^\dagger(x_2) - \text{H.c.} \right) |\emptyset\rangle, \quad (37)$$

which, apart from an additive term, represents a dimer state. Using the normalized dimer state

$$|B_\mu\rangle = \hat{b}^\dagger(\mu) |\emptyset\rangle = \sqrt{\frac{\Gamma}{4\pi v_g^2}} \int dx_1 dx_2 e^{i\frac{\mu}{2v_g}(x_1+x_2) - \frac{\Gamma}{v_g}|x_1-x_2|} \times \hat{c}^\dagger(x_1) \hat{c}^\dagger(x_2) |\emptyset\rangle$$

[where $\langle B_{\mu'} | B_\mu \rangle = \delta(\mu - \mu')$], the state in Eq. (36) can be written in the following compact form:

$$|\psi\rangle = e^{\beta_B \hat{b}^\dagger(2\omega_0) - \beta_B^* \hat{b}(2\omega_0)} |\emptyset\rangle, \quad (38)$$

where $\beta_B = -i2\kappa V e^{-i2\omega_0 t}$ and $\Gamma = \pi V^2$. The coherent state of photonic dimers is a superposition with even number photons. The expectation of the electric field $\langle \psi | \hat{E}^+(x, t) | \psi \rangle$ is zero for all positions and time.

V. CORRELATION FUNCTIONS

The correlation functions characterize the statistical properties of the optical fields. In this section, we calculate the

0th order: $\hat{c}(x)$;

1st order: $[\hat{F} - \hat{F}^\dagger, \hat{c}(x)] = \int dx_1 2\bar{\phi}^S(x_1, x) \hat{c}^\dagger(x)$;

2nd order: $[\hat{F} - \hat{F}^\dagger, [\hat{F} - \hat{F}^\dagger, \hat{c}(x)]] = \int dx_2 \left[\int dx_1 [2\bar{\phi}^S(x_1, x_2)]^* 2\bar{\phi}^S(x_1, x) \right] \hat{c}(x)$. (43)

Then the $\hat{\phi}_c(x)$ operator is a combination between single-photon creation and annihilation operators. If we further define

$$F_n(x_0, x) = \int_{-\infty}^{\infty} dx_1 \cdots dx_n e^{-\frac{\Gamma}{v_g}(|x_0-x_1|+|x_1-x_2|+|x_2-x_3|+\cdots+|x_{n-1}-x_n|+|x_n-x|)} \quad (n \geq 0),$$

$$F_{-1}(x_0, x) = \delta(x - x_0), \quad (44)$$

where $\Gamma = \pi V^2$, then $\hat{\phi}_c(x)$ can be cast as

$$\hat{\phi}_c(x_0) = \int dx \left[e^{i\frac{\omega_0}{v_g}(x_0-x)} \sum_{n=0}^{\infty} \frac{1}{(2n)!} \left(\frac{2\kappa V^2}{v_g} \right)^{2n} F_{2n-1}(x_0, x) \hat{c}(x) + i e^{i\frac{\omega_0}{v_g}(x_0+x)} \sum_{n=0}^{\infty} \frac{1}{(2n+1)!} \left(\frac{2\kappa V^2}{v_g} \right)^{2n+1} F_{2n}(x_0, x) \hat{c}^\dagger(x) \right] \quad (45)$$

$$= \int dx [\Phi(x_0, x) \hat{c}(x) + \Psi(x_0, x) \hat{c}^\dagger(x)], \quad (46)$$

correlation functions of the photons in the cavity, and of the coherent state of dimers [Eqs. (36) and (38), respectively].

A. Correlation functions of the intracavity photons

The average intracavity photon number is

$$\langle \psi(t) | \hat{a}^\dagger \hat{a} | \psi(t) \rangle = \frac{1}{3} \sinh^2 \left(\frac{\sqrt{3}\kappa}{\pi} \right) + \frac{1}{2} \sinh^2 \left(\frac{\sqrt{2}\kappa}{\pi} \right), \quad (39)$$

which exponentially increases with a strong pumping power. This growth is expected to saturate when sufficient energy is drawn from the pump so that the assumption of an undepleted pump no longer holds.

B. Correlation functions of the coherent state of dimers

The unnormalized first- and second-order correlation functions are given by

$$G^{(1)}(x) = \langle \psi | \hat{c}^\dagger(x) \hat{c}(x) | \psi \rangle = |\hat{c}(x) e^{\int dx_1 dx_2 \bar{\phi}^S(x_1, x_2) \hat{c}^\dagger(x_1) \hat{c}^\dagger(x_2) - \text{H.c.}} |\emptyset\rangle|^2,$$

$$G^{(2)}(x_1, x_2) = \langle \psi | \hat{c}^\dagger(x_2) \hat{c}^\dagger(x_1) \hat{c}(x_1) \hat{c}(x_2) | \psi \rangle = |\hat{c}(x_1) \hat{c}(x_2) e^{\int dx_1 dx_2 \bar{\phi}^S(x_1, x_2) \hat{c}^\dagger(x_1) \hat{c}^\dagger(x_2) - \text{H.c.}} |\emptyset\rangle|^2, \quad (40)$$

where $|\psi\rangle$ is the coherent state of dimers given by Eq. (36). To simplify the calculation, similar to the previous case, we also define an auxiliary operator

$$\hat{\phi}_c(x) \equiv e^{\hat{F} - \hat{F}^\dagger} \hat{c}(x) e^{\hat{F}^\dagger - \hat{F}}, \quad (41)$$

where $\hat{F}^\dagger = \int dx_1 dx_2 \bar{\phi}^S(x_1, x_2) \hat{c}^\dagger(x_1) \hat{c}^\dagger(x_2)$. Using the following formula:

$$e^{\alpha A} B e^{-\alpha A} = B + \alpha [A, B] + \frac{\alpha^2}{2!} [A, [A, B]] + \cdots, \quad (42)$$

one then can calculate each terms in the expansion of $\hat{\phi}_c(x)$ in the order of $\bar{\phi}^S(x_1, x_2)$; the first few terms are given below:

where

$$\begin{aligned}\Phi(x_0, x) &= e^{i\frac{\omega_0}{v_g}(x_0-x)} \sum_{n=0}^{\infty} \frac{1}{(2n)!} \left(\frac{2\kappa V^2}{v_g}\right)^{2n} F_{2n-1}(x_0, x), \\ \Psi(x_0, x) &= i e^{i\frac{\omega_0}{v_g}(x_0+x)} \sum_{n=0}^{\infty} \frac{1}{(2n+1)!} \left(\frac{2\kappa V^2}{v_g}\right)^{2n+1} F_{2n}(x_0, x).\end{aligned}\quad (47)$$

These series expansions, as we shall see below, not only enable a perturbative calculations in the weak-pumping limit, but also an efficient computational means in the strong-pumping limit.

In terms of the auxiliary operators, the correlation functions are

$$G^{(1)}(x_0, x'_0) = \langle \emptyset | \hat{\phi}_c^\dagger(x'_0) \hat{\phi}_c(x_0) | \emptyset \rangle = \int dx \Psi^*(x'_0, x) \Psi(x_0, x), \quad (48)$$

$$G^{(1)}(x_0) = |\hat{\phi}_c(x_0) | \emptyset \rangle|^2 = \int dx |\Psi(x_0, x)|^2,$$

$$\begin{aligned}G^{(2)}(x_0, x'_0) &= |\hat{\phi}_c(x_0) \hat{\phi}_c(x'_0) | \emptyset \rangle|^2 \\ &= \left| \int dx [\Phi(x_0, x) \hat{c}(x) + \Psi(x_0, x) \hat{c}^\dagger(x)] \int dx' \Psi(x'_0, x') \hat{c}^\dagger(x') | \emptyset \rangle \right|^2 \\ &= \left| \int dx \Phi(x_0, x) \Psi(x'_0, x) \right|^2 + \int dx_1 dx_2 |\Psi(x_0, x_1)|^2 |\Psi(x'_0, x_2)|^2 \\ &\quad + \int dx_1 dx_2 \Psi^*(x_0, x_2) \Psi^*(x'_0, x_1) \Psi(x_0, x_1) \Psi(x'_0, x_2),\end{aligned}\quad (49)$$

$$g^{(2)}(x_0, x'_0) = 1 + \frac{|\int dx \Phi(x_0, x) \Psi(x'_0, x)|^2 + |\int dx \Psi^*(x'_0, x) \Psi(x_0, x)|^2}{(\int dx |\Psi(x_0, x)|^2)(\int dx |\Psi(x'_0, x)|^2)}.\quad (50)$$

We now apply these exact expressions to the weak-pumping limit and to the scenarios beyond the weak-pumping limit, respectively.

1. Correlation functions in the weak-pumping limit

In the weak-pumping limit, the higher-order term of $\hat{\phi}_c(x)$ can be neglected. Up to the order of κ ,

$$\begin{aligned}\Phi(x_0, x) &= \delta(x - x_0), \\ \Psi(x_0, x) &= i \frac{2\kappa V^2}{v_g} e^{i\frac{\omega_0}{v_g}(x_0+x) - \frac{\pi v^2}{v_g}|x_0-x|}, \\ \hat{\phi}_c(x_0) &= \hat{c}(x_0) + \int dx i \frac{2\kappa V^2}{v_g} e^{i\frac{\omega_0}{v_g}(x_0+x) - \frac{\pi v^2}{v_g}|x_0-x|} \hat{c}^\dagger(x).\end{aligned}\quad (51)$$

Under this approximation,

$$\begin{aligned}G^{(1)}(x_0, x'_0) &= \int dx \Psi^*(x'_0, x) \Psi(x_0, x) = \frac{4\kappa^2 V^2}{\pi V^2} e^{i\frac{\omega_0}{v_g}(x_0-x'_0) - \frac{\pi v^2}{v_g}|x_0-x'_0|} \left(1 + \frac{\pi V^2}{v_g} |x_0 - x'_0|\right), \\ G^{(1)}(x_0) &= \int dx |\Psi(x_0, x)|^2 = \frac{4\kappa^2 V^2}{\pi v_g}, \\ g^{(1)}(x_0, x'_0) &= e^{i\frac{\omega_0}{v_g}(x_0-x'_0) - \frac{\pi v^2}{v_g}|x_0-x'_0|} \left(1 + \frac{\pi V^2}{v_g} |x_0 - x'_0|\right), \\ G^{(2)}(x_0, x'_0) &= \left(\frac{2\kappa V^2}{v_g}\right)^2 e^{-\frac{2\pi v^2}{v_g}|x_0-x'_0|} + \left(\frac{4\kappa^2 V^2}{\pi v_g}\right)^2 \left[1 + \left(1 + \frac{\pi V^2}{v_g} |x_0 - x'_0|\right)^2\right], \\ g^{(2)}(x_0, x'_0) &= 1 + \left[\left(1 + \frac{\pi V^2}{v_g} |x_0 - x'_0|\right)^2 + \frac{\pi^2}{4\kappa^2}\right] e^{-\frac{2\pi v^2}{v_g}|x_0-x'_0|}.\end{aligned}\quad (52)$$

Thus the first-order correlation is a constant. The second-order correlation is

$$g^{(2)}(\tau) = 1 + \left[\frac{\pi^2}{4\kappa^2} + (1 + \pi V^2 |\tau|)^2 \right] e^{-2\pi V^2 |\tau|}, \quad \text{and thus} \quad (53)$$

$$g^{(2)}(0) = 2 + \frac{\pi^2}{4\kappa^2}. \quad (54)$$

In the weak-pumping limit, $\kappa \ll 1$ so that $(1 + \pi V^2 |\tau|)^2 \ll \pi^2/4\kappa^2$,

$$g^{(2)}(\tau) = 1 + \frac{\pi^2}{4\kappa^2} e^{-2\pi V^2 |\tau|}. \quad (55)$$

Omitting the $(1 + \pi V^2 |\tau|)^2$ term leads to a different $g^{(2)}(0)$, but as $\pi^2/4\kappa^2$ is a large number, this will only have a negligible change to the result. In the weak-pumping limit, $g^{(2)}(\tau)$ is an exponentially decaying function from $2 + \pi^2/4\kappa^2$ to 1 with a decay rate of $2\pi V^2$. Figure 6 plots $g^{(2)}(\tau)$ as a function of $\pi V^2 \tau$ for various values of κ .

We note that the correlation functions are identical to those of a two-photon dimer state $|B_\mu\rangle$ in Eq. (1). That is, in the weak-pumping limit, $g^{(2)}(\tau)$ exhibits the correlation signatures of individual photonic dimers. The photon generation rate, the probability to find a photon per unit time, is $R \equiv v_g G^{(1)}(x) = \frac{4\kappa^2 V^2}{\pi}$ (see Appendix C for details), then the second-order correlation function is

$$g^{(2)}(\tau) = 1 + \frac{1}{2R\tau_c} e^{-\frac{|\tau|}{\tau_c}}, \quad (56)$$

where τ_c , the coherence time, is the inverse of the bandwidth $\tau_c = 1/\Delta B = 1/2\pi V^2$. The identical result has been reported in the literature [28,29], albeit using a different approach. The behaviors of the correlation functions are also in agreement with recent biphoton experiments [30].

C. Beyond the weak-pumping limit

For a pumping power that is beyond the weak-pumping limit, all orders of κ must be considered. The series expansion of the auxiliary operator $\hat{\phi}_c(x)$ in Eq. (46) facilitates an efficient computational approach, as detailed in Appendix D. Here we present and discuss the numerical results.

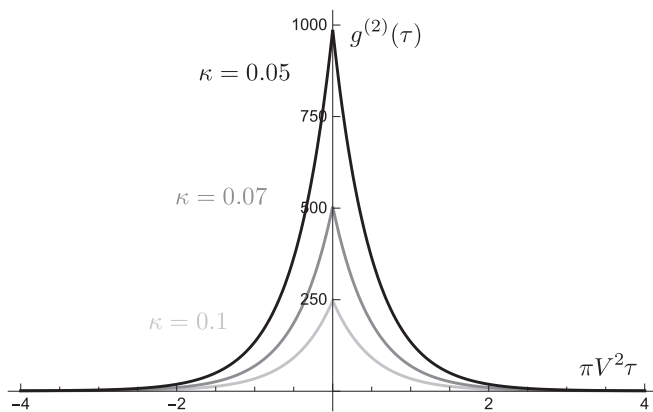


FIG. 6. In the weak-pumping limit, $g^{(2)}(\tau)$ as a function of $\pi V^2 \tau$ when $\kappa = 0.1, 0.07, 0.05$.

I. Numerical results of $G^{(1)}(x)$

Figure 7 plots $G^{(1)}(x)$ of the coherent state of dimers as a function of β , where $\beta = 2\kappa V^2/\Gamma = 2\kappa/\pi$ is a dimensionless quantity proportion to the electric field of the pumping optical field.

When β is small ($\lesssim 0.1$), the numerical results are in good agreement with that from the weak-pumping limit in Sec. VB 1. In this regime, $G^{(1)}(x)$ is proportional to β^2 (i.e., proportional to the pumping power). When β is increased further, $G^{(1)}(x)$ increases exponentially (i.e., $\ln G^{(1)}(x)$ proportional to β), as shown in Fig. 7.

Figure 7 also plots $G^{(1)}(x)/(\frac{\Gamma}{v_g})$ and $2n_{\text{cavity}}$ versus various values of β . When β is small ($\beta \lesssim 0.2$), $G^{(1)}(x) = 2\frac{\Gamma}{v_g} n_{\text{cavity}}$. The physical picture is that each dimer consists of two photons and is released from the cavity in a timescale of $1/\Gamma$. When β is increased, $G^{(1)}(x)$ increases faster than $2n_{\text{cavity}}$, although both functions increase exponentially.

2. Numerical results of $g^{(2)}(x_0, x'_0)$ function

Figure 8 plots the numerical $g^{(2)}(x_0, x'_0)$ as a function of $\frac{\Gamma}{v_g}(x_0 - x'_0)$ for various values of β . When β is small, the $g^{(2)}$ function is in good agreement with that calculated in the weak-pumping limit.

Figure 9 plots the numerical $g^{(2)}$ for increasing β (\propto the squared root of the pumping power). When β is increased, the qualitative behavior of $g^{(2)}$ transitions from a pronounced cusp peak (signatures of individual dimers) to a lower and rounded shape. In the small β weak-pumping regime, $g^{(2)}(0)$ is proportional to $\frac{1}{\beta^2}$ and the full width at half maximum (FWHM) is proportional to the cavity bandwidth, which is independent of β . When β is increased beyond the weak-pumping regime, numerically it is found that $g^{(2)}(0)$ decreases and eventually

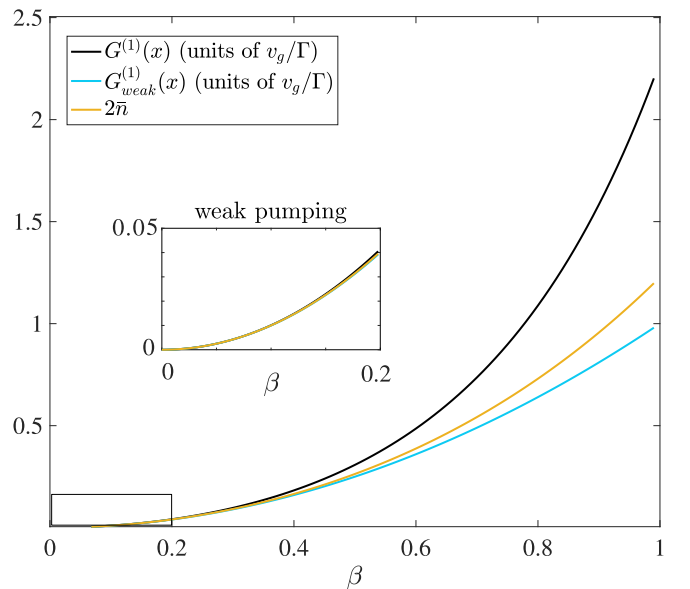


FIG. 7. Numerical $G^{(1)}(x)$ function (black), the weak-pumping limit result $G_{\text{weak}}^{(1)}(x)$ (blue) and average cavity photon number \bar{n} (yellow) with $\beta = 0-1$.

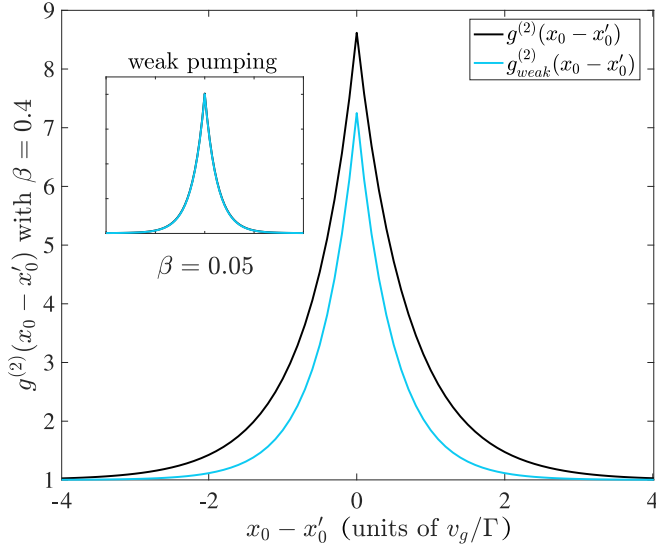


FIG. 8. Numerical $g^{(2)}(x_0, x'_0)$ (black) as a function of $\frac{\Gamma}{v_g}(x_0 - x'_0)$ for $\beta = 0.4$ and $\beta = 0.05$. Also plotted is the weak-pumping results (blue).

stabilizes to the value of three. The width of $g^{(2)}$ function also increases, indicating multidimer scenarios.

As will be discussed in Sec. VIII, the above results show that increasing pumping power makes the dimer-dimer overlap increases and influences the statistical property. As the overlaps can be characterized by comparing average interphoton distance,

$$\begin{aligned} \bar{d} &= \frac{\text{Length of any section } (v_g \Delta t)}{\text{Average photon number in this length } [G^{(1)}(t) \Delta t]} \\ &= \frac{v_g}{G^{(1)}(t)}, \end{aligned}$$

and dimer spatial width (v_g/Γ), we can also increase dimer spatial width to change the overlaps. Figure 10 plots the numerical $g^{(2)}$ for decreasing Γ with a fixed pumping power ($2\kappa V^2$). When Γ is decreased, the similar behavior of $g^{(2)}$ is observed, which transitions from a pronounced peak to a

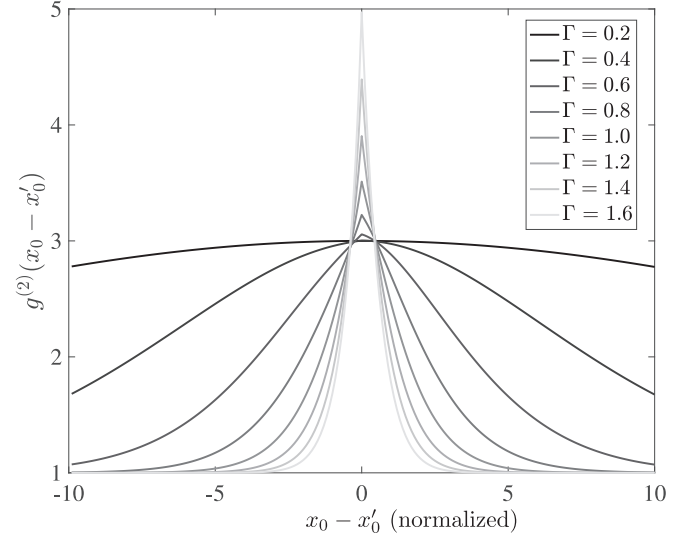
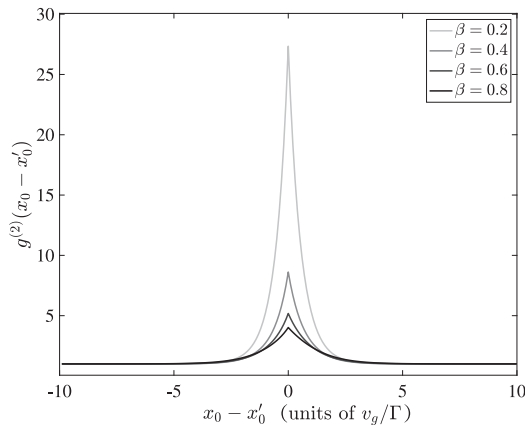


FIG. 10. Numerical $g^{(2)}(x_0, x'_0)$ as a function of $x_0 - x'_0$ [in units of $1/(2\kappa V^2)$] for various values of Γ (in units of $2\kappa V^2$) with a fixed pumping power κV^2 .

lower and rounded shape. With a smaller and smaller Γ , it is found that $g^{(2)}$ stabilizes to the value of three. Analytically, by taking the limit $\frac{\Gamma}{v_g}|x_0 - x'_0| \ll 1$, it is found that

$$g^{(2)}(x_0, x'_0) = 3 + \frac{1}{\sinh^2\left(\frac{2\kappa V^2}{v_g} \int dx\right)} = 3$$

is a constant. In fact, with this limit, the exponentially decaying relative function [$\exp(-\frac{\Gamma}{v_g}|x_1 - x_2|)$] of the photonic dimer can be neglected and the coherent state of photonic dimers approaches a squeezed vacuum state.

VI. THE QUADRATURE PROPERTIES

In this section, we provide a detailed discussion of the quadrature properties of the coherent state of dimers and compare our results to those in the literature.

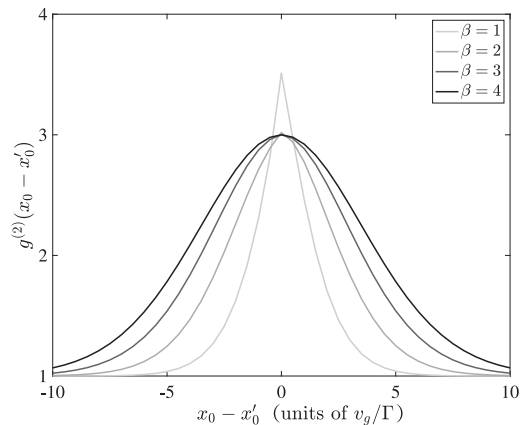


FIG. 9. Numerical $g^{(2)}$ in the weak-pumping limit (left, $\beta = 0.2, 0.4, 0.6, 0.8$) and beyond the weak-pumping limit (right, $\beta = 1, 2, 3, 4$). Two figures have different scales where $g^{(2)}$ -axis scales from 0 to 30 in the weak-pumping limit and scales from one to four beyond the weak-pumping limit.

Recall the form of the dimer coherent state,

$$\begin{aligned}
|\psi\rangle &= e^{\beta_B \hat{b}^\dagger(2\omega_0) - \beta_B \hat{b}(2\omega_0)} |\emptyset\rangle \\
&= \exp \left[\beta_B V \int d\omega \frac{\Gamma}{(\omega - \omega_0)^2 + \Gamma^2} \hat{c}_\omega^\dagger \hat{c}_{2\omega_0 - \omega}^\dagger - \text{H.c.} \right] |\emptyset\rangle \\
&= \exp \left(\beta_B V \int d\omega \frac{\Gamma}{\omega^2 + \Gamma^2} \hat{c}_{\omega_0 + \omega}^\dagger \hat{c}_{\omega_0 - \omega}^\dagger - \text{H.c.} \right) |\emptyset\rangle,
\end{aligned} \tag{57}$$

where $\beta_B = -i2\kappa V e^{-2i\omega_0 t}$ and $\Gamma = \pi V^2$.

A. Compare with the definition of Collett and Gardiner [20]

Similar to Eq. (31) in Ref. [20], we transform to a rotating frame with $a \rightarrow e^{i\omega_0 t} a$. The coherent state of dimers becomes

$$|\psi\rangle = \exp \left(-2i\kappa V^2 \int d\omega \frac{\Gamma}{\omega^2 + \Gamma^2} \hat{c}_{\omega_0 + \omega}^\dagger \hat{c}_{\omega_0 - \omega}^\dagger - \text{H.c.} \right) |\emptyset\rangle. \tag{58}$$

The single-frequency quadrature is a Hermitian operator defined by

$$\begin{aligned}
\hat{X}_1(\omega) &= \frac{e^{-i\theta/2} \hat{c}_\omega + e^{i\theta/2} \hat{c}_\omega^\dagger}{2}, \\
\hat{X}_2(\omega) &= \frac{e^{-i\theta/2} \hat{c}_\omega - e^{i\theta/2} \hat{c}_\omega^\dagger}{2i}.
\end{aligned} \tag{59}$$

To characterize the squeezing effect, the normal-ordered variances and the normal-ordered spectrum of the quadrature are defined, respectively, as

$$\begin{aligned}
\langle : \hat{X}_i, \hat{X}_i : \rangle &= \int d\omega d\omega' \langle : \hat{X}_i(\omega_0 + \omega), \hat{X}_i(\omega_0 + \omega') : \rangle, \\
:S_i(\omega) : &= \int d\omega' \langle : \hat{X}_i(\omega_0 + \omega), \hat{X}_i(\omega_0 + \omega') : \rangle.
\end{aligned} \tag{60}$$

Here, the normal-ordered (also called the Wick-ordered) operator is defined so that all creation operators are to the left of all annihilation operators in the product. This definition yields that the normal-ordered variance of the vacuum is zero. Any state with a negative normal-ordered variance is a nonclassical squeezed state. As the quadrature operator has a unit $[\omega]^{-\frac{1}{2}}$, the quadrature variance $\langle : \hat{X}_i, \hat{X}_i : \rangle$ has a unit $[\omega]$.

The covariances for creation and annihilation operators are given by

$$\begin{aligned}
\langle \hat{c}_{\omega_0 + \omega}^\dagger, \hat{c}_{\omega_0 + \omega'} \rangle &= \sinh^2 \left(\frac{2\beta\Gamma^2}{\omega^2 + \Gamma^2} \right) \delta(\omega - \omega'), \quad \langle \hat{c}_{\omega_0 + \omega}, \hat{c}_{\omega_0 + \omega'}^\dagger \rangle = \cosh^2 \left(\frac{2\beta\Gamma^2}{\omega^2 + \Gamma^2} \right) \delta(\omega - \omega'), \\
\langle \hat{c}_{\omega_0 + \omega}, \hat{c}_{\omega_0 + \omega'} \rangle &= -i \sinh \left(\frac{2\beta\Gamma^2}{\omega^2 + \Gamma^2} \right) \cosh \left(\frac{2\beta\Gamma^2}{\omega^2 + \Gamma^2} \right) \delta(\omega + \omega'), \\
\langle \hat{c}_{\omega_0 + \omega}^\dagger, \hat{c}_{\omega_0 + \omega'}^\dagger \rangle &= i \sinh \left(\frac{2\beta\Gamma^2}{\omega^2 + \Gamma^2} \right) \cosh \left(\frac{2\beta\Gamma^2}{\omega^2 + \Gamma^2} \right) \delta(\omega + \omega').
\end{aligned} \tag{61}$$

More details can be found in Appendix E. The normal-ordered quadrature variances with two modes can be computed:

$$\langle : \hat{X}_1(\omega_0 + \omega), \hat{X}_1(\omega_0 + \omega') : \rangle = \frac{1}{2} \sinh \left(\frac{2\beta\Gamma^2}{\omega^2 + \Gamma^2} \right) \left[-2 \sin \theta \cosh \left(\frac{2\beta\Gamma^2}{\omega^2 + \Gamma^2} \right) \delta(\omega + \omega') + \sinh \left(\frac{2\beta\Gamma^2}{\omega^2 + \Gamma^2} \right) \delta(\omega - \omega') \right]. \tag{62}$$

The normal-ordered variance of the full-bandwidth quadrature and the spectrum are

$$\begin{aligned}
\langle : \hat{X}_1, \hat{X}_1 : \rangle &= \int_{-\infty}^{\infty} d\omega \frac{1}{4} \left[-2 \sin \theta \sinh \left(\frac{2\beta\Gamma^2}{\omega^2 + \Gamma^2} \right) \cosh \left(\frac{2\beta\Gamma^2}{\omega^2 + \Gamma^2} \right) + 2 \sinh^2 \left(\frac{2\beta\Gamma^2}{\omega^2 + \Gamma^2} \right) \right], \\
:S_1(\omega) : &= \frac{1}{4} \left[-2 \sin \theta \sinh \left(\frac{2\beta\Gamma^2}{\omega^2 + \Gamma^2} \right) \cosh \left(\frac{2\beta\Gamma^2}{\omega^2 + \Gamma^2} \right) + 2 \sinh^2 \left(\frac{2\beta\Gamma^2}{\omega^2 + \Gamma^2} \right) \right].
\end{aligned} \tag{63}$$

As the coefficient $\int dx \sinh(\frac{2\beta}{x^2+1}) \cosh(\frac{2\beta}{x^2+1}) > 0$, the maximum squeezing occurs in the direction $\theta = \frac{\pi}{2}$ and thus yields the following results:

$$\langle : \hat{X}_1, \hat{X}_1 : \rangle = \Gamma \int_{-\infty}^{\infty} dx \frac{1}{4} \left[-2 \sinh \left(\frac{2\beta}{x^2 + 1} \right) \cosh \left(\frac{2\beta}{x^2 + 1} \right) + 2 \sinh^2 \left(\frac{2\beta}{x^2 + 1} \right) \right], \tag{64}$$

$$:S_1(\omega) : = \frac{1}{4} \left[-2 \sinh \left(\frac{2\beta\Gamma^2}{\omega^2 + \Gamma^2} \right) \cosh \left(\frac{2\beta\Gamma^2}{\omega^2 + \Gamma^2} \right) + 2 \sinh^2 \left(\frac{2\beta\Gamma^2}{\omega^2 + \Gamma^2} \right) \right] = \frac{1}{4} \left(e^{-\frac{4\beta\Gamma^2}{\omega^2 + \Gamma^2}} - 1 \right), \tag{65}$$

$$:S_1(0) : = \frac{1}{2} \sinh(2\beta) [\sinh(2\beta) - \cosh(2\beta)] = \frac{1}{4} (e^{-4\beta} - 1). \tag{66}$$

In their seminal paper, Collett and Gardiner (CG) employed the input-output formalism to compute the quadrature properties [20]. We note that our definitions are slightly different from theirs: In their paper, they used the \hat{X}_2 operator with $\theta = 0$, which is the same as \hat{X}_1 with $\theta = \pi$. Expressed in terms of our notations, their results are

$$\begin{aligned} & \langle : \hat{X}_2(\omega_0 + \omega), \hat{X}_2(\omega_0 + \omega') : \rangle_{CG} \\ &= -\frac{\beta \Gamma^2}{\omega^2 + (\Gamma + \beta \Gamma)^2} \delta(\omega + \omega'), \end{aligned} \quad (67)$$

$$\langle : \hat{X}_2, \hat{X}_2 : \rangle_{CG} = -\frac{\Gamma}{2} \frac{\beta}{1 + \beta} \leq \frac{\Gamma}{4}, \quad (68)$$

$$: S_2(\omega) :_{th;CG} = -\frac{\Gamma^2}{\omega^2 + 4\Gamma^2}, \quad (69)$$

$$: S_2(0) :_{th;CG} = -\frac{1}{4}. \quad (70)$$

The maximum squeezing is attained at the threshold ($\beta = 1$), which is exactly the same as our prediction, although the numerical squeezing factors differ. Figure 11 plots the variances in the two approaches, Eq. (68) in the CG approach and Eq. (E10) in our approach, respectively, as a function of β . The numerical results indicate that the coherent states of dimers provides a larger squeezing factor; equivalently, for the same level of squeezing, the dimer coherent states requires a smaller β values (i.e., weaker pumping).

Figure 12 further illustrates the behavior of the normal-ordered variance of the full-bandwidth quadrature of the dimer coherent state, Eq. (E8). The left figure plots the variance as a function of β for various local oscillator directions θ , and the right figure plots variance as a function of θ for various pumping power β . The squeezing occurs when the variance becomes negative.

B. Compare with the definition of Scully and Zubairy [18]

Other widely cited quadrature variance results for describing squeezing are those of Scully and Zubairy (SZ) [18]. They considered the quadrature variance at the resonant frequency, instead of the full-bandwidth variance. Another distinction is that their definition of the variance is not normal-ordered, and thus the vacuum (coherent) state has a quadrature variance $\frac{1}{4} > 0$.

The following SZ result of the ratio of the variances is derived using the input-output formalism:

$$\frac{[\Delta \hat{X}_{1,\text{out}}(\omega_0)_{SZ}]^2}{[\Delta \hat{X}_{1,\text{in}}(\omega_0)]^2} = \left(\frac{1 - \beta}{1 + \beta} \right)^2, \quad (71)$$

while in our approach, the ratio is given by (at the maximum squeezing direction $\theta = \frac{\pi}{2}$)

$$\begin{aligned} \frac{[\Delta \hat{X}_{1,\text{out}}(\omega_0)]^2}{[\Delta \hat{X}_{1,\text{in}}(\omega_0)]^2} &= 1 + 2 \sinh(2\beta) [\sinh(2\beta) - \cosh(2\beta)] \\ &= e^{-4\beta}. \end{aligned} \quad (72)$$

Figure 13 compares the ratios of the variances between the SZ result [Eq. (71)] and our result for the dimer coherent state [Eq. (72)] as a function of β . For $0 \leq \beta \leq 1$ (upper figure), the two results are in numerically agreement with each other.

The SZ result shows a perfect OPO squeezing at the threshold $\beta = 1$,

$$\frac{[\Delta \hat{X}_{1,\text{out}}(\omega_0)_{SZ}]^2}{[\Delta \hat{X}_{1,\text{in}}(\omega_0)]^2}_{\beta=1} = 0,$$

while our results yields a nearly perfect squeezing at the threshold,

$$\frac{[\Delta \hat{X}_{1,\text{out}}(\omega_0)]^2}{[\Delta \hat{X}_{1,\text{in}}(\omega_0)]^2}_{\beta=1} = 0.0183.$$

On the other hand, when $\beta > 1$, the SZ result increases as the input-output formalism does not reach a steady state in this range, while the dimer coherent state remains squeezed (both approaches assuming the undepleted pumping field).

The squeezing factor for Eqs. (71) and (72) can be computed using

$$\begin{aligned} R &= -10 \log_{10} \left(\frac{[\Delta \hat{X}_{1,\text{out}}(\omega_0)]^2}{[\Delta \hat{X}_{1,\text{in}}(\omega_0)]^2} \right), \\ R_{SZ} &= -20 \log_{10} \left(\frac{1 - \beta}{1 + \beta} \right) \quad (\text{dB}), \\ R_{our} &= -10 \log_{10}(e^{-4\beta}) \quad (\text{dB}) \\ &= 17.4\beta \quad (\text{dB}). \end{aligned} \quad (73)$$

At threshold ($\beta = 1$), the SZ result employing the input-output formalism predicts a squeezing factor of $+\infty$, while our approach predicts a squeezing factor for the dimer coherent state which is linearly dependent of β and yields a value of 17.4 dB at the threshold. The input-output formalism yields no stationary states above the threshold (thus the extension part of the curve of the SZ result beyond the threshold is indicated by a dashed line in the lower figure in Fig. 13).

VII. EXPERIMENTAL COMPARISONS AND REALIZATIONS

In this section, we apply the results that are developed in the previous sections to compare with the experimental results and to estimate the required pumping power in different regimes.

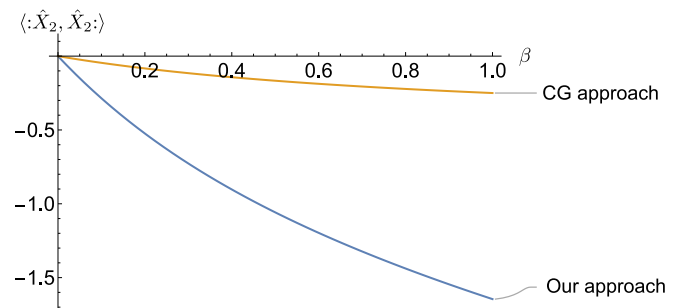


FIG. 11. Comparison of the normal-ordered quadrature variances in the maximal squeezing direction between the CG result (68) and our result (E10). The variances are plotted in units of Γ .

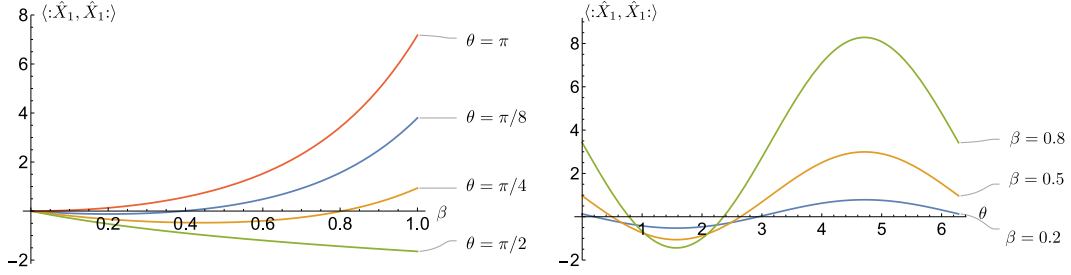


FIG. 12. Normal-ordered variance of the full-bandwidth quadrature of the dimer coherent state, Eq. (E8). The variances are plotted in unit of Γ . (left) The variance as a function of β for various local oscillator directions θ . (right) The variance as a function of θ for various pumping power β .

A. Small- β regime

We first compare the quadrature variances at small- β regime between our theoretical results and that of the squeezed states of the electromagnetic field generated by degenerate parametric down conversion in an optical cavity [31].

Using the quadrature definition in Ref. [31],

$$\hat{X}(\theta) = (\hat{c} + \hat{c}^\dagger) \cos \theta - i(\hat{c} - \hat{c}^\dagger) \sin \theta, \quad (74)$$

the ratio of the variances by our approach is given by

$$\frac{[\Delta \hat{X}(\theta)]^2}{[\Delta \hat{X}_{vac}]^2} = 1 + 2 \sinh(2\beta) [\sinh(2\beta) - \sin(2\theta) \cosh(2\beta)]. \quad (75)$$

Here the ratio is evaluated at the resonant frequency due to the narrow bandwidth of ≈ 100 kHz of the detector. Figure 14 plots the quadrature variance as a function of the local oscillator direction θ . The experimental result (blue curve) and the theoretical result (red curve, with a choice of $\beta = 0.16$) are

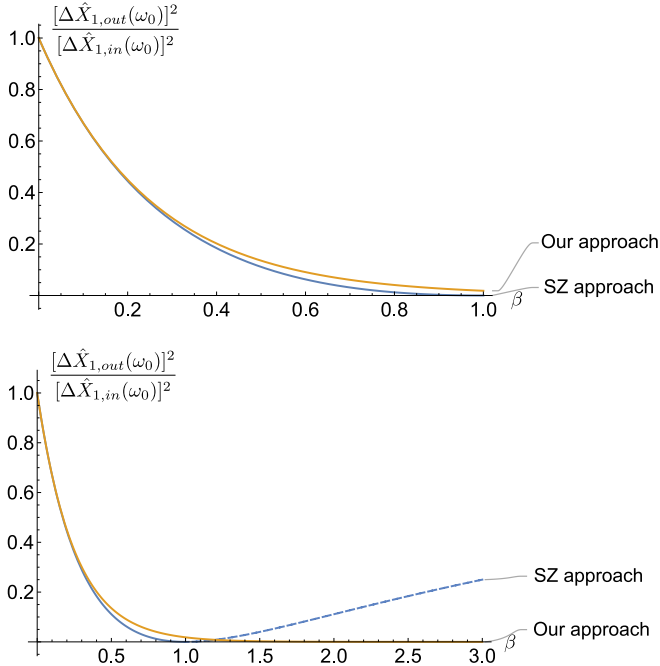


FIG. 13. Comparison of the ratios of the variances between the SZ result [Eq. (71)] and our result for the dimer coherent state [Eq. (72)] as a function of β for $0 \leq \beta \leq 1$ (upper) and $\beta > 1$ (lower).

in good agreement and provide the same qualitative behavior: The period of the phase is π , the average quadrature variance is above the vacuum state, and the squeezing only occurs within a small range of θ .

B. Large- β regime

We start by expressing the parameter κ ,

$$\begin{aligned} \kappa &= \frac{\Gamma_{0,0}L}{\hbar V^2} \\ &= \frac{L}{\hbar V^2} \frac{\hbar \omega_0}{2\epsilon_0 n_{\text{eff}}^2 V_{\text{crystal}}} 2\pi \epsilon_0 \chi^{(2)} E_p A_{\text{crystal}}, \end{aligned} \quad (76)$$

where n_{eff} is the effective refractive index for signal or idler photons in nonlinear crystal. $\chi^{(2)}$ is the second-order nonlinear coefficient of the crystal. A_{crystal} and V_{crystal} are the cross-sectional area and the volume of the crystal, respectively. ω_0 is the frequency of single-mode cavity or signal or idler photons. It follows that the pumping electric field and pumping power can be written as

$$\begin{aligned} E_p &= \frac{\kappa n_{\text{eff}}^2 A_{\text{cavity}} |T|^2 c}{4\pi^2 \chi^{(2)} \omega_0 V_{\text{crystal}}}, \quad \text{and} \\ P_{\text{pump}} &= \frac{\epsilon_0}{2} |E_p|^2 A_{\text{beam}}, \end{aligned} \quad (77)$$

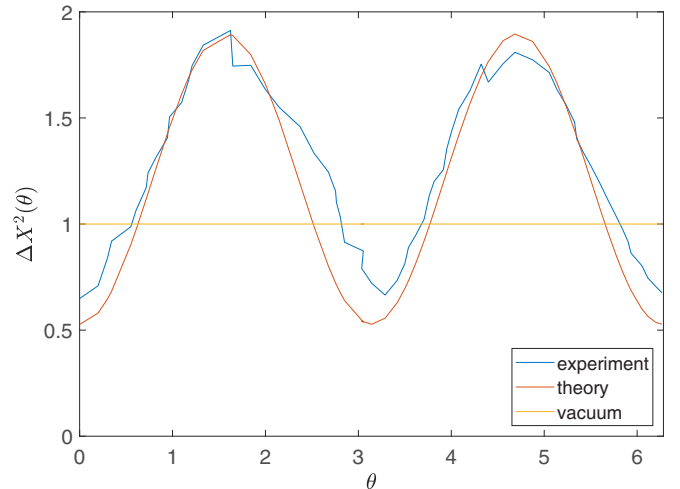


FIG. 14. Quadrature variances as a function of the local oscillator direction θ , for extracted experimental data (blue), theoretical predictions (red, with $\beta = 0.16$), and the vacuum (yellow).

TABLE I. Experimental values from the literature.

Crystal type [31]	Crystal size [31]	$\chi^{(2)}$ [32]	n_{eff} [32]	T [31]	Wavelength [31]	Beam radius [33]
MgO:LiNbO ₃	8 mm × 9 mm × 25 mm	4.4 pm/V	2.20	4.3%	1.06 μm	64 μm

where A_{cavity} is the cross-sectional area of the cavity, T is the transmittance, and A_{beam} is the cross-sectional area of the laser beam. We take $A_{\text{cavity}} = A_{\text{crystal}}$.

Recall that the average photon number inside the cavity is given by $\bar{n} = \frac{1}{3} \sinh^2(\frac{\sqrt{3}\kappa}{\pi}) + \frac{1}{2} \sinh^2(\frac{\sqrt{2}\kappa}{\pi})$. With the experimental values from the literature (see Table I), the exact values of our results can be estimated. When the average interphoton distance [$v_g/G^{(1)}(t) \simeq v_g/2\Gamma\bar{n}$] is comparable with single dimer spatial width (v_g/Γ), the average cavity photon number is about 0.5. It is estimated numerically that when $\bar{n} = 0.5$ ($\kappa = 1.44$ and $\beta = 0.92$), the pumping power is approximately 1.44×10^{-14} W. For photons in the visible spectrum ($\lambda = 533$ nm), average cavity photon $\bar{n} = 0.5$ requires 3.87×10^4 pumping photons per second. The output photon number per unit time is $G^{(1)}(t) = 1.70\Gamma = 9.38 \times 10^6$ photon/s. Here $\Gamma = \pi V^2 = 5.5 \times 10^6$ s⁻¹ represents a correlation time [width of $g^{(2)}(\tau)$] of ≈ 10 ns. The estimates for the KTP crystal are of the same orders of magnitude.

In the weak-pumping limit, as both $G^{(1)}$ and the pumping power is proportional to κ^2 , the output photon number per unit time is proportional to the pumping photon number ($\bar{n}_{\text{out}} = \alpha\bar{n}_{\text{pump}}$). Using the above values, when $\bar{n} = 0.005$ ($\kappa = \pi/20$), the output photon number is 1.11×10^5 s⁻¹ and the pumping power is 1.71×10^{-16} W (4.6×10^2 s⁻¹ photons). Then the ratio between output photons and pumping photons is $\alpha = 241$. Numerically we found that this ratio is sensitive to some experimental values. The ratio depends on all experimental parameters. For example, the ratio is proportional to the square of the beam radius and changes from $\alpha = 9.9 \times 10^5$ (beam radius 1 μm) to $\alpha = 0.99$ (beam radius 1 mm).

VIII. STATISTICAL PROPERTIES OF COHERENT STATES OF DIMERS IN BEC AND BCS LIMIT

An important element of the discussion in this paper will be the two-photon operators that create and annihilate the dimers, which are introduced by rewriting the dimer state in Eq. (1) as

$$|B_\mu\rangle = \int \frac{dx}{\sqrt{2\pi v_g}} e^{i\frac{\mu}{v_g}x} \hat{b}_x^\dagger(x)|\emptyset\rangle, \quad (78a)$$

$$\hat{b}_x^\dagger(x) \equiv \int dx_d \sqrt{\frac{\Gamma}{v_g}} e^{-2\frac{\Gamma}{v_g}|x_d|} \frac{1}{\sqrt{2}} \hat{c}^\dagger\left(x + \frac{x_d}{2}\right) \hat{c}^\dagger\left(x - \frac{x_d}{2}\right), \quad (78b)$$

with $x \equiv (x_1 + x_2)/2$ denoting the center of two photons and $x_d \equiv x_1 - x_2$ the relative position of two photons.

To explore the properties of the photonic states in the reciprocal frequency space, the relevant single-photon operators

are represented by the Fourier integral:

$$\hat{c}_\omega^\dagger \equiv \int \frac{dx}{\sqrt{2\pi v_g}} e^{i\frac{\omega}{v_g}x} \hat{c}^\dagger(x), \quad (79a)$$

$$\hat{c}_\omega \equiv \int \frac{dx}{\sqrt{2\pi v_g}} e^{-i\frac{\omega}{v_g}x} \hat{c}(x). \quad (79b)$$

These two operators satisfy the commutator relation: $[\hat{c}_\omega, \hat{c}_{\omega'}^\dagger] = \delta(\omega - \omega')$. Accordingly, the two-photon dimer operators in the frequency representation for a dimer mode with a total frequency μ (the energy is $\hbar\mu$) are introduced as follows:

$$|B_\mu\rangle = \sqrt{\frac{\Gamma}{\pi}} \int d\omega \frac{\Gamma}{\left(\frac{\mu}{2} - \omega\right)^2 + \Gamma^2} \hat{c}_\omega^\dagger \hat{c}_{\mu-\omega}^\dagger |\emptyset\rangle \quad (80a)$$

$$\equiv \hat{b}^\dagger(\mu)|\emptyset\rangle, \quad (80b)$$

$$\hat{b}^\dagger(\mu) \equiv \sqrt{\frac{\Gamma}{\pi}} \int d\omega \frac{\Gamma}{\left(\frac{\mu}{2} - \omega\right)^2 + \Gamma^2} \hat{c}_\omega^\dagger \hat{c}_{\mu-\omega}^\dagger. \quad (80c)$$

It follows from the frequency dependence of the two single-photon operators in the integrand that the energies of the two photons in the dimer are anticorrelated, and that the dimer has a frequency bandwidth $\approx \Gamma$. For each individual photon, its frequency spectrum follows a Lorentzian form, which is plotted in Fig. 1(c).

We shall be interested in the quantum statistical properties of an ensemble of photonic dimers. As the two photons in a dimer stay apart with a finite distance that is described in the relative wave function, the statistical properties depend on the degree of overlap between dimers in the ensemble. Similar scenarios occur for the systems of interacting fermions. In the context of attractively interacting Fermi gases, the properties of the gases, e.g., the ground-state energy, momentum distribution, and low-energy excitations, all depend on the degree of overlap of the diatomic molecules. By varying the length scale of the pair correlations (or the size of the fermion pairs), the gases can transition from the Bardeen-Cooper-Schrieffer (BCS) limits of Cooper-like pairs to the Bose-Einstein condensation (BEC) limit of diatomic molecules. The crossover can be driven by fixing the interactions and changing the particle density (density-driven), or by tuning the interactions at a fixed density (interaction-driven), and has been observed in dilute atomic gases [34–37] and recently in two-dimensional superconductors [38].

Although the many-body system is in principle described by the same wave function in both BCS and BEC limits, the theoretical descriptions are however rather different. In this paper, we confine our attention to an ensemble of photonic dimers in the BEC limit and formulate the theory from the outset. In photonic gases, even though the fundamental statistics of the constituent particles are different from that in the Fermi gases, the descriptions of the two systems in the BEC

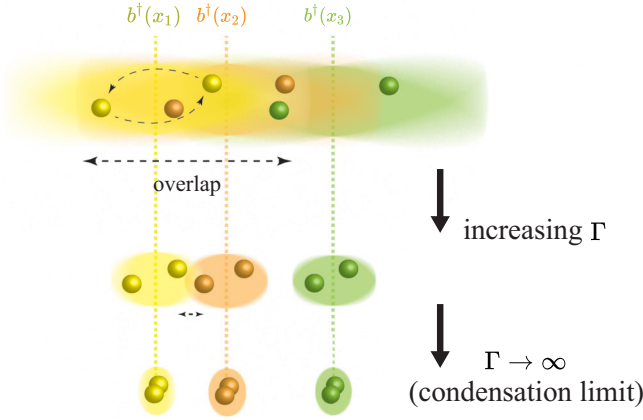


FIG. 15. The spatial overlap of three photonic dimer relative wave functions. When bunching factor Γ is not sufficiently large compared with average distance between photons, the overlap of relative wave functions is significant. With increasing Γ , such overlaps gradually decrease, and eventually disappear at condensation limit when $\Gamma \rightarrow \infty$. The two strictly collocated photons now behave like a grouped giant particle.

limit however are similar as the building blocks in both gases are bosons in the BEC limit. As shown in the following, in the BEC limit, the quantum optical field of a many-dimer system is described by a coherent state of dimers, which is a natural generalization of conventional lasers outputting a coherent state of single photons. In the BEC limit, the optical field also possesses unique optical properties, such as strong quantum optical nonlinearity. Figure 15 shows schematically the transition of the many-dimer system from the BCS limit to the BEC limit by varying the interaction strength Γ .

The information of the dimer-dimer overlap is captured by the commutator of the dimer operators:

$$[\hat{b}_x(x), \hat{b}_x^\dagger(x')] = \delta(x - x') + 2 \int dx \frac{\Gamma}{v_g} e^{-\frac{\Gamma}{v_g}|x_d|} \times \left(e^{-\frac{\Gamma}{v_g}|2x' - 2x - x_d|} + e^{-\frac{\Gamma}{v_g}|2x' - 2x + x_d|} \right) \hat{c}^\dagger \times \left(2x' - x + \frac{x_d}{2} \right) \hat{c} \left(x + \frac{x_d}{2} \right), \quad (81)$$

whereas the second term describing the dimer correlation is due to the overlap of the dimer relative wave functions with a finite spatial range and becomes significant when Γ is small ($\Gamma \lesssim v_g/|x - x'|$). When Γ increases, the overlap between the relative wave functions becomes less and the dimer correlation between the neighboring dimers becomes weaker. When Γ is further increased ($\Gamma \gg v_g/|x - x'|$), the spatial extension of the relative wave functions reduces to a sufficiently small size compared with the average distance between dimers and the overlap is negligible. In this BEC limit, the two photons in the dimer bind tightly and the dimers become the building blocks of the many-photon system.

To further simplify the description so that the theory becomes tractable, we investigate the dimer operators and

commutator at the large- Γ limit:

$$\begin{aligned} \lim_{\Gamma \rightarrow \infty} \hat{b}_x^\dagger(x) &= \int dx_d \lim_{\Gamma \rightarrow \infty} \sqrt{\Gamma e^{-2\frac{\Gamma}{v_g}|x_d|}/v_g} \frac{1}{\sqrt{2}} \hat{c}^\dagger \left(x + \frac{x_d}{2} \right) \\ &\quad \times \hat{c}^\dagger \left(x - \frac{x_d}{2} \right) \\ &= \int dx_d \sqrt{\delta(x_d)} \frac{1}{\sqrt{2}} \hat{c}^\dagger \left(x + \frac{x_d}{2} \right) \hat{c}^\dagger \left(x - \frac{x_d}{2} \right) \\ &= \frac{1}{\sqrt{2\Delta_\omega}} \hat{c}^\dagger(x) \hat{c}^\dagger(x), \end{aligned} \quad (82)$$

where $\lim_{\Gamma \rightarrow \infty} \Gamma e^{-2\frac{\Gamma}{v_g}|x|}/v_g = \delta(x)$ is used and the normalization factor $\Delta_\omega \equiv \int d\omega e^{i\omega x/v_g}/(2\pi v_g)|_{x=0}$ is proportional to the available bandwidth. The commutation relation of the dimer creation operator and its adjoint annihilation operator follows:

$$\begin{aligned} [\hat{b}_x(x), \hat{b}_x^\dagger(x')] &= \frac{1}{2\Delta_\omega} [\hat{c}(x)\hat{c}(x), \hat{c}^\dagger(x')\hat{c}^\dagger(x')] \\ &= \delta(x - x') \left(1 + \frac{2}{\Delta_\omega} \hat{c}^\dagger(x)\hat{c}(x) \right). \end{aligned} \quad (83)$$

The second term in the parentheses is $O(\frac{1}{\Delta_\omega})$ as $\Delta_\omega \rightarrow \infty$.

In the BEC limit ($\Gamma \rightarrow \infty$), the frequency representations of the dimer operator and the commutator can be obtained straightforwardly:

$$\hat{b}^\dagger(\mu) = \int \frac{d\omega}{\sqrt{2\pi}} \frac{1}{\sqrt{2\Delta_\omega v_g}} \hat{c}_\omega^\dagger \hat{c}_{\mu-\omega}^\dagger. \quad (84a)$$

$$[\hat{b}(\mu), \hat{b}^\dagger(\mu')] = \delta(\mu - \mu') + \int \frac{d\omega}{2\pi} \frac{1}{\Delta_\omega v_g} (\hat{c}_{\mu'-\mu+\omega}^\dagger \hat{c}_\omega) \quad (84b)$$

$$+ \hat{c}_{\mu'-\omega}^\dagger \hat{c}_{\mu-\omega}. \quad (84c)$$

Similarly, the second term in the integral is $O(\frac{1}{\Delta_\omega})$ as $\Delta_\omega \rightarrow \infty$ and the commutator $[b(\mu), b^\dagger(\mu')] = \delta(\mu - \mu')$ in the BEC limit.

IX. CONCLUSION AND OUTLOOK

In this section, we discuss the major approximations and the consequences of the approach presented in this work, followed by a brief comparison with the approach of others.

A. Neglecting time ordering

In Eq. (18) and the calculations followed, the time-ordering operator \hat{T} is neglected for mathematical simplicity. The time-ordering operator \hat{T} determines the order of Hamiltonian operators of different times in the expansions. As the Hamiltonians at different times do not commute, the time-ordering operator cannot be neglected in general. The effects of time ordering in quantum nonlinear optics have been discussed in details in Ref. [39] using the Magnus expansions.

Specifically, for an interacting Hamiltonian involving a bosonic quadratic term,

$$\begin{aligned} \hat{H}(t) &= \kappa \int d\omega_1 d\omega_2 e^{-i(\omega_p - \omega_1 - \omega_2)t} \phi(\omega_1, \omega_2) \hat{A}^\dagger(\omega_1) \hat{A}^\dagger(\omega_2) \\ &\quad + \text{H.c.} \end{aligned} \quad (85)$$

As shown above, the output state without time ordering contains only the dimer Lorentzian amplitude in the exponent. In contrast, the evolution operator with the proper time-ordering consists of contributions from the frequency-conversion part and the squeezed state part, respectively. For the initial vacuum state in the current problem, the frequency-conversion corrections disappear; the only correction is an additional two-photon amplitude of higher-order in κ in the exponent. Consequently, in the weak-pumping limit ($\kappa \ll 1$), the time-ordering effect indeed can be neglected. In Ref. [39], it is also indicated that the time-order corrections vanish for a broad bandwidth amplitude $\phi(\omega_1, \omega_2)$ in the Hamiltonian, which is exactly the conditions for the BEC limit in the photonic dimer laser. In the strong-pumping limit ($\kappa \gg 1$), the correction cannot be neglected.

B. Undepleted assumption

The formalism developed in this work is in the undepleted pump regime, so that the pumping field remains the same. Here we briefly discuss some of the artifacts due to the undepleted pump assumption. In the undepleted pump regime, beyond the weak-pumping limit, the input photon number is proportional to κ^2 , while the output photon number and the average cavity photon number increase exponentially when κ increases. In contrast, as shown in Ref. [40], in the depleted pump regime, it is found that the number of the output photons eventually becomes proportional to the input power ($\propto \kappa^2$). We note that it is possible to extend the formalism to the depleted regime of the pumping field [41]; nonetheless, we shall leave this endeavor to future work. The general observation is that the range of agreement in both regimes is relatively wide (specific range of agreement for this work would require working out the depleted-pump case).

C. Comparison with the input-output formalism and quantum Langevin approach

The input-output formalism and quantum Langevin approach have provided viable predictions below the threshold. Above the threshold, however, both approaches yield the results that the average cavity photon number (and $G^{(1)}$) increases exponentially over time and that steady states no longer exist. In our formalism, however, an OPO can always reach a steady state. The average cavity photon number of the steady states in our approach also increases exponentially with increasing pumping field. In the input-output formalism and quantum Langevin approach, it has been argued that the cavity photon number is ultimately constrained by the depletion effect and the time-ordering effect and reaches a steady state.

With an understanding of the limitations in our approach, we show that a new class of quantum photonic states, namely, the coherent states of photonic dimers, can be emerged in the cavity-SPDC system. As a final remark, we would like to emphasize that the coherent states of photonic dimers may also be engineered in different physical platforms, just like the coherent states of single photons can be created in different systems. For example, our preliminary results indicate that the coherent states of dimers can also be created when an ensemble of biexcitons is coupled to a cavity [42]. The unique

quantum statistical properties of these new states, as detailed in this work, may open up new opportunities in nonlinear quantum optic researches.

ACKNOWLEDGMENTS

J.-T.S. thanks Chih-Sung Chuu for many fruitful discussions on the SPDC experiment. This project has been made possible in part by Grant No. 2020-225832 from the Chan Zuckerberg Initiative DAF, an advised fund of the Silicon Valley Community Foundation.

APPENDIX A: EFFECTIVE INTERACTIONS OF GAIN MEDIUM

Consider an ensemble of two-level atoms inside a cavity. The Hamiltonian for the interaction of the active atoms with the single-mode optical field and the state of the system in the interaction picture and the rotating-wave approximation are

$$\hat{V}(t) = \hbar g(\hat{a}\hat{\sigma}^+ e^{i(\omega-\Omega)t} + \hat{a}^\dagger \hat{\sigma}^- e^{-i(\omega-\Omega)t}), \quad (\text{A1a})$$

$$|\Psi(t)\rangle = \sum_n A_{n,-}(t)|n, -\rangle + \sum_n A_{n,+}(t)|n, +\rangle, \quad (\text{A1b})$$

where g denotes the atom-cavity photon interaction strength, and \hat{a}^\dagger is the annihilation (creation) operator of the cavity photons. ω and Ω are the cavity-mode frequency and the atom transition frequency, respectively. $|+\rangle$ and $|-\rangle$ denote the excited and ground state of the atom, respectively. The damping of the optical field can be accounted for by the interaction of the radiation field inside the cavity with a reservoir of vacuum modes representing the outside world (modes of the universe) as seen through the partially transmitting mirrors at cavity boundary, or by including a phenomenological decay factor in the in density-matrix approach [18]. This dissipation mechanism will be considered in the later discussions.

At well above threshold, when the quantum fluctuation of the atom states can be neglected, the atomic degrees of freedom are replaced by the average values:

$$\begin{aligned} \hat{V}_p(t) &= \hbar g(\hat{a}\langle\hat{\sigma}^+\rangle e^{i(\omega-\Omega)t} + \hat{a}^\dagger \langle\hat{\sigma}^-\rangle e^{-i(\omega-\Omega)t}) \\ &= \hbar g \sum_n A_{n,+}^*(t) A_{n,-}(t) \hat{a} e^{i(\Omega-\omega)t} \\ &\quad + \hbar g \sum_n A_{n,+}^*(t) A_{n,-}(t) \hat{a}^\dagger e^{i(\omega-\Omega)t}. \end{aligned} \quad (\text{A2})$$

We are interested when the system is on resonance $\omega = \Omega$. Under the resonance condition, the oscillation terms $e^{\pm i(\omega-\Omega)t}$ vanish and the amplitudes are

$$A_{n,+}(t) = B_{n,1} e^{i\sqrt{n+1}gt} + B_{n,2} e^{-i\sqrt{n+1}gt}, \quad (\text{A3a})$$

$$A_{n,-}(t) = C_{n,1} e^{i\sqrt{n}gt} + C_{n,2} e^{-i\sqrt{n}gt}, \quad (\text{A3b})$$

with complex coefficients $B_{n,1}$, $B_{n,2}$, $C_{n,1}$, and $C_{n,2}$. The coefficients in Eq. (A2) become

$$\begin{aligned} &A_{n,+}^*(t) A_{n,-}(t) \\ &= B_{n,1}^* C_{n,1} e^{i(\sqrt{n}-\sqrt{n+1})gt} + B_{n,2}^* C_{n,1} e^{i(\sqrt{n}+\sqrt{n+1})gt} \\ &\quad + B_{n,1}^* C_{n,2} e^{-i(\sqrt{n+1}+\sqrt{n})gt} + B_{n,2}^* C_{n,2} e^{i(\sqrt{n+1}-\sqrt{n})gt}. \end{aligned} \quad (\text{A4})$$

For strongly pumped materials, the average photon number \bar{n} in the cavity is large so that $n \simeq \bar{n}$. Average over a short period $\simeq 1/\bar{n}g$, we have

$$\sum_n \overline{A_{n,+}^*(t)A_{n,-}(t)} = \sum_{n \simeq \bar{n}} B_{n,1}^* C_{n,1} + B_{n,2}^* C_{n,2}. \quad (\text{A5})$$

The overbar denotes a temporal average over the period $1/\bar{n}g$. The effective interaction now takes the following form:

$$\hat{\mathcal{V}}_p(t) = \hbar(\chi \hat{a} e^{i(\omega-\Omega)t} + \chi^* \hat{a}^\dagger e^{-i(\omega-\Omega)t}), \quad (\text{A6})$$

where $\chi \equiv g(\sum_{n \simeq \bar{n}} B_{n,1}^* C_{n,1} + B_{n,2}^* C_{n,2})$.

APPENDIX B: FREQUENCY REPRESENTATION AND REAL-SPACE REPRESENTATION IN THE SCHRÖDINGER PICTURE

To obtain a direct expression of the photonic state in the laboratory frame, here we calculate the state in the Schrödinger picture. It turns out that it is rather involved to transform the state in the interaction picture, Eq. (22), to the Schrödinger picture of the state. Here we employ the dressed operator \hat{A} [Eq. (3b)] that the diagonalized Hamiltonian \hat{H}_0 [Eq. (3b)] to get the final state in the Schrödinger picture. The relation of the state between the two pictures yields

$$|\psi(t)\rangle_S = e^{-i\frac{\hat{H}_0}{\hbar}t} |\psi(t)\rangle_I = e^{-i\frac{\hat{H}_0}{\hbar}t} e^{-\frac{i}{\hbar} \int_0^t dt' \hat{H}_I(t')} |\emptyset\rangle_I = e^{-i\frac{\hat{H}_0}{\hbar}t} e^{-\frac{i}{\hbar} \int_0^t dt' \hat{H}_I(t')} e^{i\frac{\hat{H}_0}{\hbar}t} |\emptyset\rangle_S, \quad (\text{B1})$$

where

$$\begin{aligned} \hat{H}_0 &= \hbar \int d\omega \omega \hat{A}^\dagger(\omega) \hat{A}(\omega), \\ \hat{H}_I(t) &= \Gamma_{0,0} L \int d\omega_1 d\omega_2 e^{-i\omega_p t + i\omega_1 t + i\omega_2 t} \alpha(\omega_1) \alpha(\omega_2) \hat{A}^\dagger(\omega_1) \hat{A}^\dagger(\omega_2) + \text{H.c.} \end{aligned} \quad (\text{B2})$$

Inserting identity operator $\hat{\mathbb{1}} = e^{-i\frac{\hat{H}_0}{\hbar}t} e^{i\frac{\hat{H}_0}{\hbar}t}$ into the evolution operator,

$$\begin{aligned} \hat{U}_S(t) &= e^{-i\frac{\hat{H}_0}{\hbar}t} e^{-\frac{i}{\hbar} \int_0^t dt' \hat{H}_I(t')} e^{i\frac{\hat{H}_0}{\hbar}t} \\ &= e^{-i\frac{\hat{H}_0}{\hbar}t} \left[1 - \frac{i}{\hbar} \int_0^t dt' \hat{H}_I(t') + \frac{1}{2} \left(-\frac{i}{\hbar} \int_0^t dt' \hat{H}_I(t') \right) \left(-\frac{i}{\hbar} \int_0^t dt' \hat{H}_I(t') \right) + \dots \right] e^{i\frac{\hat{H}_0}{\hbar}t} \\ &= 1 + e^{-i\frac{\hat{H}_0}{\hbar}t} \left(-\frac{i}{\hbar} \int_0^t dt' \hat{H}_I(t') \right) e^{i\frac{\hat{H}_0}{\hbar}t} + \frac{1}{2} e^{-i\frac{\hat{H}_0}{\hbar}t} \left(-\frac{i}{\hbar} \int_0^t dt' \hat{H}_I(t') \right) e^{i\frac{\hat{H}_0}{\hbar}t} e^{-i\frac{\hat{H}_0}{\hbar}t} \left(-\frac{i}{\hbar} \int_0^t dt' \hat{H}_I(t') \right) e^{i\frac{\hat{H}_0}{\hbar}t} + \dots \\ &= \exp \left[e^{-i\frac{\hat{H}_0}{\hbar}t} \left(-\frac{i}{\hbar} \int_0^t dt' \hat{H}_I(t') \right) e^{i\frac{\hat{H}_0}{\hbar}t} \right] \end{aligned} \quad (\text{B3})$$

The exponent of the time-evolution operator in the Schrödinger picture now becomes

$$\begin{aligned} \ln[\hat{U}_S(t)] &= e^{-i\frac{\hat{H}_0}{\hbar}t} \left(-\frac{i}{\hbar} \int_0^t dt' \hat{H}_I(t') \right) e^{i\frac{\hat{H}_0}{\hbar}t} \\ &= -\frac{i\Gamma_{0,0}L}{\hbar} \int_0^t dt' \int d\omega_1 d\omega_2 e^{-i\omega_p t' + i\omega_1(t'-t) + i\omega_2(t'-t)} \alpha(\omega_1) \alpha(\omega_2) \hat{A}^\dagger(\omega_1) \hat{A}^\dagger(\omega_2) - \text{H.c.} \\ &= \frac{i\Gamma_{0,0}L e^{-i\omega_p t}}{\hbar} \int_0^t dt' \int d\omega_1 d\omega_2 e^{i(\omega_p - \omega_1 - \omega_2)t'} \alpha(\omega_1) \alpha(\omega_2) \hat{A}^\dagger(\omega_1) \hat{A}^\dagger(\omega_2) - \text{H.c.} \\ &= \frac{i\Gamma_{0,0}L e^{-i\omega_p t}}{\hbar} \int_0^t dt' \int d\omega_1 d\omega_2 e^{i(\omega_p - \omega_1 - \omega_2)t'} \alpha(\omega_1) \alpha(\omega_2) \left[\alpha^*(\omega_1) \hat{a}^\dagger + \int d\eta_1 \beta^*(\omega_1, \eta_1) \hat{c}_{\eta_1}^\dagger \right] \\ &\quad \times \left[\alpha^*(\omega_2) \hat{a}^\dagger + \int d\eta_2 \beta^*(\omega_2, \eta_2) \hat{c}_{\eta_2}^\dagger \right] - \text{H.c.} \\ &= \xi^S \hat{a}^\dagger \hat{a}^\dagger + \int d\eta f_\eta^S \hat{a}^\dagger \hat{c}_\eta^\dagger + \int d\eta_1 d\eta_2 \phi_{\eta_1, \eta_2}^S \hat{c}_{\eta_1}^\dagger \hat{c}_{\eta_2}^\dagger - \text{H.c.} \end{aligned} \quad (\text{B4})$$

(1) The first term contains two cavity-mode photons,

$$\begin{aligned}
 \ln[\hat{U}_S(t)]_1 &= \frac{i\Gamma_{0,0}Le^{-i\omega_p t}}{\hbar} \int_0^t dt' \int d\omega_1 d\omega_2 e^{i(\omega_p - \omega_1 - \omega_2)t'} |\alpha(\omega_1)|^2 |\alpha(\omega_2)|^2 \hat{a}^\dagger \hat{a}^\dagger - \text{H.c.} \\
 &= \frac{i\Gamma_{0,0}Le^{-i\omega_p t}}{\hbar} \int_0^t dt' e^{-\pi V^2 t'} \times e^{-\pi V^2 t'} \hat{a}^\dagger \hat{a}^\dagger - \text{H.c.} \\
 &= \frac{i\Gamma_{0,0}Le^{-i2\omega_0 t}}{2\pi \hbar V^2} \hat{a}^\dagger \hat{a}^\dagger - \text{H.c.} \\
 &= \xi^S \hat{a}^\dagger \hat{a}^\dagger - \text{H.c.}
 \end{aligned}$$

where

$$\xi^S = \frac{i\Gamma_{0,0}Le^{-i2\omega_0 t}}{2\pi \hbar V^2} = \frac{i\kappa e^{-i2\omega_0 t}}{2\pi}.$$

(2) The second term contains both cavity-mode operator and free-space operator,

$$\begin{aligned}
 \ln[\hat{U}_S(t)]_2 &= \frac{i\Gamma_{0,0}Le^{-i\omega_p t}}{\hbar} \int_0^t dt' \int d\omega_1 d\omega_2 e^{i(\omega_p - \omega_1 - \omega_2)t'} \alpha(\omega_1) \alpha(\omega_2) \\
 &\quad \times \int d\eta [\alpha^*(\omega_1) \beta^*(\omega_2, \eta) + \alpha^*(\omega_2) \beta^*(\omega_1, \eta)] \hat{a}^\dagger \hat{c}_\eta^\dagger - \text{H.c.} \\
 &= \frac{2i\Gamma_{0,0}Le^{-i\omega_p t}}{\hbar} \int_0^t dt' \int d\omega_1 e^{i(\omega_0 - \omega_1)t'} |\alpha(\omega_1)|^2 \int d\omega_2 d\eta e^{i(\omega_0 - \omega_2)t'} \alpha(\omega_2) \beta^*(\omega_2, \eta) \hat{a}^\dagger \hat{c}_\eta^\dagger - \text{H.c.} \\
 &= \frac{2i\Gamma_{0,0}Le^{-i\omega_p t}}{\hbar} \int_0^t dt' e^{-\pi V^2 t'} \int d\eta \frac{V}{\eta - \omega_0 + i\pi V^2} [e^{i(\omega_0 - \eta)t'} - e^{-\pi V^2 t'}] \hat{a}^\dagger \hat{c}_\eta^\dagger - \text{H.c.} \\
 &= \frac{-i\Gamma_{0,0}Le^{-i2\omega_0 t}}{\pi \hbar V} \int d\eta \frac{1}{\eta - \omega_0 - i\pi V^2} \hat{a}^\dagger \hat{c}_\eta^\dagger - \text{H.c.} \\
 &= \int d\eta f_\eta^S \hat{a}^\dagger \hat{c}_\eta^\dagger - \text{H.c.}, \tag{B5}
 \end{aligned}$$

where

$$f_\eta^S = \frac{-i\Gamma_{0,0}Le^{-i2\omega_0 t}}{\pi \hbar V} \frac{1}{\eta - \omega_0 - i\pi V^2} = \frac{-i\kappa e^{-i2\omega_0 t}}{\pi} \frac{V}{\eta - \omega_0 - i\pi V^2}.$$

(3) The third term contains only the free-space operator,

$$\begin{aligned}
 \ln[\hat{U}_S(t)]_3 &= \frac{i\Gamma_{0,0}Le^{-i\omega_p t}}{\hbar} \int_0^t dt' \int d\omega_1 d\omega_2 e^{i(\omega_p - \omega_1 - \omega_2)t'} \alpha(\omega_1) \alpha(\omega_2) \int d\eta_1 d\eta_2 \beta^*(\omega_1, \eta_1) \beta^*(\omega_2, \eta_2) \hat{c}_{\eta_1}^\dagger \hat{c}_{\eta_2}^\dagger - \text{H.c.} \\
 &= \frac{i\Gamma_{0,0}Le^{-i\omega_p t}}{\hbar} \int_0^t dt' \left[\int d\omega_1 d\eta_1 e^{i(\omega_0 - \omega_1)t'} \alpha(\omega_1) \beta^*(\omega_1, \eta_1) \hat{c}_{\eta_1}^\dagger \right] \left[\int d\omega_2 d\eta_2 e^{i(\omega_0 - \omega_2)t'} \alpha(\omega_2) \beta^*(\omega_2, \eta_2) \hat{c}_{\eta_2}^\dagger \right] - \text{H.c.} \\
 &= \frac{i\Gamma_{0,0}Le^{-i\omega_p t}}{\hbar} \int d\eta_1 d\eta_2 \int_0^t dt' \frac{V^2}{(\eta_1 - \omega_0 + i\pi V^2)(\eta_2 - \omega_0 + i\pi V^2)} [e^{i(\omega_0 - \eta_1)t'} - e^{-\pi V^2 t'}] \\
 &\quad \times [e^{i(\omega_0 - \eta_2)t'} - e^{-\pi V^2 t'}] \hat{c}_{\eta_1}^\dagger \hat{c}_{\eta_2}^\dagger - \text{H.c.} \\
 &= \frac{i\Gamma_{0,0}Le^{-2i\omega_0 t}}{\hbar} \int d\eta_1 d\eta_2 \frac{V^2}{(\eta_1 - \omega_0 + i\pi V^2)(\eta_2 - \omega_0 + i\pi V^2)} \\
 &\quad \times \left[\pi \delta(2\omega_0 - \eta_1 - \eta_2) + iP \frac{1}{2\omega_0 - \eta_1 - \eta_2} + \frac{i}{\eta_1 - \omega_0 - i\pi V^2} + \frac{i}{\eta_2 - \omega_0 - i\pi V^2} + \frac{1}{2\pi V^2} \right] \hat{c}_{\eta_1}^\dagger \hat{c}_{\eta_2}^\dagger - \text{H.c.} \\
 &= \int d\eta_1 d\eta_2 \phi_{\eta_1, \eta_2}^S \hat{c}_{\eta_1}^\dagger \hat{c}_{\eta_2}^\dagger - \text{H.c.}, \tag{B6}
 \end{aligned}$$

where

$$\begin{aligned}
 \phi_{\eta_1, \eta_2}^S &= \frac{i\Gamma_{0,0}Le^{-2i\omega_0 t}}{\hbar} \frac{V^2}{(\eta_1 - \omega_0 + i\pi V^2)(\eta_2 - \omega_0 + i\pi V^2)} \\
 &\quad \times \left[\pi \delta(2\omega_0 - \eta_1 - \eta_2) + iP \frac{1}{2\omega_0 - \eta_1 - \eta_2} + \frac{i}{\eta_1 - \omega_0 - i\pi V^2} + \frac{i}{\eta_2 - \omega_0 - i\pi V^2} + \frac{1}{2\pi V^2} \right]
 \end{aligned}$$

$$\begin{aligned}
 &= ikV^2 e^{-2i\omega_0 t} \frac{V^2}{(\eta_1 - \omega_0 + i\pi V^2)(\eta_2 - \omega_0 + i\pi V^2)} \\
 &\times \left[\pi \delta(2\omega_0 - \eta_1 - \eta_2) + iP \frac{1}{2\omega_0 - \eta_1 - \eta_2} + \frac{i}{\eta_1 - \omega_0 - i\pi V^2} + \frac{i}{\eta_2 - \omega_0 - i\pi V^2} + \frac{1}{2\pi V^2} \right].
 \end{aligned}$$

To better understand the state, we perform the Fourier transform [$\hat{c}_\eta^\dagger = \frac{1}{\sqrt{2\pi v_g}} \int_{-\infty}^{\infty} dx e^{inx/v_g} \hat{c}^\dagger(x)$] to get the wave function in the real-space representation.

For the second term $\int d\eta f_\eta^S \hat{a}^\dagger \hat{c}_\eta^\dagger$:

$$\begin{aligned}
 \int d\eta f_\eta^S \hat{a}^\dagger \hat{c}_\eta^\dagger - \text{H.c.} &= \frac{2i\Gamma_{0,0} L e^{-i2\omega_0 t}}{\hbar} \int d\eta \frac{V}{\eta - \omega_0 + i\pi V^2} \left[\frac{e^{i(\omega_0 - \eta)t - \pi V^2 t} - 1}{i(\omega_0 - \eta) - \pi V^2} + \frac{e^{-2\pi V^2 t} - 1}{2\pi V^2} \right] \hat{a}^\dagger \hat{c}_\eta^\dagger - \text{H.c.} \\
 &= \frac{2i\Gamma_{0,0} L e^{-i\omega_0 t}}{\hbar} \hat{a}^\dagger \int d\eta \frac{V}{\eta - \omega_0 + i\pi V^2} \left[\frac{e^{-i\eta t} - e^{-i\omega_0 t}}{i(\omega_0 - \eta) - \pi V^2} + \frac{e^{-i\omega_0 t - 2\pi V^2 t} - e^{-i\omega_0 t}}{2\pi V^2} \right] \hat{c}_\eta^\dagger - \text{H.c.} \\
 &= \frac{2i\Gamma_{0,0} L e^{-i\omega_0 t}}{\sqrt{2\pi v_g} \hbar} \hat{a}^\dagger \int dx \int d\eta \frac{V e^{inx/v_g}}{\eta - \omega_0 + i\pi V^2} \left[\frac{e^{-i\eta t} - e^{-i\omega_0 t}}{i(\omega_0 - \eta) - \pi V^2} + \frac{e^{-i\omega_0 t - 2\pi V^2 t} - e^{-i\omega_0 t}}{2\pi V^2} \right] \hat{c}^\dagger(x) - \text{H.c.} \\
 &= \frac{2i\Gamma_{0,0} L e^{-i\omega_0 t}}{\sqrt{2\pi v_g} \hbar} \hat{a}^\dagger \int dx \left[\frac{i}{V} e^{i\omega_0(x/v_g - t) - \pi V^2 t - \pi V^2 |x/v_g - t|} + \frac{-i}{V} e^{i\omega_0(x/v_g - t) - \pi V^2 |x|} \right. \\
 &\quad \left. + \frac{-i}{V} e^{i\omega_0(x/v_g - t) - \pi V^2(2t - x)} \Theta(-x) + \frac{i}{V} e^{i\omega_0(x/v_g - t) + \pi V^2 x} \Theta(-x) \right] \hat{c}^\dagger(x) - \text{H.c.} \\
 &= \frac{2i\Gamma_{0,0} L e^{-i\omega_0 t}}{\sqrt{2\pi v_g} \hbar} \hat{a}^\dagger \int dx \left[\frac{i}{V} e^{i\omega_0(x/v_g - t) - \pi V^2 t - \pi V^2 |x/v_g - t|} + \frac{-i}{V} e^{i\omega_0(x/v_g - t) - \pi V^2 |x|} \right] \Theta(x) \hat{c}^\dagger(x) - \text{H.c.} \\
 &= \frac{2i\Gamma_{0,0} L e^{-i\omega_0 t}}{\sqrt{2\pi v_g} \hbar} \hat{a}^\dagger \int dx \frac{-i}{V} e^{i\omega_0(x/v_g - t) - \pi V^2 x} [1 - e^{-\pi V^2(t - x/v_g) - \pi V^2 |t - x/v_g|}] \Theta(x) \hat{c}^\dagger(x) - \text{H.c.} \\
 &\equiv a^\dagger \int dx \bar{f}^S(x, t) \hat{c}^\dagger(x) - \text{H.c.}, \tag{B7}
 \end{aligned}$$

where

$$\begin{aligned}
 \bar{f}^S(x, t) &= \frac{2\Gamma_{0,0} L e^{-i\omega_0 t}}{\sqrt{2\pi v_g} \hbar V} e^{i\omega_0(x/v_g - t) - \pi V^2 x/v_g} [1 - e^{-\pi V^2(t - x/v_g) - \pi V^2 |t - x/v_g|}] \Theta(x) \\
 &= \frac{2\Gamma_{0,0} L e^{-i\omega_0 t}}{\sqrt{2\pi v_g} \hbar V} e^{i\omega_0(x/v_g - t) - \pi V^2 x/v_g} [1 - e^{-2\pi V^2(t - x/v_g)}] \Theta(x) \Theta(t - x/v_g) \tag{B8}
 \end{aligned}$$

$$\begin{aligned}
 &\approx \frac{2\Gamma_{0,0} L e^{-i\omega_0 t}}{\sqrt{2\pi v_g} \hbar V} e^{i\omega_0(x/v_g - t) - \pi V^2 x/v_g} \Theta(x) \quad (t \rightarrow \infty) \\
 &= \frac{2\kappa V e^{-i\omega_0 t}}{\sqrt{2\pi v_g}} e^{i\omega_0(x/v_g - t) - \pi V^2 x/v_g} \Theta(x) \quad (t \rightarrow \infty). \tag{B9}
 \end{aligned}$$

For the third term $\int d\eta_1 d\eta_2 \phi_{\eta_1, \eta_2}^S \hat{c}_{\eta_1}^\dagger \hat{c}_{\eta_2}^\dagger$ in Eq. (B4):

$$\begin{aligned}
 &\int d\eta_1 d\eta_2 \phi_{\eta_1, \eta_2}^S \hat{c}_{\eta_1}^\dagger \hat{c}_{\eta_2}^\dagger - \text{H.c.} \\
 &= \frac{1}{2\pi v_g} \int dx_1 dx_2 \int d\eta_1 d\eta_2 \phi_{\eta_1, \eta_2}^S e^{i\eta_1 x_1/v_g + i\eta_2 x_2/v_g} \hat{c}^\dagger(x_1) \hat{c}^\dagger(x_2) - \text{H.c.} \\
 &= \frac{ikV^2}{2\pi v_g} \int dx_1 dx_2 \int d\eta_1 d\eta_2 \frac{V^2 e^{-2i\omega_0 t + i\eta_1 x_1/v_g + i\eta_2 x_2/v_g}}{(\eta_1 - \omega_0 + i\pi V^2)(\eta_2 - \omega_0 + i\pi V^2)} \\
 &\quad \times \left[\pi \delta(2\omega_0 - \eta_1 - \eta_2) + iP \frac{1}{2\omega_0 - \eta_1 - \eta_2} + \frac{i}{\eta_1 - \omega_0 - i\pi V^2} + \frac{i}{\eta_2 - \omega_0 - i\pi V^2} + \frac{1}{2\pi V^2} \right] \hat{c}^\dagger(x_1) \hat{c}^\dagger(x_2) - \text{H.c.}
 \end{aligned}$$

$$\begin{aligned}
 &= \frac{i\kappa V^2}{2\pi v_g} \int dx_1 dx_2 \int d\eta_1 \frac{e^{-2i\omega_0 t + i\eta_1 x_1 / v_g}}{\eta_1 - \omega_0 + i\pi V^2} \left\{ \frac{-\pi V^2 e^{i(2\omega_0 - \eta_1)x_2 / v_g}}{\eta_1 - \omega_0 - i\pi V^2} + \frac{-\pi V^2 e^{i(2\omega_0 - \eta_1)x_2 / v_g}}{\eta_1 - \omega_0 - i\pi V^2} \Theta(x_2) \right. \\
 &+ \frac{\pi V^2 e^{i(2\omega_0 - \eta_1)x_2 / v_g}}{\eta_1 - \omega_0 - i\pi V^2} \Theta(-x_2) + \frac{-2\pi V^2 e^{i(\omega_0 - i\pi V^2)x_2 / v_g}}{\eta_1 - \omega_0 - i\pi V^2} \Theta(-x_2) + \frac{2\pi V^2 e^{i(\omega_0 - i\pi V^2)x_2 / v_g}}{\eta_1 - \omega_0 - i\pi V^2} \Theta(-x_2) \\
 &\left. + i e^{i\omega_0 x_2 / v_g - \pi V^2 |x_2| / v_g} - i e^{i\omega_0 x_2 / v_g + \pi V^2 x_2 / v_g} \Theta(-x_2) \right\} \hat{c}^\dagger(x_1) \hat{c}^\dagger(x_2) - \text{H.c.} \\
 &= \frac{i\kappa V^2}{2\pi v_g} \int dx_1 dx_2 \int d\eta_1 \frac{e^{-2i\omega_0 t + i\eta_1 x_1 / v_g}}{\eta_1 - \omega_0 + i\pi V^2} \left\{ \frac{-2\pi V^2 e^{i(2\omega_0 - \eta_1)x_2 / v_g}}{\eta_1 - \omega_0 - i\pi V^2} \Theta(x_2) + i e^{i\omega_0 x_2 / v_g - \pi V^2 x_2 / v_g} \Theta(x_2) \right\} \hat{c}^\dagger(x_1) \hat{c}^\dagger(x_2) - \text{H.c.} \\
 &= \frac{i\kappa V^2}{2\pi v_g} \int dx_1 dx_2 \left[-2\pi e^{i2\omega_0(\frac{x_1+x_2}{2v_g} - t) - \pi V^2 |x_1 - x_2| / v_g} \Theta(x_2) + 2\pi e^{i2\omega_0(\frac{x_1+x_2}{2v_g} - t) + \pi V^2 (x_1 - x_2) / v_g} \Theta(x_2) \Theta(-x_1) \right] \hat{c}^\dagger(x_1) \hat{c}^\dagger(x_2) - \text{H.c.} \\
 &= -\frac{i\kappa V^2}{v_g} \int dx_1 dx_2 e^{i2\omega_0(\frac{x_1+x_2}{2v_g} - t) - \pi V^2 |x_1 - x_2| / v_g} \Theta(x_1) \Theta(x_2) \hat{c}^\dagger(x_1) \hat{c}^\dagger(x_2) - \text{H.c.} \\
 &\equiv \int dx_1 dx_2 \bar{\phi}^S(x_1, x_2) \hat{c}^\dagger(x_1) \hat{c}^\dagger(x_2) - \text{H.c.}, \tag{B10}
 \end{aligned}$$

where

$$\bar{\phi}^S(x_1, x_2, t) = -\frac{i\kappa V^2}{v_g} e^{i2\omega_0(\frac{x_1+x_2}{2v_g} - t) - \pi V^2 |x_1 - x_2| / v_g} \Theta(x_1) \Theta(x_2). \tag{B11}$$

In the above calculation, the large- t limit is also taken. $\Theta(x)$ factors are contributed by the last four terms of the wave function in the frequency domain. Figure 5 plots the probability distribution of the two-photon dimer state.

In the real-space domain, state of the system is

$$|\psi(t)\rangle_S = \exp \left[\xi^S \hat{a}^\dagger \hat{a}^\dagger + \int dx \bar{f}^S(x, t) \hat{a}^\dagger \hat{c}^\dagger(x) + \int dx_1 dx_2 \bar{\phi}^S(x_1, x_2, t) \hat{c}^\dagger(x_1) \hat{c}^\dagger(x_2) - \text{H.c.} \right] |\emptyset\rangle, \tag{B12}$$

where

$$\begin{aligned}
 \xi^S &= \frac{i\kappa e^{-i2\omega_0 t}}{2\pi}, \\
 \bar{f}^S(x, t) &= \frac{2\kappa V e^{-i\omega_0 t}}{\sqrt{2\pi} v_g} e^{i\omega_0(x/v_g - t) - \pi V^2 x / v_g} \Theta(x), \\
 \bar{\phi}^S(x_1, x_2, t) &= -\frac{i\kappa V^2}{v_g} e^{i2\omega_0(\frac{x_1+x_2}{2v_g} - t) - \pi V^2 |x_1 - x_2| / v_g} \Theta(x_1) \Theta(x_2).
 \end{aligned}$$

APPENDIX C: CORRELATION FUNCTIONS IN THE INTERACTION PICTURE

In this section, we discuss the correlation functions calculated in the interaction picture. As the physically measurable quantities are identical in different pictures, we expect the same result in this section as we calculated in the Schrödinger's picture.

1. Interaction picture (frequency domain)

In the interaction picture, the state is

$$\begin{aligned}
 |\psi\rangle &= e^{\xi \hat{a}^\dagger \hat{a}^\dagger + \int d\eta f_\eta \hat{a}^\dagger \hat{c}_\eta^\dagger + \int d\eta_1 d\eta_2 \phi_{\eta_1, \eta_2} \hat{c}_{\eta_1}^\dagger \hat{c}_{\eta_2}^\dagger} - \text{H.c.} |\emptyset\rangle \\
 &= e^{\hat{F}^\dagger - \hat{F}} |\emptyset\rangle,
 \end{aligned}$$

where $\hat{F}^\dagger = \xi \hat{a}^\dagger \hat{a}^\dagger + \int d\eta f_\eta \hat{a}^\dagger \hat{c}_\eta^\dagger + \int d\eta_1 d\eta_2 \phi_{\eta_1, \eta_2} \hat{c}_{\eta_1}^\dagger \hat{c}_{\eta_2}^\dagger$. In the experiment, only free-space photons will be measured:

$$\begin{aligned}
 G^{(1)}(t + \tau, t) &= \frac{1}{2\pi} \int dk dk' e^{i\omega_{k'}(t+\tau) - i\omega_k t} \langle \emptyset | e^{\hat{F} - \hat{F}^\dagger} \hat{c}_k^\dagger \hat{c}_k e^{\hat{F}^\dagger - \hat{F}} | \emptyset \rangle, \\
 G^{(2)}(t + \tau, t) &= \left| \frac{1}{2\pi} \int dk_1 dk_2 e^{-i\omega_{k_1}(t+\tau) - i\omega_{k_2} t} \hat{c}_{k_1} \hat{c}_{k_2} e^{\hat{F}^\dagger - \hat{F}} | \emptyset \rangle \right|^2.
 \end{aligned}$$

(1) Here the coefficient $1/2\pi$ does not influence the value of normalized correlation but is important because it makes the photon count $\int dt G^{(1)}(t, t) = 1$ for a one-photon state.

(2) The time variable t in $G^{(2)}(t + \tau, t)$ cannot be chosen as 0 before doing the integration.

If we define $\hat{\varphi}_{\hat{O}}(s) = e^{s(\hat{F}-\hat{F}^\dagger)}\hat{O}e^{s(\hat{F}^\dagger-\hat{F})}$, and let $\hat{\varphi}_{\hat{O}} = \hat{\varphi}_{\hat{O}}(1)$. Inserting the identity operator $\hat{1} = e^{\hat{F}-\hat{F}^\dagger}e^{\hat{F}^\dagger-\hat{F}}$,

$$G^{(1)}(t+\tau, t) = \frac{1}{2\pi} \int dk dk' e^{i\omega_{k'}(t+\tau) - i\omega_k t} \langle \emptyset | \hat{\varphi}_{\hat{c}_k} \hat{\varphi}_{\hat{c}_k} | \emptyset \rangle,$$

$$G^{(2)}(t+\tau, t) = \left| \frac{1}{2\pi} \int dk_1 dk_2 e^{-i\omega_{k_1}(t+\tau) - i\omega_{k_2} t} \hat{\varphi}_{\hat{c}_{k_1}} \hat{\varphi}_{\hat{c}_{k_2}} | \emptyset \rangle \right|^2.$$

Based on the experience in previous calculation, we may guess that $\hat{\varphi}_{\hat{c}_k}$ is a linear combination of \hat{c}_k , \hat{c}_k^\dagger , \hat{a} , and \hat{a}^\dagger . Once we get the form of $\hat{\varphi}_{\hat{c}_k}$ operator, we can use it to calculate the $g^{(2)}$ function. Similar to the previous calculation, first differentiate s ,

$$\frac{d}{ds} \hat{\varphi}_{\hat{O}}(s) = e^{s(\hat{F}-\hat{F}^\dagger)} [\hat{O}, \hat{F}^\dagger - \hat{F}] e^{s(\hat{F}^\dagger-\hat{F})}. \quad (C1)$$

Using the following commutation relations:

$$\begin{aligned} [\hat{c}_k, \hat{F}^\dagger - \hat{F}] &= f_k \hat{a}^\dagger + \int d\eta (2\phi_{\eta,k}) \hat{c}_\eta^\dagger, \\ [\hat{c}_k^\dagger, \hat{F}^\dagger - \hat{F}] &= f_k^* \hat{a} + \int d\eta (2\phi_{\eta,k}^*) \hat{c}_\eta, \\ [\hat{a}, \hat{F}^\dagger - \hat{F}] &= 2\xi \hat{a}^\dagger + \int d\eta f_\eta \hat{c}_\eta^\dagger, \\ [\hat{a}^\dagger, \hat{F}^\dagger - \hat{F}] &= 2\xi^* \hat{a} + \int d\eta f_\eta^* \hat{c}_\eta, \end{aligned} \quad (C2)$$

we have a set of differential equations for $\hat{\varphi}_{\hat{O}}(s)$ operators,

$$\begin{aligned} \frac{d}{ds} \hat{\varphi}_{\hat{c}_k}(s) &= f_k \hat{\varphi}_{\hat{a}^\dagger}(s) + \int d\eta (2\phi_{\eta,k}) \hat{\varphi}_{\hat{c}_\eta^\dagger}(s), \\ \frac{d}{ds} \hat{\varphi}_{\hat{c}_k^\dagger}(s) &= f_k^* \hat{\varphi}_{\hat{a}}(s) + \int d\eta (2\phi_{\eta,k}^*) \hat{\varphi}_{\hat{c}_\eta}(s), \\ \frac{d}{ds} \hat{\varphi}_{\hat{a}}(s) &= 2\xi \hat{\varphi}_{\hat{a}^\dagger}(s) + \int d\eta f_\eta \hat{\varphi}_{\hat{c}_\eta^\dagger}(s), \\ \frac{d}{ds} \hat{\varphi}_{\hat{a}^\dagger}(s) &= 2\xi^* \hat{\varphi}_{\hat{a}}(s) + \int d\eta f_\eta^* \hat{\varphi}_{\hat{c}_\eta}(s). \end{aligned} \quad (C3)$$

The first-order differential equations transfer each $\hat{\varphi}_{\hat{O}}$ operator into other operators, which makes it difficult to calculate.

The above calculation is nothing but using the formula

$$e^X Y e^{-X} = Y + [X, Y] + \frac{1}{2!} [X, [X, Y]] + \frac{1}{3!} [X, [X, [X, Y]]] + \dots \quad (C8)$$

In the strong-coupling or weak-pumping limit, notice that ξ , f_k , and $\phi_{\eta,k}$ are all of order $O[\frac{\Gamma_{0,0}L}{\hbar V^2}]$. Then α_k , $\beta_{k,\eta}$, γ , and ζ_η are of order $O[(\Gamma_{0,0}L/\hbar V^2)^2]$. Here we only consider the order of $O[\Gamma_{0,0}L/\hbar V^2]$. Then,

$$\hat{\varphi}_{\hat{c}_k} = \hat{c}_k + \int d\eta (2\phi_{k,\eta}) \hat{c}_\eta^\dagger + f_k \hat{a}^\dagger, \quad (C9)$$

Then we take the second-order differentiation,

$$\begin{aligned} \frac{d^2}{ds^2} \hat{\varphi}_{\hat{c}_k}(s) &= \alpha_k^* \hat{\varphi}_{\hat{a}}(s) + \int d\eta \beta_{k,\eta}^* \hat{\varphi}_{\hat{c}_\eta}(s), \\ \frac{d^2}{ds^2} \hat{\varphi}_{\hat{c}_k^\dagger}(s) &= \alpha_k \hat{\varphi}_{\hat{a}^\dagger}(s) + \int d\eta \beta_{k,\eta} \hat{\varphi}_{\hat{c}_\eta^\dagger}(s), \\ \frac{d^2}{ds^2} \hat{\varphi}_{\hat{a}}(s) &= \gamma^* \hat{\varphi}_{\hat{a}}(s) + \int d\eta \zeta_\eta^* \hat{\varphi}_{\hat{c}_\eta}(s), \\ \frac{d^2}{ds^2} \hat{\varphi}_{\hat{a}^\dagger}(s) &= \gamma \hat{\varphi}_{\hat{a}^\dagger}(s) + \int d\eta \zeta_\eta \hat{\varphi}_{\hat{c}_\eta^\dagger}(s), \end{aligned} \quad (C4)$$

where

$$\begin{aligned} \alpha_k &= 2f_k^* \xi + \int d\eta (2\phi_{\eta,k}^*) f_\eta, \\ \beta_{k,\eta} &= f_k^* f_\eta + \int d\eta' (2\phi_{\eta',k}^*) (2\phi_{\eta',\eta}), \\ \gamma &= |2\xi|^2 + \int d\eta |f_\eta|^2, \\ \zeta_\eta &= 2\xi^* f_\eta + \int d\eta' f_{\eta'}^* (2\phi_{\eta',\eta}). \end{aligned} \quad (C5)$$

In principle, we are able to write arbitrary-order equations. Expanding the $\hat{\varphi}_{\hat{O}}(1)$

$$\hat{\varphi}_{\hat{O}}(1) = \hat{\varphi}_{\hat{O}}(0) + \frac{d}{ds} \hat{\varphi}_{\hat{O}}(0) + \frac{1}{2!} \frac{d^2}{ds^2} \hat{\varphi}_{\hat{O}}(0) + \dots \quad (C6)$$

Using the fact $\hat{\varphi}_{\hat{O}}(0) = \hat{O}$,

$$\begin{aligned} \hat{\varphi}_{\hat{c}_k}(0) &= \hat{c}_k, \\ \frac{d}{ds} \hat{\varphi}_{\hat{c}_k}(0) &= f_k \hat{a}^\dagger + \int d\eta (2\phi_{\eta,k}) \hat{c}_\eta^\dagger, \\ \frac{d^2}{ds^2} \hat{\varphi}_{\hat{c}_k}(0) &= \alpha_k^* \hat{a} + \int d\eta \beta_{k,\eta}^* \hat{c}_\eta, \\ &\vdots \end{aligned}$$

From the above two sets of differential equations, all the odd-order $(1/n!)(d^n/ds^n)\hat{\varphi}_{\hat{c}_k}(0)$ terms are simply a linear combination of \hat{c}_k and \hat{a} , while all the even terms are a linear combination of \hat{c}_k^\dagger and \hat{a}^\dagger . A general form of $\hat{\varphi}_{\hat{c}_k}$ operator can be written as

$$\hat{\varphi}_{\hat{c}_k} = \int d\eta (\Phi_{k,\eta} \hat{c}_\eta + \Psi_{k,\eta} \hat{c}_\eta^\dagger) + \mu_k \hat{a}^\dagger + \lambda_k \hat{a}. \quad (C7)$$

where

$$f_\eta = i \frac{\Gamma_{0,0}L}{\pi \hbar V} \frac{1}{\eta - \omega_0 + i\pi V^2}, \quad \phi_{\eta_1, \eta_2} = -i \frac{\Gamma_{0,0}L}{\hbar} \frac{V^2}{(\eta_1 - \omega_0 - i\pi V^2)(\eta_2 - \omega_0 - i\pi V^2)} \\ \times \left[\pi \delta(\eta_1 + \eta_2 - \omega_p) + iP \frac{1}{\eta_1 + \eta_2 - \omega_p} - \frac{i}{\eta_1 - \omega_0 + i\pi V^2} - \frac{i}{\eta_2 - \omega_0 + i\pi V^2} + \frac{1}{2\pi V^2} \right].$$

The $\hat{\phi}_{\hat{c}_k}$ operator indicates that expected value of annihilation operator is zero:

$$\langle \psi | \hat{c}_k | \psi \rangle = \langle \emptyset | \hat{\phi}_{\hat{c}_k} | \emptyset \rangle = 0,$$

which is because the state is two-photon coherent state. The photons can be in cavity or in free space, and photon number is always even. As the cavity-mode photons cannot be separated, the state is different from $e^{\int d\eta f_\eta \hat{c}_\eta^\dagger + \int d\eta_1 d\eta_2 \phi_{\eta_1, \eta_2} \hat{c}_{\eta_1}^\dagger \hat{c}_{\eta_2}^\dagger - \text{H.c.}} | \emptyset \rangle$, where expected value of annihilation operator is not zero.

This approximation is similar to the expansion of wave function,

$$|\psi\rangle = e^{\xi \hat{a}^\dagger \hat{a}^\dagger + \int d\eta f_\eta \hat{a}^\dagger \hat{c}_\eta^\dagger + \int d\eta_1 d\eta_2 \phi_{\eta_1, \eta_2} \hat{c}_{\eta_1}^\dagger \hat{c}_{\eta_2}^\dagger - \text{H.c.}} | \emptyset \rangle = \left(1 + \xi \hat{a}^\dagger \hat{a}^\dagger + \int d\eta f_\eta \hat{a}^\dagger \hat{c}_\eta^\dagger + \int d\eta_1 d\eta_2 \phi_{\eta_1, \eta_2} \hat{c}_{\eta_1}^\dagger \hat{c}_{\eta_2}^\dagger \right) | \emptyset \rangle. \quad (\text{C10})$$

Here we can use the first-order expansion to calculate $G^{(1)}$. But we have to use the second-order expansion to calculate $G^{(2)}$ to get the same result under our approximation. In the first-order expansion, $G^{(2)}(\tau)$ is only related the ϕ_{η_1, η_2} term and this term is the leading one in the weak-pumping limit. Under our approximation,

$$G^{(1)}(t + \tau, t) = \frac{1}{2\pi} \int dk dk' e^{i\omega_{k'}(t+\tau) - i\omega_k t} \langle \emptyset | \hat{\phi}_{\hat{c}_{k'}} \hat{\phi}_{\hat{c}_k} | \emptyset \rangle \\ = \frac{1}{2\pi} \int dk dk' e^{i\omega_{k'}(t+\tau) - i\omega_k t} \langle \emptyset | \left[\int d\eta' (2\phi_{k', \eta'}^*) \hat{c}_{\eta'} + f_{k'}^* \hat{a} \right] \left[\int d\eta (2\phi_{k, \eta}) \hat{c}_\eta^\dagger + f_k \hat{a}^\dagger \right] | \emptyset \rangle \\ = \langle \emptyset | \left[\int d\eta' \tilde{\phi}_{\eta'}^*(t + \tau) \hat{c}_{\eta'} + \tilde{f}^*(t + \tau) \hat{a} \right] \left[\int d\eta \tilde{\phi}_\eta(t) \hat{c}_\eta^\dagger + \tilde{f}(t) \hat{a}^\dagger \right] | \emptyset \rangle \\ = \int d\eta \tilde{\phi}_\eta^*(t + \tau) \tilde{\phi}_\eta(t) + \tilde{f}^*(t + \tau) \tilde{f}(t), \quad (\text{C11})$$

$$G^{(1)}(t, t) = |\tilde{f}(t)|^2 + \int d\eta |\tilde{\phi}_\eta(t)|^2. \quad (\text{C12})$$

Here we define $\tilde{\phi}_\eta(\tau) = \frac{1}{\sqrt{2\pi}} \int dk e^{-i\omega_k \tau} (2\phi_{k, \eta})$ and $\tilde{f}(\tau) = \frac{1}{\sqrt{2\pi}} \int dk e^{-i\omega_k \tau} f_k$.

$$G^{(2)}(t + \tau, t) = \left| \frac{1}{2\pi} \int dk_1 dk_2 e^{-i\omega_{k_1}(t+\tau) - i\omega_{k_2} t} \hat{\phi}_{\hat{c}_{k_1}} \hat{\phi}_{\hat{c}_{k_2}} | \emptyset \rangle \right|^2 \\ = \left| \frac{1}{2\pi} \int dk_1 dk_2 e^{-i\omega_{k_1}(t+\tau) - i\omega_{k_2} t} \left[\hat{c}_{k_1} + \int d\eta (2\phi_{k_1, \eta}) \hat{c}_\eta^\dagger + f_{k_1} \hat{a}^\dagger \right] \left[\int d\eta (2\phi_{k_2, \eta}) \hat{c}_\eta^\dagger + f_{k_2} \hat{a}^\dagger \right] | \emptyset \rangle \right|^2 \\ = \frac{1}{2\pi} \left| \int d\eta \tilde{\phi}_\eta(t) e^{-i\eta(t+\tau)} \right|^2 + \int d\eta_1 d\eta_2 [|\tilde{\phi}_{\eta_1}(t + \tau)|^2 |\tilde{\phi}_{\eta_2}(t)|^2 + \tilde{\phi}_{\eta_2}^*(t + \tau) \tilde{\phi}_{\eta_1}^*(t) \tilde{\phi}_{\eta_1}(t + \tau) \tilde{\phi}_{\eta_2}(t)] \\ + \int d\eta |\tilde{f}(t + \tau) \tilde{\phi}_\eta(t) + \tilde{f}(t) \tilde{\phi}_\eta(t + \tau)|^2 + 2|\tilde{f}(t + \tau) \tilde{f}(t)|^2 \\ = \frac{1}{2\pi} \left| \int d\eta \tilde{\phi}_\eta(t) e^{-i\eta(t+\tau)} \right|^2 + \left(\int d\eta_1 |\tilde{\phi}_{\eta_1}(t + \tau)|^2 \right) \left(\int d\eta_2 |\tilde{\phi}_{\eta_2}(t)|^2 \right) + \left| \int d\eta \tilde{\phi}_\eta^*(t + \tau) \tilde{\phi}_\eta(t) \right|^2 \\ + |\tilde{f}(t + \tau)|^2 \int d\eta |\tilde{\phi}_\eta(t)|^2 + |\tilde{f}(t)|^2 \int d\eta |\tilde{\phi}_\eta(t + \tau)|^2 + \left(\tilde{f}^*(t) \tilde{f}(t + \tau) \int d\eta \tilde{\phi}_\eta^*(t + \tau) \tilde{\phi}_\eta(t) + \text{H.c.} \right) \\ + 2|\tilde{f}(t + \tau)|^2 |\tilde{f}(t)|^2 \quad (\text{C13})$$

$$= G^{(1)}(t + \tau) G^{(1)}(t) + \frac{1}{2\pi} \left| \int d\eta \tilde{\phi}_\eta(t) e^{-i\eta(t+\tau)} \right|^2 + \left| \int d\eta \tilde{\phi}_\eta^*(t + \tau) \tilde{\phi}_\eta(t) \right|^2 + |\tilde{f}(t + \tau)|^2 |\tilde{f}(t)|^2 \\ + \left(\tilde{f}^*(t) \tilde{f}(t + \tau) \int d\eta \tilde{\phi}_\eta^*(t + \tau) \tilde{\phi}_\eta(t) + \text{H.c.} \right), \quad (\text{C14})$$

$$g^{(2)}(\tau) = \frac{G^{(2)}(t + \tau, t)}{G^{(1)}(t + \tau, t + \tau) G^{(1)}(t, t)}. \quad (\text{C15})$$

To calculate $\tilde{\phi}_\eta(\tau)$ and $\tilde{f}(\tau)$ only terms with singularities on the x axis or the lower half have contributions. Let $\kappa = \Gamma_{0,0}L/\hbar V^2$,

$$\tilde{f}(t) = \frac{1}{\sqrt{2\pi}} \int d\eta e^{-i\eta t} i \frac{\Gamma_{0,0}L}{\pi \hbar V} \frac{1}{\eta - \omega_0 + i\pi V^2} = \frac{2\kappa V}{\sqrt{2\pi}} e^{-i\omega_0 t - \pi V^2 t}. \quad (\text{C16})$$

$\tilde{f}(t)$ is the effect of the ‘‘single-photon part.’’

$$\begin{aligned} \tilde{\phi}_\eta(t) &= -i \frac{2\Gamma_{0,0}L}{\sqrt{2\pi}\hbar} \int dke^{-i\omega_k t} \frac{V^2}{(\omega_k - \omega_0 - i\pi V^2)(\eta - \omega_0 - i\pi V^2)} \\ &\quad \times \left[\pi \delta(\omega_k + \eta - 2\omega_0) + iP \frac{1}{\omega_k + \eta - 2\omega_0} - \frac{i}{\omega_k - \omega_0 + i\pi V^2} - \frac{i}{\eta - \omega_0 + i\pi V^2} + \frac{1}{2\pi V^2} \right] \\ &= -i \frac{2\kappa V^2}{\sqrt{2\pi}} [I_1 + I_2 + I_3 + 0 + 0], \end{aligned}$$

where

$$\begin{aligned} I_1 &= \int dke^{-i\omega_k t} \frac{V^2}{(\omega_k - \omega_0 - i\pi V^2)(\eta - \omega_0 - i\pi V^2)} \pi \delta(\omega_k + \eta - 2\omega_0) = \frac{-\pi V^2}{(\eta - \omega_0)^2 + \pi^2 V^4} e^{-i(2\omega_0 - \eta)t}, \\ I_2 &= \int dke^{-i\omega_k t} \frac{V^2}{(\omega_k - \omega_0 - i\pi V^2)(\eta - \omega_0 - i\pi V^2)} iP \frac{1}{\omega_k + \eta - 2\omega_0} = \frac{-\pi V^2}{(\eta - \omega_0)^2 + \pi^2 V^4} e^{-i(2\omega_0 - \eta)t}, \\ I_3 &= \int dke^{-i\omega_k t} \frac{V^2}{(\omega_k - \omega_0 - i\pi V^2)(\eta - \omega_0 - i\pi V^2)} \frac{-i}{\omega_k - \omega_0 + i\pi V^2} = -i \frac{e^{-i\omega_0 t - \pi V^2 t}}{\eta - \omega_0 - i\pi V^2}. \end{aligned}$$

Here we can see that the first two terms (photon bound state) play an important role in the $\tilde{\phi}_\eta$ function:

$$\tilde{\phi}_\eta(t) = -i \frac{2\kappa V^2}{\sqrt{2\pi}} \left[\frac{-2\pi V^2}{(\eta - \omega_0)^2 + \pi^2 V^4} e^{-i(2\omega_0 - \eta)t} - i \frac{e^{-i\omega_0 t - \pi V^2 t}}{\eta - \omega_0 - i\pi V^2} \right]. \quad (\text{C17})$$

To calculate correlation functions, we need to use the following results,

$$\begin{aligned} \int d\eta \tilde{\phi}_\eta(t) e^{-i\eta(t+\tau)} &= -i \frac{2\kappa V^2}{\sqrt{2\pi}} \int d\eta \left[\frac{-2\pi V^2}{(\eta - \omega_0)^2 + \pi^2 V^4} e^{-i\eta\tau - i2\omega_0 t} - i \frac{e^{-i\omega_0 t - \pi V^2 t - i\eta(t+\tau)}}{\eta - \omega_0 - i\pi V^2} \right] \\ &= -i \frac{2\kappa V^2}{\sqrt{2\pi}} [-2\pi e^{-i\omega_0\tau - \pi V^2|\tau| - i2\omega_0 t} + 0] \\ &= i \frac{4\pi\kappa V^2}{\sqrt{2\pi}} e^{-i\omega_0\tau - \pi V^2|\tau| - i2\omega_0 t}, \end{aligned} \quad (\text{C18})$$

$$\begin{aligned} \int d\eta |\tilde{\phi}_\eta(t)|^2 &= \frac{2\kappa^2 V^4}{\pi} \int d\eta \left[\frac{-2\pi V^2}{(\eta - \omega_0)^2 + \pi^2 V^4} e^{i(2\omega_0 - \eta)t} + i \frac{e^{i\omega_0 t - \pi V^2 t}}{\eta - \omega_0 + i\pi V^2} \right] \\ &\quad \times \left[\frac{-2\pi V^2}{(\eta - \omega_0)^2 + \pi^2 V^4} e^{-i(2\omega_0 - \eta)t} - i \frac{e^{-i\omega_0 t - \pi V^2 t}}{\eta - \omega_0 - i\pi V^2} \right] \\ &= \frac{2\kappa^2 V^4}{\pi} \int d\eta \left[\frac{4\pi^2 V^4}{[(\eta - \omega_0)^2 + \pi^2 V^4]^2} + \frac{2i\pi V^2 e^{i(\omega_0 - \eta)t - \pi V^2 t}}{[(\eta - \omega_0)^2 + \pi^2 V^4](\eta - \omega_0 - i\pi V^2)} \right. \\ &\quad \left. + \frac{-2i\pi V^2 e^{-i(\omega_0 - \eta)t - \pi V^2 t}}{[(\eta - \omega_0)^2 + \pi^2 V^4](\eta - \omega_0 + i\pi V^2)} + \frac{e^{-2\pi V^2 t}}{(\eta - \omega_0)^2 + \pi^2 V^4} \right] \\ &= \frac{2\kappa^2 V^4}{\pi} \left[\frac{2}{V^2} - \frac{e^{-2\pi V^2 t}}{V^2} - \frac{e^{-2\pi V^2 t}}{V^2} - \frac{e^{-2\pi V^2 t}}{V^2} \right] \\ &= \frac{2\kappa^2 V^2}{\pi} (2 - e^{-2\pi V^2 t}), \end{aligned} \quad (\text{C19})$$

$$\begin{aligned}
 \int d\eta \tilde{\phi}_\eta^*(t+\tau) \tilde{\phi}_\eta(t) &= \frac{2\kappa^2 V^4}{\pi} \int d\eta \left[\frac{-2\pi V^2}{(\eta - \omega_0)^2 + \pi^2 V^4} e^{i(2\omega_0 - \eta)(t+\tau)} + i \frac{e^{-i\omega_0(t+\tau) - \pi V^2(t+\tau)}}{\eta - \omega_0 + i\pi V^2} \right] \\
 &\quad \times \left[\frac{-2\pi V^2}{(\eta - \omega_0)^2 + \pi^2 V^4} e^{-i(2\omega_0 - \eta)t} - i \frac{e^{-i\omega_0 t - \pi V^2 t}}{\eta - \omega_0 - i\pi V^2} \right] \\
 &= \frac{2\kappa^2 V^4}{\pi} \left[\frac{2(1 + \pi V^2 |\tau|)}{V^2} e^{i\omega_0 \tau - \pi V^2 |\tau|} - \frac{e^{i\omega_0 \tau - \pi V^2 (2t+\tau)}}{V^2} \times 2 + \frac{e^{i\omega_0 \tau - \pi V^2 (2t+\tau)}}{V^2} \right] \\
 &= \frac{2\kappa^2 V^2}{\pi} \left[2(1 + \pi V^2 |\tau|) - e^{-2\pi V^2 t} \right] e^{i\omega_0 \tau - \pi V^2 |\tau|}. \tag{C20}
 \end{aligned}$$

Using these result, the $G^{(1)}$ and $G^{(2)}$ functions are

$$\begin{aligned}
 G^{(1)}(t+\tau, t) &= \int d\eta \tilde{\phi}_\eta^*(t+\tau) \tilde{\phi}_\eta(t) + \tilde{f}^*(t+\tau) \tilde{f}(t) \\
 &= \frac{2\kappa^2 V^2}{\pi} \left[2(1 + \pi V^2 |\tau|) - e^{-2\pi V^2 t} \right] e^{i\omega_0 \tau - \pi V^2 |\tau|} + \frac{2\kappa^2 V^2}{\pi} e^{i\omega_0 \tau - \pi V^2 (2t+\tau)} \\
 &= \frac{4\kappa^2 V^2}{\pi} (1 + \pi V^2 |\tau|) e^{i\omega_0 \tau - \pi V^2 |\tau|}, \tag{C21}
 \end{aligned}$$

$$G^{(1)}(t, t) = \frac{4\kappa^2 V^2}{\pi}, \tag{C22}$$

$$\begin{aligned}
 G^{(2)}(t+\tau, t) &= G^{(1)}(t+\tau) G^{(1)}(t) + \frac{1}{2\pi} \left| \int d\eta \tilde{\phi}_\eta(t) e^{-i\eta(t+\tau)} \right|^2 + \left| \int d\eta \tilde{\phi}_\eta^*(t+\tau) \tilde{\phi}_\eta(t) \right|^2 + |\tilde{f}(t+\tau)|^2 |\tilde{f}(t)|^2 \\
 &\quad + \left(\tilde{f}^*(t) \tilde{f}(t+\tau) \int d\eta \tilde{\phi}_\eta^*(t+\tau) \tilde{\phi}_\eta(t) + \text{H.c.} \right) \\
 &= \left(\frac{4\kappa^2 V^2}{\pi} \right)^2 + \frac{1}{2\pi} \frac{(4\pi\kappa V^2)^2}{2\pi} e^{-2\pi V^2 |\tau|} + \left(\frac{2\kappa^2 V^2}{\pi} \right)^2 [2(1 + \pi V^2 |\tau|) - e^{-2\pi V^2 t}]^2 e^{-2\pi V^2 |\tau|} \\
 &\quad + \left(\frac{2\kappa^2 V^2}{\pi} \right)^2 e^{-2\pi V^2 (2t+\tau)} + \left(\frac{2\kappa^2 V^2}{\pi} \right)^2 [2(1 + \pi V^2 |\tau|) - e^{-2\pi V^2 t}]^2 e^{-2\pi V^2 (t+\tau)} \\
 &\approx \left(\frac{4\kappa^2 V^2}{\pi} \right)^2 \left[1 + \frac{\pi^2}{4\kappa^2} e^{-2\pi V^2 |\tau|} + (1 + \pi V^2 |\tau|)^2 e^{-2\pi V^2 |\tau|} \right]. \tag{C23}
 \end{aligned}$$

The only difference between these results and the correlation functions in the main text is the v_g factor. Here $G^{(1)}(t)$ is the probability per unit time (t), while $G^{(1)}(x)$ is the probability per unit distance (x). The probability to detect one photon is a constant. The second-order correlation is

$$g^{(2)}(\tau) = 1 + \left[\frac{\pi^2}{4\kappa^2} + (1 + \pi V^2 |\tau|)^2 \right] e^{-2\pi V^2 |\tau|}. \tag{C24}$$

$$g^{(2)}(0) = 2 + \frac{\pi^2}{4\kappa^2}. \tag{C25}$$

Here κ is very small. Then the $\frac{\pi^2}{4\kappa^2} e^{-2\pi V^2 |\tau|}$ term from $\left| \int d\eta \tilde{\phi}_\eta(t) e^{-i\eta(t+\tau)} \right|^2$ dominates the behavior of $g^{(2)}(\tau)$. As mentioned before, the photon bound-state term is a major part in $\tilde{\phi}_\eta(t)$. We can say that $g^{(2)}(\tau)$ exhibits the correlation signatures of the photon bound state component.

2. Interaction picture (real-space domain in the weak-pumping limit)

In the real-space domain in the interaction picture, the state is

$$|\psi\rangle = e^{\xi \hat{a}^\dagger \hat{a}^\dagger + \int d\eta f \eta \hat{a}^\dagger \hat{c}_\eta^\dagger + \int d\eta_1 d\eta_2 \phi_{\eta_1, \eta_2} \hat{c}_{\eta_1}^\dagger \hat{c}_{\eta_2}^\dagger - \text{H.c.}} |\emptyset\rangle = e^{\xi \hat{a}^\dagger \hat{a}^\dagger + \int dx \bar{f}(x) \hat{a}^\dagger \hat{c}^\dagger(x) + \int dx_1 dx_2 \bar{\phi}(x_1, x_2) \hat{c}^\dagger(x_1) \hat{c}^\dagger(x_2) - \text{H.c.}} |\emptyset\rangle, \tag{C26}$$

where

$$\bar{f}(x) = \frac{1}{\sqrt{2\pi v_g}} \int d\eta f_\eta e^{i\eta x} = \frac{1}{\sqrt{2\pi v_g}} 2\kappa V e^{i\frac{\omega_0}{v_g}x + \frac{\pi v^2}{v_g}x} \Theta(-x), \quad (C27)$$

$$\bar{\phi}(x_1, x_2) = \frac{1}{2\pi v_g} \int d\eta_1 d\eta_2 \phi_{\eta_1, \eta_2} e^{i\eta_1 x_1 + i\eta_2 x_2} = \frac{i\kappa V^2}{v_g} e^{i\frac{\omega_0}{v_g}(x_1+x_2) - \frac{\pi v^2}{v_g}|x_1-x_2|} \Theta(-x_1) \Theta(-x_2). \quad (C28)$$

In the weak-pumping limit, the state can be written as

$$|\psi\rangle = |\emptyset\rangle + \left[\xi \hat{a}^\dagger \hat{a}^\dagger + \int dx \bar{f}(x) \hat{a}^\dagger \hat{c}^\dagger(x) + \int dx_1 dx_2 \bar{\phi}(x_1, x_2) \hat{c}^\dagger(x_1) \hat{c}^\dagger(x_2) \right] |\emptyset\rangle, \quad (C29)$$

which contains a one-photon state $\bar{f}(x)$ and a two-photon state $\bar{\phi}(x_1, x_2)$. Obviously we get the similar correlation functions as in the last section:

$$\begin{aligned} G^{(1)}(x) &= |\hat{c}(x)|\psi\rangle|^2 = |\bar{f}(x)|^2 + \int dx_1 |2\bar{\phi}(x, x_1)|^2 \\ &= \frac{2\kappa^2 V^2}{\pi v_g} e^{\frac{2\pi v^2}{v_g}x} \Theta(-x) + \int_{-\infty}^0 dx_1 \frac{4\kappa^2 V^4}{v_g^2} e^{-\frac{2\pi v^2}{v_g}|x-x_1|} \Theta(-x) \Theta(-x_1) \\ &= \frac{2\kappa^2 V^2}{\pi v_g} e^{\frac{2\pi v^2}{v_g}x} \Theta(-x) + \frac{2\kappa^2 V^2}{\pi v_g} (2 - e^{\frac{2\pi v^2}{v_g}x}) \Theta(-x) = \frac{4\kappa^2 V^2}{\pi v_g} \Theta(-x), \\ G^{(2)}(x_1, x_2) &= |\hat{c}(x_1) \hat{c}(x_2)|\psi\rangle|^2 = |2\bar{\phi}(x_1, x_2)|^2 = \frac{4\kappa^2 V^4}{v_g^2} e^{-\frac{2\pi v^2}{v_g}|x_1-x_2|} \Theta(-x_1) \Theta(-x_2), \\ g^{(2)}(x_1 - x_2) &= \frac{G^{(2)}(x_1, x_2)}{G^{(1)}(x_1) G^{(1)}(x_2)} = \frac{\pi^2}{4\kappa^2} e^{-\frac{2\pi v^2}{v_g}|x_1-x_2|}. \end{aligned} \quad (C30)$$

APPENDIX D: CORRELATION FUNCTIONS IN THE SCHRÖDINGER PICTURE

1. Correlation function for intracavity photons

Here we calculate the average photon number inside the cavity. Let $\hat{F}^\dagger = \xi^S \hat{a}^\dagger \hat{a}^\dagger + \int dx \bar{f}^S(x, t) \hat{a}^\dagger \hat{c}^\dagger(x) + \int dx_1 dx_2 \bar{\phi}^S(x_1, x_2, t) \hat{c}^\dagger(x_1) \hat{c}^\dagger(x_2)$, the state of the system. Then,

$$|\psi(t)\rangle_S = \exp \left[\xi^S \hat{a}^\dagger \hat{a}^\dagger + \int dx \bar{f}^S(x, t) \hat{a}^\dagger \hat{c}^\dagger(x) + \int dx_1 dx_2 \bar{\phi}^S(x_1, x_2, t) \hat{c}^\dagger(x_1) \hat{c}^\dagger(x_2) - \text{H.c.} \right] |\emptyset\rangle \quad (D1)$$

can be written as $|\psi(t)\rangle_S = e^{\hat{F}^\dagger - \hat{F}} |\emptyset\rangle$. The average photon number inside the cavity is

$$\bar{n} = \langle \psi(t) | \hat{a}^\dagger \hat{a} | \psi(t) \rangle = \langle \emptyset | e^{\hat{F} - \hat{F}^\dagger} \hat{a}^\dagger e^{\hat{F}^\dagger - \hat{F}} e^{\hat{F} - \hat{F}^\dagger} \hat{a} e^{\hat{F}^\dagger - \hat{F}} | \emptyset \rangle.$$

Expand $e^{\hat{F} - \hat{F}^\dagger} \hat{a} e^{\hat{F}^\dagger - \hat{F}} = \hat{a} + [\hat{F} - \hat{F}^\dagger, \hat{a}] + \frac{1}{2!} [\hat{F} - \hat{F}^\dagger, [\hat{F} - \hat{F}^\dagger, \hat{a}]] + \dots$. The first few terms are computed as follows (here we consider only the weak-pumping limit):

0th term: \hat{a} ;

$$1\text{st term: } [\hat{F} - \hat{F}^\dagger, \hat{a}] = 2\xi^S \hat{a}^\dagger + \int dx \bar{f}^S(x, t) \hat{c}^\dagger(x);$$

2nd term: $[\hat{F} - \hat{F}^\dagger, [\hat{F} - \hat{F}^\dagger, \hat{a}]]$

$$\begin{aligned} &= \left[\hat{F}, 2\xi^S \hat{a}^\dagger + \int dx \bar{f}^S(x, t) \hat{c}^\dagger(x) \right] \\ &= \left(4|\xi^S|^2 + \int dx |\bar{f}^S|^2 \right) \hat{a} + 2\xi^S \int dx (\bar{f}^S)^* \hat{c}(x); \end{aligned}$$

3rd term: $[\hat{F} - \hat{F}^\dagger, [\hat{F} - \hat{F}^\dagger, [\hat{F} - \hat{F}^\dagger, \hat{a}]]]$

$$\begin{aligned} &= \left[-\hat{F}^\dagger, \left(4|\xi^S|^2 + \int dx |\bar{f}^S|^2 \right) \hat{a} + 2\xi^S \int dx (\bar{f}^S)^* \hat{c}(x) \right] \\ &= \left(4|\xi^S|^2 + 2 \int dx |\bar{f}^S|^2 \right) 2\xi^S \hat{a}^\dagger + \left(4|\xi^S|^2 + \int dx |\bar{f}^S|^2 \right) \int dx \bar{f}^S(x, t) \hat{c}^\dagger(x). \end{aligned} \quad (D2)$$

To calculate average photon number, we note that the even-numbered terms can be omitted as $\langle \emptyset | \hat{a}^\dagger \hat{a} | \emptyset \rangle = 0$. Thus,

$$e^{\hat{F}-\hat{F}^\dagger} \hat{a} e^{\hat{F}^\dagger-\hat{F}} | \emptyset \rangle = \left\{ \frac{1}{1!} 2\xi^S + \frac{1}{3!} \left(4|\xi^S|^2 + 2 \int dx |\bar{f}^S|^2 \right) 2\xi^S + \frac{1}{5!} \left(4|\xi^S|^2 + 2 \int dx |\bar{f}^S|^2 \right)^2 2\xi^S + \dots \right\} \hat{a}^\dagger | \emptyset \rangle + \left\{ \frac{1}{1!} + \frac{1}{3!} \left(4|\xi^S|^2 + \int dx |\bar{f}^S|^2 \right) + \frac{1}{5!} \left(4|\xi^S|^2 + \int dx |\bar{f}^S|^2 \right)^2 + \dots \right\} \int dx \bar{f}^S(x, t) \hat{c}^\dagger(x) | \emptyset \rangle. \quad (\text{D3})$$

Using $|\xi^S|^2 = \kappa^2/4\pi^2$ and

$$\int dx |\bar{f}^S|^2 = \int_0^\infty dx \frac{4\kappa^2 V^2}{2\pi v_g} e^{-\frac{2\pi V^2}{v_g} x} = \frac{\kappa^2}{\pi^2}$$

from Eq. (C1), one has

$$\begin{aligned} e^{\hat{F}-\hat{F}^\dagger} \hat{a} e^{\hat{F}^\dagger-\hat{F}} | \emptyset \rangle &= 2\xi^S \left\{ \frac{1}{1!} + \frac{1}{3!} \left(\frac{3\kappa^2}{\pi^2} \right) + \frac{1}{5!} \left(\frac{3\kappa^2}{\pi^2} \right)^2 + \dots \right\} \hat{a}^\dagger | \emptyset \rangle \\ &+ \left\{ \frac{1}{1!} + \frac{1}{3!} \left(\frac{2\kappa^2}{\pi^2} \right) + \frac{1}{5!} \left(\frac{2\kappa^2}{\pi^2} \right)^2 + \dots \right\} \int dx \bar{f}^S(x, t) \hat{c}^\dagger(x) | \emptyset \rangle \\ &= 2\xi^S \frac{\sinh\left(\frac{\sqrt{3}\kappa}{\pi}\right)}{\frac{\sqrt{3}\kappa}{\pi}} \hat{a}^\dagger | \emptyset \rangle + \frac{\sinh\left(\frac{\sqrt{2}\kappa}{\pi}\right)}{\frac{\sqrt{2}\kappa}{\pi}} \int dx \bar{f}^S(x, t) \hat{c}^\dagger(x) | \emptyset \rangle. \end{aligned} \quad (\text{D4})$$

In the above, we have used the relation

$$\sum_{n=0}^{\infty} \frac{\alpha^n}{(2n+1)!} = \frac{\sinh(\sqrt{\alpha})}{\sqrt{\alpha}}.$$

The average intracavity photon number is

$$\langle \psi(t) | \hat{a}^\dagger \hat{a} | \psi(t) \rangle = 4|\xi^S|^2 \left(\frac{\sinh\left(\frac{\sqrt{3}\kappa}{\pi}\right)}{\frac{\sqrt{3}\kappa}{\pi}} \right)^2 + \int dx |\bar{f}^S|^2 \left(\frac{\sinh\left(\frac{\sqrt{2}\kappa}{\pi}\right)}{\frac{\sqrt{2}\kappa}{\pi}} \right)^2 = \frac{1}{3} \sinh^2\left(\frac{\sqrt{3}\kappa}{\pi}\right) + \frac{1}{2} \sinh^2\left(\frac{\sqrt{2}\kappa}{\pi}\right), \quad (\text{D5})$$

which will exponentially increase with a strong pumping power. This growth is expected to saturate when sufficient energy is drawn from the pump so that the assumption of an undepleted pump no longer holds.

2. Beyond the weak-pumping limit

For an arbitrary pumping power beyond the weak-pumping limit, all orders of κ must be considered. Recall the expression for $\hat{\varphi}_c(x)$ operator,

$$\begin{aligned} \hat{\varphi}_c(x_0) &= \int dx \left[e^{i\frac{\omega_0}{v_g}(x_0-x)} \sum_{n=0}^{\infty} \frac{1}{(2n)!} \left(\frac{2\kappa V^2}{v_g} \right)^{2n} F_{2n-1}(x_0, x) \hat{c}(x) + i e^{i\frac{\omega_0}{v_g}(x_0+x)} \sum_{n=0}^{\infty} \frac{1}{(2n+1)!} \left(\frac{2\kappa V^2}{v_g} \right)^{2n+1} F_{2n}(x_0, x) \hat{c}^\dagger(x) \right] \\ &= \int dx [\Phi(x_0, x) \hat{c}(x) + \Psi(x_0, x) \hat{c}^\dagger(x)]. \end{aligned} \quad (\text{D6})$$

$$(\text{D7})$$

First we need to derive a general expression for $F_n(x_0, x)$ function. Let $\Delta = |x - x_0|$ and $\Gamma = \pi V^2$,

$$\begin{aligned} F_n(x_0, x) &= \int dx_1 dx_2 \dots dx_n e^{-\frac{\Gamma}{v_g}|x_0-x_1| - \frac{\Gamma}{v_g}|x_1-x_2| - \dots - \frac{\Gamma}{v_g}|x_n-x|}, \\ F_{-1}(x_0, x) &= \delta(x - x_0), \\ F_0(x_0, x) &= e^{-\frac{\Gamma}{v_g}\Delta}, \\ F_1(x_0, x) &= \left(\frac{v_g}{\Gamma} + \Delta \right) e^{-\frac{\Gamma}{v_g}\Delta}, \\ &\vdots \end{aligned} \quad (\text{D8})$$

for $n \geq 1$,

$$\begin{aligned}
 F_n(x_0, x) &= \int dx_1 \cdots dx_{n-1} e^{-\frac{\Gamma}{v_g}|x_0-x_1|-\frac{\Gamma}{v_g}|x_1-x_2|-\cdots-\frac{\Gamma}{v_g}|x_{n-2}-x_{n-1}|} \int dx_n e^{-\frac{\Gamma}{v_g}(|x_{n-1}-x_n|+|x_n-x|)} \\
 &= \int dx_1 \cdots dx_{n-1} e^{-\frac{\Gamma}{v_g}|x_0-x_1|-\frac{\Gamma}{v_g}|x_1-x_2|-\cdots-\frac{\Gamma}{v_g}|x_{n-1}-x|} \left(\frac{v_g}{\Gamma} + |x_{n-1}-x| \right) \\
 &= \int dx_1 \cdots dx_{n-1} e^{-\frac{\Gamma}{v_g}|x_0-x_1|-\frac{\Gamma}{v_g}|x_1-x_2|-\cdots-\frac{\Gamma}{v_g}|x_{n-1}-x|} \left[\frac{v_g}{\Gamma} + \frac{1}{n}(|x_0-x_1| + \cdots + |x_{n-1}-x|) \right] \\
 &= \left(\frac{v_g}{\Gamma} - \frac{v_g}{n} \frac{d}{d\Gamma} \right) \int dx_1 \cdots dx_{n-1} e^{-\frac{\Gamma}{v_g}|x_0-x_1|-\frac{\Gamma}{v_g}|x_1-x_2|-\cdots-\frac{\Gamma}{v_g}|x_{n-1}-x|}, \\
 F_n(\Delta) &= \left(\frac{v_g}{\Gamma} - \frac{v_g}{n} \frac{d}{d\Gamma} \right) F_{n-1}(\Delta). \tag{D9}
 \end{aligned}$$

Then we get an iteration equation for $F_n(x_0, x)$ function. Given $F_0(\Delta) = e^{-\frac{\Gamma}{v_g}\Delta}$,

$$F_n(\Delta) = \left(\frac{v_g}{\Gamma} - \frac{v_g}{n} \frac{d}{d\Gamma} \right) \left(\frac{v_g}{\Gamma} - \frac{v_g}{n-1} \frac{d}{d\Gamma} \right) \cdots \left(\frac{v_g}{\Gamma} - \frac{v_g}{1} \frac{d}{d\Gamma} \right) e^{-\frac{\Gamma}{v_g}\Delta}. \tag{D10}$$

To avoid the integration in numerical calculation, here I write F_n in the form of

$$F_n(\Delta) = \sum_{k=0}^n a_{k,n} \frac{v_g^n}{\Gamma^k} \frac{d^{n-k}}{d\Gamma^{n-k}} e^{-\frac{\Gamma}{v_g}\Delta}. \tag{D11}$$

The coefficients are given by the following equations:

$$\begin{aligned}
 a_{0,n+1} &= -\frac{1}{n+1} a_{0,n}, & a_{n+1,n+1} &= \frac{2n+1}{n+1} a_{n,n}, \\
 a_{k,n+1} &= \left(1 + \frac{k-1}{n+1} \right) a_{k-1,n} - \frac{1}{n+1} a_{k,n} \quad (1 \leq k \leq n), \tag{D12}
 \end{aligned}$$

with the initial coefficient $a_{0,0} = 1$, we have $a_{0,n} = (-1)^n/n!$ and $a_{n,n} = (2n-1)!!/n!$, but the arbitrary $a_{k,n}$ is numerically calculated in my code. Given a general expression for F_n , $G^{(1)}$ can be written in the following way,

$$\begin{aligned}
 G^{(1)}(x) &= \left| \int dx i e^{i\frac{\omega_0}{v_g}(x_0+x)} \sum_{n=0}^{\infty} \frac{1}{(2n+1)!} \left(\frac{2\kappa V^2}{v_g} \right)^{2n+1} F_{2n}(x_0, x) \hat{c}^\dagger(x) |\emptyset \rangle \right|^2 \\
 &= \left| \int dx e^{i\frac{\omega_0}{v_g}(x_0+x)} \sum_{n=0}^{\infty} \frac{1}{(2n+1)!} \left(\frac{2\kappa V^2}{v_g} \right)^{2n+1} \sum_{k=0}^{2n} a_{k,2n} \frac{-|x-x_0|^{2n-k}}{(\Gamma/v_g)^k} e^{-\frac{\Gamma}{v_g}|x-x_0|} \hat{c}^\dagger(x) |\emptyset \rangle \right|^2 \\
 &= \int dx \left| \sum_{n=0}^{\infty} \frac{1}{(2n+1)!} \left(\frac{2\kappa V^2}{v_g} \right)^{2n+1} \sum_{k=0}^{2n} a_{k,2n} \frac{-|x-x_0|^{2n-k}}{(\Gamma/v_g)^k} \right|^2 e^{-2\frac{\Gamma}{v_g}|x-x_0|} \\
 &= \int dx \left| \sum_{n=0}^{\infty} \frac{1}{(2n+1)!} \left(\frac{2\kappa V^2}{v_g} \right)^{2n+1} \sum_{k=0}^{2n} a_{2n-k,2n} \frac{-|x-x_0|^k}{(\Gamma/v_g)^{2n-k}} \right|^2 e^{-2\frac{\Gamma}{v_g}|x-x_0|} \\
 &= \left(\frac{\Gamma}{v_g} \right)^2 \int_{-\infty}^{\infty} dx \left| \sum_{n=0}^{\infty} \left(\frac{2\kappa V^2}{\Gamma} \right)^{2n+1} \sum_{k=0}^{2n} a_{2n-k,2n} \frac{-\Gamma^k |x-x_0|^k}{v_g^k (2n+1)!} \right|^2 e^{-2\frac{\Gamma}{v_g}|x-x_0|} \\
 &= 2 \frac{\Gamma}{v_g} \int_0^{\infty} dy \left| \sum_{n=0}^{\infty} \frac{\beta^{2n+1}}{(2n+1)!} \sum_{k=0}^{2n} a_{2n-k,2n} (-y)^k \right|^2 e^{-2y} \\
 &= 2 \frac{\Gamma}{v_g} \int_0^{\infty} dy \left| \sum_{k=0}^{\infty} \left(\sum_{n=k/2}^{\infty} \frac{\beta^{2n+1}}{(2n+1)!} a_{2n-k,2n} (-1)^k \right) y^k \right|^2 e^{-2y} \\
 &= 2 \frac{\Gamma}{v_g} \int_0^{\infty} dy \left| \sum_{k=0}^{\infty} c_k^{(1)} y^k \right|^2 e^{-2y} = 2 \frac{\Gamma}{v_g} \sum_{k=0}^{\infty} b_k \left(\int_0^{\infty} dy y^k e^{-2y} \right) = \frac{\Gamma}{v_g} \sum_{k=0}^{\infty} b_k \frac{k!}{2^k}. \tag{D13}
 \end{aligned}$$

Here

$$c_k^{(1)} = \sum_{n=k/2}^{\infty} \frac{\beta^{2n+1}}{(2n+1)!} a_{2n-k,2n} (-1)^k,$$

b_k are the coefficients of the squared polynomial, and $\beta = 2\kappa V^2/\Gamma = 2\kappa/\pi$ is a dimensionless quantity proportion to the electric field of the pumping light. In the last equal sign, we used an integral,

$$\int dx x^n e^x = \left[\sum_{k=0}^n (-1)^{n-k} \frac{n!}{k!} x^k \right] e^x + C, \quad \int_0^{\infty} dy y^k e^{-2y} = \frac{1}{(-2)^{k+1}} \int_0^{\infty} dy y^k e^y = \frac{1}{(-2)^{k+1}} (-1)^{k+1} k! = \frac{k!}{2^{k+1}}. \quad (\text{D14})$$

In the code, we only need to use the iteration equations to get the $a_{k,n}$ coefficients and do the polynomial operations. Below is the $G^1(x)$ (units of Γ/v_g) as a function of β in different pumping scales. In the weak-pumping limit, the G^1 function is proportional to β^2 , which is in agreement with the result in last section. Under the large pumping power, $G^{(1)}$ function grows exponentially with β [$\ln[G^{(1)}(x)] \propto \beta$].

Similarly, we can calculate the two other integrals in the second-order correlation function

$$g^{(2)}(x_0, x'_0) = 1 + \frac{|\int dx \Phi(x_0, x) \Psi(x'_0, x)|^2 + |\int dx \Psi^*(x'_0, x) \Psi(x_0, x)|^2}{[\int dx |\Psi(x_0, x)|^2][\int dx |\Psi(x'_0, x)|^2]}.$$

(a) Define $I_1 = |\int dx \Phi(x_0, x) \Psi(x'_0, x)|^2$

$$\begin{aligned} I_1 &= \left| \int dx \left[e^{i\frac{\omega_0}{v_g}(x_0-x)} \sum_{n=0}^{\infty} \frac{1}{(2n)!} \left(\frac{2\kappa V^2}{v_g} \right)^{2n} F_{2n-1}(x_0, x) \right] \left[e^{i\frac{\omega_0}{v_g}(x'_0+x)} \sum_{m=0}^{\infty} \frac{1}{(2m+1)!} \left(\frac{2\kappa V^2}{v_g} \right)^{2m+1} F_{2m}(x'_0, x) \right] \right|^2 \\ &= \left| \int dx \left[\delta(x-x_0) + \sum_{n=1}^{\infty} \frac{1}{(2n)!} \left(\frac{2\kappa V^2}{v_g} \right)^{2n} \sum_{k=0}^{2n-1} a_{k,2n-1} \frac{(-|x-x_0|)^{2n-1-k}}{(\Gamma/v_g)^k} \right] e^{-\frac{\Gamma}{v_g}|x-x_0|} \right. \\ &\quad \times \left. \left[\sum_{m=0}^{\infty} \frac{1}{(2m+1)!} \left(\frac{2\kappa V^2}{v_g} \right)^{2m+1} \sum_{j=0}^{2m} a_{j,2m} \frac{(-|x-x'_0|)^{2m-j}}{(\Gamma/v_g)^j} \right] e^{-\frac{\Gamma}{v_g}|x-x'_0|} \right|^2 \\ &= \left| \frac{\Gamma}{v_g} \sum_{m=0}^{\infty} \frac{1}{(2m+1)!} \left(\frac{2\kappa V^2}{\Gamma} \right)^{2m+1} \sum_{j=0}^{2m} a_{j,2m} \left(-\frac{\Gamma}{v_g} |x_0-x'_0| \right)^{2m-j} e^{-\frac{\Gamma}{v_g}|x_0-x'_0|} \right. \\ &\quad + \int dx \left[\frac{\Gamma}{v_g} \sum_{n=0}^{\infty} \frac{\beta^{2n}}{(2n)!} \sum_{k=0}^{2n-1} a_{2n-1-k,2n-1} \left(-\frac{\Gamma}{v_g} |x-x_0| \right)^k \right] e^{-\frac{\Gamma}{v_g}|x-x_0|} \\ &\quad \times \left. \left[\frac{\Gamma}{v_g} \sum_{m=0}^{\infty} \frac{\beta^{2m+1}}{(2m+1)!} \sum_{j=0}^{2m} a_{2m-j,2m} \left(-\frac{\Gamma}{v_g} |x-x'_0| \right)^j \right] e^{-\frac{\Gamma}{v_g}|x-x'_0|} \right|^2 \\ &= \left| \frac{\Gamma}{v_g} I_{11} + \int dx \left[\frac{\Gamma}{v_g} \sum_{k=0}^{\infty} \left(\sum_{n=\frac{k+1}{2}}^{\infty} \frac{\beta^{2n}}{(2n)!} a_{2n-1-k,2n-1} \right) \left(-\frac{\Gamma}{v_g} |x-x_0| \right)^k \right] e^{-\frac{\Gamma}{v_g}|x-x_0|} \right. \\ &\quad \times \left. \left[\frac{\Gamma}{v_g} \sum_{j=0}^{\infty} \left(\sum_{m=\frac{j}{2}}^{\infty} \frac{\beta^{2m+1}}{(2m+1)!} a_{2m-j,2m} \right) \left(-\frac{\Gamma}{v_g} |x-x'_0| \right)^j \right] e^{-\frac{\Gamma}{v_g}|x-x'_0|} \right|^2 \\ &= \left(\frac{\Gamma}{v_g} \right)^2 \left| I_{11} + \int dy \left[\sum_{k=0}^{\infty} c_k^{(2)} \left| \frac{\Gamma}{v_g} x_0 - y \right|^k \sum_{j=0}^{\infty} c_j^{(1)} \left| \frac{\Gamma}{v_g} x'_0 - y \right|^j \right] e^{-|\frac{\Gamma}{v_g} x_0 - y| - |\frac{\Gamma}{v_g} x'_0 - y|} \right|^2 \\ &= \left(\frac{\Gamma}{v_g} \right)^2 \left| I_{11} + \sum_{k=0}^{\infty} \sum_{j=0}^{\infty} c_k^{(2)} c_j^{(1)} \int_{-\infty}^{\infty} dy \left| \frac{\Gamma}{v_g} x_0 - y \right|^k \left| \frac{\Gamma}{v_g} x'_0 - y \right|^j e^{-|\frac{\Gamma}{v_g} x_0 - y| - |\frac{\Gamma}{v_g} x'_0 - y|} \right|^2 \\ &= \left(\frac{\Gamma}{v_g} \right)^2 \left| I_{11} + \sum_{k=0}^{\infty} \sum_{j=0}^{\infty} c_k^{(2)} c_j^{(1)} \int_{-\infty}^{\infty} dy |y|^k \left| \frac{\Gamma}{v_g} (x'_0 - x_0) - y \right|^j e^{-|y| - |\frac{\Gamma}{v_g} (x'_0 - x_0) - y|} \right|^2, \end{aligned} \quad (\text{D15})$$

where

$$I_{11} = \sum_{m=0}^{\infty} \frac{\beta^{2m+1}}{(2m+1)!} \sum_{j=0}^{2m} a_{j,2m} \left(-\frac{\Gamma}{v_g} |x_0 - x'_0| \right)^{2m-j} e^{-\frac{\Gamma}{v_g} |x_0 - x'_0|}.$$

Here the coefficients

$$c_k^{(2)} = \sum_{n=\frac{k+1}{2}}^{\infty} \frac{\beta^{2n}}{(2n)!} a_{2n-1-k,2n-1} (-1)^k$$

and

$$c_j^{(1)} = \sum_{m=\frac{j}{2}}^{\infty} \frac{\beta^{2m+1}}{(2m+1)!} a_{2m-j,2m} (-1)^j$$

are functions of β . The integral $\int_{-\infty}^{\infty} dy |y|^k \left| \frac{\Gamma}{v_g} (x'_0 - x_0) - y \right|^j e^{-|y| - \left| \frac{\Gamma}{v_g} (x'_0 - x_0) - y \right|}$ is a function of $(\Gamma/v_g) |x_0 - x'_0|$, and is numerically calculated.

(b) Define $I_2 = \left| \int dx \Psi(x_0, x) \Psi^*(x'_0, x) \right|^2$

$$\begin{aligned} I_2 &= \left| \int dx \left[i e^{i \frac{\epsilon_0}{v_g} (x_0+x)} \sum_{n=0}^{\infty} \frac{1}{(2n+1)!} \left(\frac{2\kappa V^2}{v_g} \right)^{2n+1} F_{2n}(x_0, x) \right] \left[-i e^{-i \frac{\epsilon_0}{v_g} (x'_0+x)} \sum_{m=0}^{\infty} \frac{1}{(2m+1)!} \left(\frac{2\kappa V^2}{v_g} \right)^{2m+1} F_{2m}(x'_0, x) \right] \right|^2 \\ &= \left| \int dx \left[\sum_{n=0}^{\infty} \frac{1}{(2n+1)!} \left(\frac{2\kappa V^2}{v_g} \right)^{2n+1} \sum_{k=0}^{2n} a_{k,2n} \frac{(-|x-x_0|)^{2n-k}}{(\Gamma/v_g)^k} \right] e^{-\frac{\Gamma}{v_g} |x-x_0|} \right. \\ &\quad \times \left. \left[\sum_{m=0}^{\infty} \frac{1}{(2m+1)!} \left(\frac{2\kappa V^2}{v_g} \right)^{2m+1} \sum_{j=0}^{2m} a_{j,2m} \frac{(-|x-x'_0|)^{2m-j}}{(\Gamma/v_g)^j} \right] e^{-\frac{\Gamma}{v_g} |x-x'_0|} \right|^2 \\ &= \left| \int dx \left[\frac{\Gamma}{v_g} \sum_{n=0}^{\infty} \frac{\beta^{2n+1}}{(2n+1)!} \sum_{k=0}^{2n} a_{2n-k,2n} \left(-\frac{\Gamma}{v_g} |x-x_0| \right)^k \right] e^{-\frac{\Gamma}{v_g} |x-x_0|} \right. \\ &\quad \times \left. \left[\frac{\Gamma}{v_g} \sum_{m=0}^{\infty} \frac{\beta^{2m+1}}{(2m+1)!} \sum_{j=0}^{2m} a_{2m-j,2m} \left(-\frac{\Gamma}{v_g} |x-x'_0| \right)^j \right] e^{-\frac{\Gamma}{v_g} |x-x'_0|} \right|^2 \\ &= \left| \int dx \left[\frac{\Gamma}{v_g} \sum_{k=0}^{\infty} \left(\sum_{n=\frac{k}{2}}^{\infty} \frac{\beta^{2n+1}}{(2n+1)!} a_{2n-k,2n} \right) \left(-\frac{\Gamma}{v_g} |x-x_0| \right)^k \right] e^{-\frac{\Gamma}{v_g} |x-x_0|} \right. \\ &\quad \times \left. \left[\frac{\Gamma}{v_g} \sum_{j=0}^{\infty} \left(\sum_{m=\frac{j}{2}}^{\infty} \frac{\beta^{2m+1}}{(2m+1)!} a_{2m-j,2m} \right) \left(-\frac{\Gamma}{v_g} |x-x'_0| \right)^j \right] e^{-\frac{\Gamma}{v_g} |x-x'_0|} \right|^2 \\ &= \left(\frac{\Gamma}{v_g} \right)^2 \left| \int dy \left[\sum_{k=0}^{\infty} c_k^{(1)} \left| \frac{\Gamma}{v_g} x_0 - y \right|^k \sum_{j=0}^{\infty} c_j^{(1)} \left| \frac{\Gamma}{v_g} x'_0 - y \right|^j \right] e^{-\left| \frac{\Gamma}{v_g} x_0 - y \right| - \left| \frac{\Gamma}{v_g} x'_0 - y \right|} \right|^2 \\ &= \left(\frac{\Gamma}{v_g} \right)^2 \left| \sum_{k=0}^{\infty} \sum_{j=0}^{\infty} c_k^{(1)} c_j^{(1)} \int_{-\infty}^{\infty} dy \left| \frac{\Gamma}{v_g} x_0 - y \right|^k \left| \frac{\Gamma}{v_g} x'_0 - y \right|^j e^{-\left| \frac{\Gamma}{v_g} x_0 - y \right| - \left| \frac{\Gamma}{v_g} x'_0 - y \right|} \right|^2 \\ &= \left(\frac{\Gamma}{v_g} \right)^2 \left| \sum_{k=0}^{\infty} \sum_{j=0}^{\infty} c_k^{(1)} c_j^{(1)} \int_{-\infty}^{\infty} dy |y|^k \left| \frac{\Gamma}{v_g} (x'_0 - x_0) - y \right|^j e^{-|y| - \left| \frac{\Gamma}{v_g} (x'_0 - x_0) - y \right|} \right|^2. \end{aligned} \tag{D16}$$

The calculation is similar to I_2 , with the coefficients

$$c_j^{(1)} = \sum_{m=\frac{j}{2}}^{\infty} \frac{\beta^{2m+1}}{(2m+1)!} a_{2m-j,2m} (-1)^j.$$

Based on these results, we are able to numerically calculate the correlation functions.

APPENDIX E: QUADRATURE PROPERTIES

To evaluate the variance and spectrum of quadrature, we first calculate the following quantities:

$$\langle \hat{c}_{\omega_0+\omega}^\dagger, \hat{c}_{\omega_0+\omega'} \rangle = \langle \emptyset | e^{\hat{F}-\hat{F}^\dagger} \hat{c}_{\omega_0+\omega}^\dagger \hat{c}_{\omega_0+\omega'} e^{\hat{F}^\dagger-\hat{F}} | \emptyset \rangle = \langle \emptyset | \hat{\phi}^\dagger(\omega) \hat{\phi}(\omega') | \emptyset \rangle, \quad (\text{E1})$$

where $\hat{F}^\dagger = -2i\kappa V^2 \int d\omega \frac{\Gamma}{\omega^2 + \Gamma^2} \hat{c}_{\omega_0+\omega}^\dagger \hat{c}_{\omega_0-\omega}^\dagger$ and $\hat{\phi}(\omega) = e^{\hat{F}-\hat{F}^\dagger} \hat{c}_{\omega_0+\omega} e^{\hat{F}^\dagger-\hat{F}}$. As the two-photon amplitude contains a δ function in the dimer coherent state, the $\hat{\phi}(\omega)$ operator can be simplified as

$$\hat{\phi}(\eta) = e^{\hat{F}-\hat{F}^\dagger} \hat{c}_{\omega_0+\eta} e^{\hat{F}^\dagger-\hat{F}} = \hat{c}_{\omega_0+\eta} + [\hat{F} - \hat{F}^\dagger, \hat{c}_{\omega_0+\eta}] + \frac{1}{2!} [\hat{F} - \hat{F}^\dagger, [\hat{F} - \hat{F}^\dagger, \hat{c}_{\omega_0+\eta}]] + \dots, \quad (\text{E2})$$

$$[\hat{F} - \hat{F}^\dagger, \hat{c}_{\omega_0+\eta}] = 2i\kappa V^2 \int d\omega \frac{\Gamma}{\omega^2 + \Gamma^2} [\hat{c}_{\omega_0+\omega}^\dagger \hat{c}_{\omega_0-\omega}^\dagger, \hat{c}_{\omega_0+\eta}] = -4i\kappa V^2 \frac{\Gamma}{\eta^2 + \Gamma^2} \hat{c}_{\omega_0-\eta}^\dagger = -2i\beta \frac{\Gamma^2}{\eta^2 + \Gamma^2} \hat{c}_{\omega_0-\eta}^\dagger, \quad (\text{E3})$$

$$[\hat{F} - \hat{F}^\dagger, \hat{c}_{\omega_0-\eta}^\dagger] = 2i\kappa V^2 \int d\omega \frac{\Gamma}{\omega^2 + \Gamma^2} [\hat{c}_{\omega_0+\omega} \hat{c}_{\omega_0-\omega}, \hat{c}_{\omega_0-\eta}^\dagger] = 4i\kappa V^2 \frac{\Gamma}{\eta^2 + \Gamma^2} \hat{c}_{\omega_0+\eta} = 2i\beta \frac{\Gamma^2}{\eta^2 + \Gamma^2} \hat{c}_{\omega_0+\eta}, \quad (\text{E4})$$

where $\beta = 2\kappa/\pi$. Using the above commutator relations,

$$\begin{aligned} \hat{\phi}(\eta) &= \hat{c}_{\omega_0+\eta} - i \left(\frac{2\beta\Gamma^2}{\eta^2 + \Gamma^2} \right) \hat{c}_{\omega_0-\eta}^\dagger + \frac{1}{2!} \left(\frac{2\beta\Gamma^2}{\eta^2 + \Gamma^2} \right)^2 \hat{c}_{\omega_0+\eta} + \frac{1}{3!} (-i) \left(\frac{2\beta\Gamma^2}{\eta^2 + \Gamma^2} \right)^3 \hat{c}_{\omega_0-\eta}^\dagger + \dots \\ &= \hat{c}_{\omega_0+\eta} \left[1 + \frac{1}{2!} \left(\frac{2\beta\Gamma^2}{\eta^2 + \Gamma^2} \right)^2 + \frac{1}{4!} \left(\frac{2\beta\Gamma^2}{\eta^2 + \Gamma^2} \right)^4 + \dots \right] \\ &\quad - i \hat{c}_{\omega_0-\eta}^\dagger \left[\left(\frac{2\beta\Gamma^2}{\eta^2 + \Gamma^2} \right) + \frac{1}{3!} \left(\frac{2\beta\Gamma^2}{\eta^2 + \Gamma^2} \right)^3 + \frac{1}{5!} \left(\frac{2\beta\Gamma^2}{\eta^2 + \Gamma^2} \right)^5 + \dots \right] \\ &= \cosh \left(\frac{2\beta\Gamma^2}{\eta^2 + \Gamma^2} \right) \hat{c}_{\omega_0+\eta} - i \sinh \left(\frac{2\beta\Gamma^2}{\eta^2 + \Gamma^2} \right) \hat{c}_{\omega_0-\eta}^\dagger, \\ \hat{\phi}^\dagger(\eta) &= \cosh \left(\frac{2\beta\Gamma^2}{\eta^2 + \Gamma^2} \right) \hat{c}_{\omega_0+\eta}^\dagger + i \sinh \left(\frac{2\beta\Gamma^2}{\eta^2 + \Gamma^2} \right) \hat{c}_{\omega_0-\eta}. \end{aligned} \quad (\text{E5})$$

In terms of the $\hat{\phi}(\eta)$ operator, the covariances for creation and annihilation operators are given by

$$\begin{aligned} \langle \hat{c}_{\omega_0+\omega}^\dagger, \hat{c}_{\omega_0+\omega'} \rangle &= \langle \emptyset | \hat{\phi}^\dagger(\omega) \hat{\phi}(\omega') | \emptyset \rangle \\ &= i \sinh \left(\frac{2\beta\Gamma^2}{\omega^2 + \Gamma^2} \right) (-i) \sinh \left(\frac{2\beta\Gamma^2}{\omega'^2 + \Gamma^2} \right) \langle \emptyset | \hat{c}_{\omega_0-\omega} \hat{c}_{\omega_0-\omega'}^\dagger | \emptyset \rangle \\ &= \sinh^2 \left(\frac{2\beta\Gamma^2}{\omega^2 + \Gamma^2} \right) \delta(\omega - \omega'), \\ \langle \hat{c}_{\omega_0+\omega}, \hat{c}_{\omega_0+\omega'}^\dagger \rangle &= \cosh^2 \left(\frac{2\beta\Gamma^2}{\omega^2 + \Gamma^2} \right) \delta(\omega - \omega'), \\ \langle \hat{c}_{\omega_0+\omega}, \hat{c}_{\omega_0+\omega'} \rangle &= -i \sinh \left(\frac{2\beta\Gamma^2}{\omega^2 + \Gamma^2} \right) \cosh \left(\frac{2\beta\Gamma^2}{\omega'^2 + \Gamma^2} \right) \delta(\omega + \omega'), \\ \langle \hat{c}_{\omega_0+\omega}^\dagger, \hat{c}_{\omega_0+\omega'}^\dagger \rangle &= i \sinh \left(\frac{2\beta\Gamma^2}{\omega^2 + \Gamma^2} \right) \cosh \left(\frac{2\beta\Gamma^2}{\omega'^2 + \Gamma^2} \right) \delta(\omega + \omega'). \end{aligned} \quad (\text{E6})$$

The normal-ordered quadrature variances with two modes can be computed:

$$\begin{aligned} \langle : \hat{X}_1(\omega_0 + \omega), \hat{X}_1(\omega_0 + \omega') : \rangle &= \frac{1}{4} \left(e^{-i\theta} \langle \hat{c}_{\omega_0+\omega}, \hat{c}_{\omega_0+\omega'} \rangle + e^{i\theta} \langle \hat{c}_{\omega_0+\omega}^\dagger, \hat{c}_{\omega_0+\omega'}^\dagger \rangle + \langle \hat{c}_{\omega_0+\omega}, \hat{c}_{\omega_0+\omega'}^\dagger \rangle + \langle \hat{c}_{\omega_0+\omega'}^\dagger, \hat{c}_{\omega_0+\omega} \rangle \right) \\ &= \frac{1}{4} \left[i(e^{i\theta} - e^{-i\theta}) \sinh \left(\frac{2\beta\Gamma^2}{\omega^2 + \Gamma^2} \right) \cosh \left(\frac{2\beta\Gamma^2}{\omega'^2 + \Gamma^2} \right) \delta(\omega + \omega') + 2 \sinh^2 \left(\frac{2\beta\Gamma^2}{\omega^2 + \Gamma^2} \right) \delta(\omega - \omega') \right] \\ &= \frac{1}{2} \sinh \left(\frac{2\beta\Gamma^2}{\omega^2 + \Gamma^2} \right) \left[-2 \sin \theta \cosh \left(\frac{2\beta\Gamma^2}{\omega'^2 + \Gamma^2} \right) \delta(\omega + \omega') + \sinh \left(\frac{2\beta\Gamma^2}{\omega^2 + \Gamma^2} \right) \delta(\omega - \omega') \right]. \end{aligned} \quad (\text{E7})$$

The normal-ordered variance of the full-bandwidth quadrature and the spectrum are

$$\begin{aligned} \langle : \hat{X}_1, \hat{X}_1 : \rangle &= \int_{-\infty}^{\infty} d\omega \frac{1}{4} \left[-2 \sin \theta \sinh \left(\frac{2\beta\Gamma^2}{\omega^2 + \Gamma^2} \right) \cosh \left(\frac{2\beta\Gamma^2}{\omega^2 + \Gamma^2} \right) + 2 \sinh^2 \left(\frac{2\beta\Gamma^2}{\omega^2 + \Gamma^2} \right) \right] \\ &= \Gamma \int_{-\infty}^{\infty} dx \frac{1}{4} \left[-2 \sin \theta \sinh \left(\frac{2\beta}{x^2 + 1} \right) \cosh \left(\frac{2\beta}{x^2 + 1} \right) + 2 \sinh^2 \left(\frac{2\beta}{x^2 + 1} \right) \right], \end{aligned} \quad (\text{E8})$$

$$:S_1(\omega): = \frac{1}{4} \left[-2 \sin \theta \sinh \left(\frac{2\beta\Gamma^2}{\omega^2 + \Gamma^2} \right) \cosh \left(\frac{2\beta\Gamma^2}{\omega^2 + \Gamma^2} \right) + 2 \sinh^2 \left(\frac{2\beta\Gamma^2}{\omega^2 + \Gamma^2} \right) \right]. \quad (\text{E9})$$

As the coefficient $\int dx \sinh(\frac{2\beta}{x^2+1}) \cosh(\frac{2\beta}{x^2+1}) > 0$, the maximum squeezing occurs in the direction $\theta = \pi/2$ and thus yields the following results:

$$\langle : \hat{X}_1, \hat{X}_1 : \rangle = \Gamma \int_{-\infty}^{\infty} dx \frac{1}{4} \left[-2 \sinh \left(\frac{2\beta}{x^2 + 1} \right) \cosh \left(\frac{2\beta}{x^2 + 1} \right) + 2 \sinh^2 \left(\frac{2\beta}{x^2 + 1} \right) \right] = \Gamma \int_{-\infty}^{\infty} dx \frac{1}{4} (e^{-\frac{4\beta}{x^2+1}} - 1), \quad (\text{E10})$$

$$:S_1(\omega): = \frac{1}{4} \left[-2 \sinh \left(\frac{2\beta\Gamma^2}{\omega^2 + \Gamma^2} \right) \cosh \left(\frac{2\beta\Gamma^2}{\omega^2 + \Gamma^2} \right) + 2 \sinh^2 \left(\frac{2\beta\Gamma^2}{\omega^2 + \Gamma^2} \right) \right] = \frac{1}{4} (e^{-\frac{4\beta\Gamma^2}{\omega^2+\Gamma^2}} - 1), \quad (\text{E11})$$

$$:S_1(0): = \frac{1}{2} \sinh(2\beta) [\sinh(2\beta) - \cosh(2\beta)] = \frac{1}{4} (e^{-4\beta} - 1). \quad (\text{E12})$$

APPENDIX F: COHERENT STATES OF PHOTONIC DIMERS

At well above threshold, the steady-state photon statistical distribution is Poissonian, and the state of the optical field of the laser output is a coherent state [18]. The single-mode coherent state $|\alpha\rangle$ at frequency ω has the form

$$|\alpha\rangle = e^{\alpha \hat{c}_\omega^\dagger - \alpha^* \hat{c}_\omega} |\emptyset\rangle \quad (\text{F1a})$$

$$= e^{-\frac{|\alpha|^2}{2}} \sum_{n=0}^{\infty} \frac{\alpha^n}{\sqrt{n!}} |n\rangle, \quad (\text{F1b})$$

$$|n\rangle = \frac{(\hat{c}_\omega^\dagger)^n}{\sqrt{n!}} |\emptyset\rangle, \quad (\text{F1c})$$

where $|n\rangle$ is the n -photon Fock state and the complex number α is an eigenvalue of \hat{c}_ω . The commutator of the mode creation and annihilation operators takes the form $[\hat{c}_\omega, \hat{c}_{\omega'}^\dagger] = \delta_{\omega, \omega'}$ (Kronecker δ function). As the dimer requires a finite bandwidth to form, and also for the mathematical convenience, in the continuous frequency ω limit (which is the same as the large-volume limit), we obtain the following various expressions: $[\hat{c}_\omega, \hat{c}_{\omega'}^\dagger] = \delta(\omega - \omega')$ (Dirac δ function), and

$$|n(\omega)\rangle = \frac{(\hat{c}_\omega^\dagger)^n}{\sqrt{n! \Delta_x^{n-1}}} |\emptyset\rangle, \quad (\text{F2a})$$

$$\langle n(\omega) | n(\omega') \rangle = \delta(\omega - \omega'), \quad (\text{F2b})$$

$$\hat{c}_\omega |n(\omega)\rangle = \sqrt{n} \frac{\delta(\omega - \omega')}{\sqrt{\Delta_x}} |(n-1)(\omega)\rangle \quad \text{for } n \geq 1. \quad (\text{F2c})$$

Here the normalization factor $\Delta_x \equiv \int dx e^{i\omega x/v_g} / (2\pi v_g) |_{\omega=0}$, which is proportional to the volume.

Based on the definition in Eq. (F2a), the number state of photonic dimers can be similarly defined as

$$|n_d(\mu)\rangle = \frac{(\hat{b}^\dagger(\mu))^{n_d}}{\sqrt{n_d! \Delta_x^{n_d-1}}} |\emptyset\rangle. \quad (\text{F3})$$

In the BEC limit, it can be shown that the dimer number states have the following properties which are the natural generalizations of the single-photon number states:

$$\langle n_d(\mu) | n_d(\mu') \rangle = \delta(\mu - \mu'), \quad (\text{F4a})$$

$$\hat{b}(\mu') |n_d(\mu)\rangle = \sqrt{n_d} \frac{\delta(\mu - \mu')}{\sqrt{\Delta_x}} |n_d - 1(\mu)\rangle. \quad (\text{F4b})$$

We note that the relations in Eqs. (F4) hold only in the BEC limit while the definition of the dimer number states in Eq. (F3) always remains valid.

The photon counting rates are determined by the relevant field averages. For example, the first-order photon counting rate for an n_d -dimer Fock state in the BEC limit is proportional to

$$\begin{aligned} \langle n_d(\mu) | \iint d\omega d\omega' \hat{c}_\omega^\dagger \hat{c}_{\omega'} | n_d(\mu) \rangle &= \frac{1}{n_d! \Delta_x^{n_d-1}} \langle \emptyset | (\hat{b}(\mu))^{n_d-1} \iint d\omega d\omega' \hat{c}_\omega^\dagger \hat{c}_{\omega'} (\hat{b}^\dagger(\mu))^{n_d-1} | \emptyset \rangle \\ &= \frac{2}{(n_d - 1)! \Delta_x^{n_d-1}} \langle \emptyset | (\hat{b}(\mu))^{n_d-1} (\hat{b}^\dagger(\mu))^{n_d-1} | \emptyset \rangle \\ &\quad + \langle (n_d - 1)(\mu) | \iint d\omega d\omega' \hat{c}_\omega^\dagger \hat{c}_{\omega'} | (n_d - 1)(\mu) \rangle \\ &= 2n_d. \end{aligned} \quad (\text{F5})$$

As expected, the first-order photon counting rate for a Fock state of dimers is twice the number of the dimers. Following Glauber [1], here we assume an ideal photon detector that has a negligible size and a frequency-independent photoabsorption probability (quantum efficiency is 1).

The second-order correlation for an n_d -dimer Fock state in the BEC limit is given by the following average:

$$\begin{aligned} G^{(2)}(x, x+d) &= \langle n_d(\mu) | \hat{c}^\dagger(x) \hat{c}^\dagger(x+d) \hat{c}(x) \hat{c}(x+d) | n_d(\mu) \rangle \\ &= \frac{n_d}{\pi v_g} \delta(d) + \frac{n_d(n_d - 1)}{\pi^2 v_g^2 \Delta_x}, \end{aligned} \quad (\text{F6})$$

where d denotes the relative distance between the two detected photons (i.e., d/v_g is the difference of the arrival times of the photons). The first term describes the probability of the detection of the two photons from the same dimer, while the second term describes the detection of the two photons from different dimers.

Thus we are motivated to introduce the coherent state of the dimers in the BEC limit. The mathematical definition, not surprising, parallels to that for single photons. Possible physical realizations of the dimer coherent states will be discussed in the following sections. The single-mode coherent state of photonic dimers of total frequency μ is defined as

$$|\beta\rangle \equiv e^{-\frac{|\beta|^2}{2}} \sum_{n_d=0}^{\infty} \frac{\beta^{n_d}}{\sqrt{n_d!}} |n_d(\mu)\rangle, \quad (\text{F7})$$

which is characterized by a complex parameter β . The following field averages can be calculated straightforwardly:

$$\langle \beta | \iint d\omega d\omega' \hat{c}_\omega^\dagger \hat{c}_{\omega'} | \beta \rangle = 2|\beta|^2, \quad (\text{F8a})$$

$$\begin{aligned} G^{(2)}(x, x+d) &= \langle \beta | \hat{c}^\dagger(x) \hat{c}^\dagger(x+d) \hat{c}(x+d) \hat{c}(x) | \beta \rangle \\ &= \frac{|\beta|^2}{\pi v_g} \delta(d) + \frac{|\beta|^4}{\pi^2 v_g^2 \Delta_x}. \end{aligned} \quad (\text{F8b})$$

The average photon number for a dimer coherent state $|\beta\rangle$ is $2|\beta|^2$, a result that is similar to that for a single-photon

coherent state. The dimer coherent state, by construction, also has a Poissonian distribution of the number of dimers. The second-order correlation has a peak at coincidence $d=0$ due to the single-photon contribution from the same dimer, and is proportional to the ‘‘intensity’’ $|\beta|^2$; the background value is due to the due to the single-photon contribution from different dimers and is proportional to the square of the intensity.

For a general optical dimer field described by a density operator ρ , the field correlations in the BEC limit are obtained by augmenting the above expressions by taking the trace of the product of ρ and relevant photon operators.

APPENDIX G: SECOND-ORDER CORRELATION OF PHOTONIC DIMER NUMBER STATE

When we apply coincidence measurement to a light pulse containing multiple photonic dimers, the result correlation curve records the probability of detecting a second photon relatively to a first arriving photon at the photodetector. Intuitively, the strong bunching nature of photonic dimers and the independence between different dimers should yield a with an intense peak near relative distance between detected photons $d=0$, or even a Dirac delta peak under condensation limit. In the following, a calculation provides the mathematical evidence:

$$\begin{aligned} \langle n_d(\mu) | \hat{c}^\dagger(x) \hat{c}^\dagger(x+d) \hat{c}(x+d) \hat{c}(x) | n_d(\mu) \rangle &= \langle n_d(\mu) | \int dx_1 dx_2 \cdots dx_{n_d} \frac{e^{i\frac{\mu}{v_g}(x_1+x_2+x_3+\dots+x_{n_d})}}{(2\sqrt{\pi}\Delta_\omega v_g)^{n_d} (\sqrt{\Delta_x})^{n_d-1} \sqrt{n_d!}} \\ &\quad \times \hat{c}^\dagger(x) \hat{c}^\dagger(x+d) \hat{c}(x+d) \hat{c}(x) \hat{c}^\dagger(x_1) \hat{c}^\dagger(x_1) \cdots \hat{c}^\dagger(x_{n_d}) \hat{c}^\dagger(x_{n_d}) | \emptyset \rangle \\ &= \langle n_d(\mu) | \int dx_1 dx_2 \cdots dx_{n_d} \frac{e^{i\frac{\mu}{v_g}(x_1+x_2+x_3+\dots+x_{n_d})}}{(2\sqrt{\pi}\Delta_\omega v_g)^{n_d} (\sqrt{\Delta_x})^{n_d-1} \sqrt{n_d!}} \\ &\quad \times \left(\sum_{i=1}^{n_d} 2\delta(d)\delta(x-x_i) \hat{c}^\dagger(x_1) \hat{c}^\dagger(x_1) \cdots \hat{c}^\dagger(x_{n_d}) \hat{c}^\dagger(x_{n_d}) \right. \\ &\quad \left. + \sum_{i=1}^{n_d} \sum_{j=1, j \neq i}^{n_d} 4\delta(x-x_i)\delta(x+d-x_j) \hat{c}^\dagger(x_1) \hat{c}^\dagger(x_1) \cdots \hat{c}^\dagger(x_{n_d}) \hat{c}^\dagger(x_{n_d}) \right) | \emptyset \rangle. \end{aligned} \quad (\text{G1})$$

The first term in the parentheses above denotes that the two detected photons are from a common photonic dimer. By summarizing all the possibilities, it can be further calculated as

$$\begin{aligned} 2\delta(d) \langle n_d(\mu) | \sum_{i=1}^{n_d} \frac{e^{i\frac{\mu}{v_g}x}}{2\sqrt{\pi}\Delta_x\Delta_\omega v_g n_d} \hat{c}^\dagger(x) \hat{c}^\dagger(x) \frac{(\hat{b}^\dagger(\mu))^{n_d-1}}{\sqrt{(n_d-1)!\Delta_x^{n_d-2}}} | \emptyset \rangle \\ &= 2\delta(d) \langle n_d(\mu) | \sum_{i=1}^{n_d} \frac{e^{i\frac{\mu}{v_g}x}}{\sqrt{2\pi}v_g\Delta_x n_d} \hat{b}_x^\dagger(x) | (n_d-1)(\mu) \rangle \\ &= 2\delta(d) \langle n_d(\mu) | \sum_{i=1}^{n_d} \frac{e^{i\frac{\mu}{v_g}x}}{\sqrt{2\pi}v_g\Delta_x n_d} \int \frac{d\mu'}{\sqrt{2\pi}v_g} e^{-i\frac{\mu'}{v_g}x} \hat{b}^\dagger(\mu') | (n_d-1)(\mu) \rangle \\ &= \frac{n_d\delta(d)}{\pi v_g} \int d\mu' e^{i\frac{\mu-\mu'}{v_g}x} \langle n_d(\mu) | \frac{\hat{b}^\dagger(\mu')}{\sqrt{n_d}\Delta_x} | (n_d-1)(\mu) \rangle = \frac{n_d\delta(d)}{\pi v_g} \int d\mu' e^{i\frac{\mu-\mu'}{v_g}x} \delta(\mu-\mu') = \frac{n_d\delta(d)}{\pi v_g}. \end{aligned} \quad (\text{G2})$$

The other term in Eq. (G1) denotes the case where the two register photons are from different photonic dimers. It only exists when the dimer number $n_d \leq 2$, and it yields the result

$$\begin{aligned}
& 4\langle n_d(\mu) | \sum_{i=1}^{n_d} \sum_{j=1, j \neq i}^{n_d} \frac{e^{i\frac{\mu}{v_g}(2x+d)}}{2\pi v_g \Delta_x \sqrt{n_d(n_d-1)}} \hat{b}_x^\dagger(x) \hat{b}_x^\dagger(x+d) \frac{(b^\dagger(\mu))^{n_d-2}}{\sqrt{(n_d-2)! \Delta_x^{n_d-3}}} | \emptyset \rangle \\
&= 4n_d(n_d-1) \langle n_d(\mu) | \frac{e^{iK(2x+d)}}{2\pi v_g \Delta_x \sqrt{n_d(n_d-1)}} \iint \frac{d\mu' d\mu''}{2\pi v_g} e^{i\frac{\mu}{v_g}(2x+d) - i\frac{\mu'}{v_g}x - i\frac{\mu''}{v_g}(x+d)} \hat{b}^\dagger(\mu') \hat{b}^\dagger(\mu'') | (n_d-2)(\mu) \rangle \\
&= \frac{\sqrt{n_d(n_d-1)}}{\pi^2 v_g^2 \Delta_x} \iint d\mu' d\mu'' e^{i\frac{\mu}{v_g}(2x+d) - i\frac{\mu'}{v_g}x - i\frac{\mu''}{v_g}(x+d)} \frac{\sqrt{n_d(n_d-1)}}{\Delta_x} \delta(\mu - \mu') \delta(\mu - \mu'') \langle (n_d-2)(\mu) | (n_d-2)(\mu) \rangle \\
&= \frac{n_d(n_d-1)}{\pi^2 v_g^2 \Delta_x}. \tag{G3}
\end{aligned}$$

Clearly, the result in Eq. (G3) is an infinitesimal value compared with that in Eq. (G2). Because different photonic dimers are uncorrelated, the probability of detecting two photons from two dimers is uniform throughout the entire space, giving a value of $1/\Delta_x$, while the probability of detecting two photons together is extremely high because a peak due to the strong bunching nature that two photons always register the photodetector simultaneously when a photonic dimer arrives at it. We note that the results in Eq. (G2) and Eq. (G3) will be slightly different by a normalization factor $1/\Delta_x$ for $n_d = 1$ and $n_d = 2$, respectively. It is due to the definition that vacuum normalizes to 1, while the physics is the same as the probability of detecting two photons from different dimers is zero or a higher-order infinitesimal value.

-
- [1] R. J. Glauber, The quantum theory of optical coherence, *Phys. Rev.* **130**, 2529 (1963).
- [2] J. L. O'Brien, A. Furusawa, and J. Vučković, Photonic quantum technologies, *Nat. Photonics* **3**, 687 (2009).
- [3] H. J. Kimble, The quantum internet, *Nature (London)* **453**, 1023 (2008).
- [4] I. Carusotto and C. Ciuti, Quantum fluids of light, *Rev. Mod. Phys.* **85**, 299 (2013).
- [5] I. H. Deutsch, R. Y. Chiao, and J. C. Garrison, Diphotons in a nonlinear Fabry-Pérot resonator: Bound states of interacting photons in an optical quantum wire, *Phys. Rev. Lett.* **69**, 3627 (1992).
- [6] Z. Cheng and G. Kurizki, "Optical multiexcitons": Quantum gap solitons in nonlinear Bragg reflectors, *Phys. Rev. Lett.* **75**, 3430 (1995).
- [7] P. D. Drummond and H. He, Optical mesons, *Phys. Rev. A* **56**, R1107 (1997).
- [8] J.-T. Shen and S. Fan, Strongly correlated two-photon transport in a one-dimensional waveguide coupled to a two-level system, *Phys. Rev. Lett.* **98**, 153003 (2007).
- [9] J.-T. Shen and S. Fan, Strongly correlated multiparticle transport in one dimension through a quantum impurity, *Phys. Rev. A* **76**, 062709 (2007).
- [10] Y. Shen and J.-T. Shen, Photonic-Fock-state scattering in a waveguide-qed system and their correlation functions, *Phys. Rev. A* **92**, 033803 (2015).
- [11] O. Firstenberg, T. Peyronel, Q.-Y. Liang, A. V. Gorshkov, M. D. Lukin, and V. Vuletić, Attractive photons in a quantum nonlinear medium, *Nature (London)* **502**, 71 (2013).
- [12] Q.-Y. Liang, A. V. Venkatramani, S. H. Cantu, T. L. Nicholson, M. J. Gullans, A. V. Gorshkov, J. D. Thompson, C. Chin, M. D. Lukin, and V. Vuletić, Observation of three-photon bound states in a quantum nonlinear medium, *Science* **359**, 783 (2018).
- [13] R. J. Glauber, Coherent and incoherent states of the radiation field, *Phys. Rev.* **131**, 2766 (1963).
- [14] J. H. Strickler and W. W. Webb, Three-dimensional optical data storage in refractive media by two-photon point excitation, *Opt. Lett.* **16**, 1780 (1991).
- [15] B. Kuhn, P. Fromherz, and W. Denk, High sensitivity of Stark-shift voltage-sensing dyes by one- or two-photon excitation near the red spectral edge, *Biophys. J.* **87**, 631 (2004).
- [16] D. Meshulach and Y. Silberberg, Coherent quantum control of two-photon transitions by a femtosecond laser pulse, *Nature (London)* **396**, 239 (1998).
- [17] Y. Zhou, Z. Chen, L. V. Wang, and J.-T. Shen, Efficient two-photon excitation by photonic dimers, *Opt. Lett.* **44**, 475 (2019).
- [18] M. O. Scully and M. S. Zubairy, *Quantum Optics* (Cambridge University Press, Cambridge, 1997).
- [19] G. Agarwal, *Quantum Optics* (Cambridge University Press, Cambridge, 2012).
- [20] M. J. Collett and C. W. Gardiner, Squeezing of intracavity and traveling-wave light fields produced in parametric amplification, *Phys. Rev. A* **30**, 1386 (1984).
- [21] C. W. Gardiner and M. J. Collett, Input and output in damped quantum systems: Quantum stochastic differential equations and the master equation, *Phys. Rev. A* **31**, 3761 (1985).
- [22] S. Barnett and P. M. Radmore, *Methods in Theoretical Quantum Optics* (Oxford University Press, 2002), Vol. 15.
- [23] S. Barnett and P. Radmore, (Elsevier, 1988), Vol. 68, pp. 364–368.
- [24] J.-T. Shen and S. Fan, Theory of single-photon transport in a single-mode waveguide. II. Coupling to a whispering-gallery resonator containing a two-level atom, *Phys. Rev. A* **79**, 023838 (2009).
- [25] R. J. Glauber, Photon correlations, *Phys. Rev. Lett.* **10**, 84 (1963).

- [26] M. H. Rubin, D. N. Klyshko, Y. Shih, and A. Sergienko, *Theory of Two-Photon Entanglement in Type-II Optical Parametric Down-Conversion* (APS, 1994), Vol. 50, p. 5122.
- [27] T. E. Keller and M. H. Rubin, *Theory of Two-Photon Entanglement for Spontaneous Parametric Down-Conversion Driven by a Narrow Pump Pulse* (APS, 1997), Vol. 56, p. 1534.
- [28] C.-S. Chuu and S. E. Harris, Ultrabright backward-wave biphoton source, *Phys. Rev. A* **83**, 061803(R) (2011).
- [29] X. Guo, C.-L. Zou, C. Schuck, H. Jung, R. Cheng, and H. X. Tang, Parametric down-conversion photon-pair source on a nanophotonic chip, *Light: Sci. Appl.* **6**, e16249 (2017).
- [30] C.-H. Wu, T.-Y. Wu, Y.-C. Yeh, P.-H. Liu, C.-H. Chang, C.-K. Liu, T. Cheng, and C.-S. Chuu, Bright single photons for light-matter interaction, *Phys. Rev. A* **96**, 023811 (2017).
- [31] L.-A. Wu, H. J. Kimble, J. L. Hall, and H. Wu, *Generation of Squeezed States by Parametric Down Conversion* (American Physical Society, 1986), Vol. 57, pp. 2520–2523.
- [32] MgO:LiNbO₃ Nonlinear Crystal (<https://optics.org/products/P000022375>).
- [33] W. R. Bosenberg, A. Drobshoff, J. I. Alexander, L. E. Myers, and R. L. Byer, 93% pump depletion, 3.5-W continuous-wave, singly resonant optical parametric oscillator, *Opt. Lett.* **21**, 1336 (1996).
- [34] C. A. Regal, M. Greiner, and D. S. Jin, Observation of resonance condensation of fermionic atom pairs, *Phys. Rev. Lett.* **92**, 040403 (2004).
- [35] M. W. Zwiernlein, C. A. Stan, C. H. Schunck, S. M. F. Raupach, A. J. Kerman, and W. Ketterle, Condensation of pairs of fermionic atoms near a Feshbach resonance, *Phys. Rev. Lett.* **92**, 120403 (2004).
- [36] C. Chin, M. Bartenstein, A. Altmeyer, S. Riedl, S. Jochim, J. H. Denschlag, and R. Grimm, Observation of the pairing gap in a strongly interacting Fermi gas, *Science* **305**, 1128 (2004).
- [37] T. Bourdel, L. Khaykovich, J. Cubizolles, J. Zhang, F. Chevy, M. Teichmann, L. Tarruell, S. J. J. M. F. Kokkelmans, and C. Salomon, Experimental study of the BEC-BCS crossover region in lithium 6, *Phys. Rev. Lett.* **93**, 050401 (2004).
- [38] Y. Nakagawa, Y. Kasahara, T. Nomoto, R. Arita, T. Nojima, and Y. Iwasa, Gate-controlled BCS-BEC crossover in a two-dimensional superconductor, *Science* **372**, 190 (2021).
- [39] N. Quesada and J. E. Sipe, Effects of time ordering in quantum nonlinear optics, *Phys. Rev. A* **90**, 063840 (2014).
- [40] A. Yariv and W. Louisell, Theory of the optical parametric oscillator, *IEEE J. Quantum Electron.* **2**, 418 (1966).
- [41] J. Schneeloch, S. H. Knarr, D. F. Bogorin, M. L. Levangie, C. C. Tison, R. Frank, G. A. Howland, M. L. Fanto, and P. M. Alsing, Introduction to the absolute brightness and number statistics in spontaneous parametric down-conversion, *J. Opt. (Bristol, UK)* **21**, 043501 (2019).
- [42] Y. Zhou, Q. Liu, and J.-T. Shen (unpublished).